

# Eye Surgery Training Simulator Having 3D Microchannels

A dissertation submitted in partial fulfilment  
of the requirements for the degree of  
**Doctor of Philosophy**

Presented by

**Mahmoud GALLAB**

Department of Micro-Nano Mechanical Science and Engineering  
Graduate School of Engineering  
Nagoya University

2020



## Acknowledgement

This dissertation presents the cumulative results of my doctoral studies. During this time, I was greatly supported by a plethora of people who contributed in different ways and without whom this work would not have been possible. Foremost, I would like to express my sincere appreciation to my supervisor Professor Fumihito Arai, Department of Micro-Nano Mechanical Science and Engineering, Nagoya University in Japan, for his immense support, advice whenever I needed it, and for his inspiring guidance during my study. I really feel privileged and ecstatic to have been part of his amazing group.

I am also grateful to Professor Yasuhisa Hasegawa from Department of Micro-Nano Mechanical Science and Engineering, Professor Masahiro Ohka from Department of Complex Systems Science, Graduate School of Information Science, and Professor Hisataka Maruyama from Department of Micro-Nano Mechanical Science and Engineering for taking time out of their busy schedule to examine my PhD thesis and for kind agreement with being my doctoral committee members.

Special thanks go to Dr. Seiji Omata for the valuable scientific discussions that we had, for teaching me precious scientific writing and communication skills, and for his unconditional support. Omata, it was a joy to work with you. I would like also to thank Dr. Taisuke Masuda, Dr. Shinya Sakuma, and Dr. Takeshi Hayakawa for their kind advice, help and support.

I would like to extend my thanks to Ms. Hiroko Tsukamoto, Ms. Mari Obara, Ms. Akiko Tanaka, Mrs. Chisato Ohsumi, and Ms. Chika Fuseya for their kind help and support. I personally would like to express my gratitude to Ms. Hiroko Tsukamoto for her genuine help and support through the whole period of my study.

This work would not have been possible without the additional help of many students and collaborators so I am very grateful to all of my lab mates. Among my lab mates I especially would like to thank Bilal, Hashim, Anas, Chang Di, Kumon, Someya, Kagiya, and Hasegawa. You guys were a great help for discussions and suggestions along the way. Thank you to Takayuki Hasegawa, the first person from our group that I met, who helped with advice and guidance on equipment in my research.

My greatest gratitude must forward to my family especially my parents for their sacrifices and for being the main source of moral support and encouragement in my life. I am so indebted to all of my brothers and sisters for their support.

Last and certainly not least, huge thanks go to my beloved wife for sharing the happiness and hardship together.

***Mahmoud Gallab 2020***

## **Dedication**

*To my Parents.....who I love the most*

“I dedicate this thesis to my parents. You deserve a special  
“thank you” from your son, who is nothing without you”

## Abstract

The ability to produce artificial organ/tissue, that mimics the real organ/tissue in its physical properties, with an effective, rapid, easy, inexpensive, and reproducible techniques, is significant in a number of medical applications such as surgical training, surgical planning, evaluation of robotics systems, and tissue engineering.

Synthetic models are functional tools for training novice surgeons and for assessment of medical equipment or surgical assistant robotics systems. Currently, several of surgical simulation systems, which can be used for training apprentices or evaluation of medical devices, exist. For successful and workable simulator model however, it is necessary to: 1) the simulator imitates the target human organ or tissue in its anatomical and mechanical characteristics, 2) the simulator should exhibit properties such as reproducibility, durability and the fabrication methods of the simulator should be inexpensive and easy to use, and 3) the models do not have ethical concerns.

This dissertation aims, firstly, to introduce two fabrication methods, photolithography and femtosecond laser and mask hybrid exposure (FMEx), for fabrication of three dimensional (3D) microchannel that allow for a close simulation of the natural structure of small diameter of human microvessels ( $\leq 15 \mu\text{m}$ ) that can be used as surgical training simulator, for different types of surgeries such as eye surgeries, or other biomedical applications. The first method, photolithography with the aid of 3D printing models, enables us from creation of 3D microchannel, with rectangular

cross section, over irregular surface with different depths and a large model size. Second method, FMEx, made it possible to fabricate microchannel, having circular cross section, with part of the millimeter-scale structure with a submicrometer resolution in 3D. Both methods made it possible to fabricate a millimetre-scale 3D structure with a submicrometric resolution and achieve an easy injection of solution. This is because it was possible to fabricate typical microfluidic channels used for model inlet and outlet ports. Furthermore, in the FMEx method, we employed an acid-diffusion effect using a chemically amplified resist to form a circular channel cross-section. The acid-diffusion effect made it realizable to fabricate a smooth surface independent of the laser scanning line width. Finally, the microvessel model made from materials with controllable mechanical characteristics that can be tuned to make them close to the mechanical properties of human microvessel.

Secondly, by using a simple fabrication techniques, we successfully developed an eye surgery model, which consists of sclera with clear cornea and 3D microchannel, which simulate human micro tube named Schlemm's Canal (SC), and thin membrane, which represents the trabecular meshwork (TM), cover the microchannel, as an eye surgical training simulator for glaucoma surgery. The eye surgical simulator was fabricated by soft materials with controllable mechanical demeanor to make it similar to actual target tissues. The proposed eye surgery model can be used as a simulator for training unexperienced surgeons on glaucoma surgery. Additionally, to emulate the surgery with constraints similar to those in a real operation, the eye model was installed on a skull platform. A preliminary assessment by eye doctors showed that the model can help novice eye doctors to develop the basic skills of the surgery. We foresee a

number of applications for the proposed eye model, besides simulation and training for the surgery, including medical device testing and surgical planning.

In conclusion, two fabrication methods of 3D microchannel, which mimics human microvessel, were developed. Moreover, an eye surgery training simulator, which consists of 3D microchannel that represents human microvessel, sclera, and trabecular meshwork tissues, introduced as surgical training simulator for glaucoma surgery.



# Contents

|   |              |
|---|--------------|
| <b>Acknowledgement</b>                                  | <b>i</b>     |
| <b>Abstract</b>   | <b>iv</b>    |
| <b>Contents</b>   | <b>vii</b>   |
| <b>List of Figures</b>                                  | <b>x</b>     |
| <b>List of Tables</b>                                   | <b>xviii</b> |
| <b>Chapter 1 Introduction</b>                           | <b>1</b>     |
| 1.1 Surgical training                                   | 1            |
| 1.2 Surgical robotics systems                           | 3            |
| 1.3 Surgical simulation                                 | 17           |
| 1.4 Classification of surgical simulation               | 18           |
| 1.4.1 Cadaveric models                                  | 20           |
| 1.4.2 Live animal models                                | 23           |
| 1.4.3 Ex vivo animal tissue models                      | 26           |
| 1.4.4 Virtual reality (computer-based) models           | 27           |
| 1.4.5 Artificial models                                 | 34           |
| 1.4.6 Summary   | 36           |
| 1.5 Recent development of artificial surgical simulator | 37           |
| 1.5.1 Surgical simulator for cardiac applications       | 39           |
| 1.5.2 Surgical simulator for urology applications       | 42           |
| 1.5.3 Surgical simulator of vascular system             | 45           |
| 1.5.4 Summary   | 56           |
| 1.6 Thesis overview                                     | 57           |
| 1.6.1 Research objectives                               | 57           |
| 1.6.2 Outline of the dissertation                       | 57           |

|  |            |
|--|------------|
| <b>Chapter 2 Eye Surgery Training Simulator</b>                                      | <b>60</b>  |
| 2.1 Introduction   | 60         |
| 2.2 Bionic Humanoid  | 61         |
| 2.3 Eye surgery training simulator   | 65         |
| 2.4 Summary  | 74         |
| <b>Chapter 3 Fabrication Methods of 3D Microchannel that Mimic Human Microvessel</b> | <b>75</b>  |
| 3.1 Introduction   | 75         |
| 3.2 Microfluidic channel design and concept  | 78         |
| 3.2.1 Photolithography method  | 79         |
| 3.2.2 Femtosecond laser exposure method  | 80         |
| 3.3 Fabrication methods  | 82         |
| 3.3.1 Photolithography exposure method   | 82         |
| 3.3.2 Femtosecond laser and mask hybrid exposure (FMEx)                              | 85         |
| 2.3.2.1 Femtosecond laser exposure system  | 85         |
| 3.4 Experimental results   | 90         |
| 3.4.1 Photolithography method  | 90         |
| 3.4.2 FMEx method  | 92         |
| 3.5 Discussion   | 95         |
| 3.6 Summary  | 101        |
| <b>Chapter 4 Eye Model as Surgical Simulator for Glaucoma Surgery</b>                | <b>102</b> |
| 4.1 Introduction   | 102        |
| 4.2 Materials and Methods  | 106        |
| 4.2.1 Design concept   | 106        |
| 4.2.2 Fabrication of the eyeball model   | 110        |
| 4.2.3 Fabrication of the TM  | 111        |
| 4.2.4 Measurement of the thickness and mechanical properties of TM                   | 113        |
| 4.3 Results  | 114        |
| 4.3.1 Eyeball model  | 114        |

|       |  |            |
|-------|--|------------|
| 4.3.2 | Fabrication results of the TM                        | 114        |
| 4.3.3 | Evaluation of the TM thickness                       | 116        |
| 4.3.4 | Evaluation of mechanical properties of the TM        | 117        |
| 4.3.5 | Simulation of surgery with the eye model             | 119        |
| 4.4   | Discussion   | 121        |
| 4.5   | Summary  | 123        |
|       | <b>Chapter 5</b>                                     | <b>124</b> |
|       | <b>Conclusions and Future Outlook</b>                | <b>124</b> |
| 5.1   | Conclusions  | 124        |
| 5.2   | Future Outlook                                       | 126        |
| 5.2.1 | For surgical training and planning applications      | 126        |
| 5.2.2 | For tissue engineering and implantation applications | 127        |
|       | <b>Bibliography</b>                                  | <b>128</b> |
|       | <b>Accomplishments</b>                               | <b>153</b> |

## List of Figures

- Figure 1.1. Robodoc surgical system. The surgeon's console is shown on the left and the robot arm tower on the right [30]. 5
- Figure 1.2. Automated Endoscopic System for Optimal Positioning 1000 (AESOP 1000) [31]. 5
- Figure 1.3. Simulated setup of the operating room for a telerobotic laparoscopic cholecystectomy using the da vinci telerobotic surgical system[34]. 6
- Figure 1.4 . DOF for retinal surgery tool [39] 9
- Figure 1.5. (A) The new steady-hand manipulator for retinal surgery during a CAM vein cannulation. (B) The tool holder and micro-injection tool during a cannulation. (C) Chicken embryo with a micro-pipette [39]. 9
- Figure 1.6. Successive images of a cannulation taken through a microscope: (A) tip is positioned near target vein. (B) tip is touching target vein. (C) tip is pushed against target vein. (D) tip is pulled up using hooking motion. (E) tip is pulled back to allow vein to un-distort. (F) tip has not been moved; vein is filled with clear marker [39]. 10
- Figure 1.7. (A) system overview (B) Workspace [45]. 12
- Figure 1.8. Ex vivo experiment: (a) experimental setup, (b) insertion of surgical tools into the eye [45]. 13
- Figure 1.9. Result of microcannulation: a insertion of the tip, b drug being injected and replacing the blood [45]. 13
- Figure 1.10. (A) Pathologic conditions in hard-to-reach areas across the human body where small-scale soft continuum robots with active

|  |    |
|--|----|
| steering and navigating capabilities have utility. (B) Illustration of the active steerability of a submillimeter-scale soft continuum robot navigating a complex vasculature with an aneurysm [51].   | 15 |
| Figure 1.11. The various simulator categories [62].  | 19 |
| Figure 1.12. Pictorial demonstration of left femoral artery cannulation. Red and blue dyes are used for arterial and venous perfusion respectively. The arterial system is perfused using a centrifugal pump [72].   | 21 |
| Figure 1.13. Practicing of different posterior and anterior segments eye surgeries with cadaveric eye model. (a). The continuous circular capsulorrhexis and a strong red reflex are evident. (b) A deep groove is phacoemulsified in the nucleus. (c) Injection of a foldable intraocular lens into the capsular bag. The capsulotomy margin can be clearly appreciated [76]. | 21 |
| Figure 1.14. Trabectome (NeoMedix Inc, Tustin, California) handpiece approaching the trabecular meshwork viewed through a modified Swan-Jacobs gonioscopy lens in a prepared practice cadaveric eye [77].  | 22 |
| Figure 1.15. Microsurgical skills training using live rat model simulation [62].   | 25 |
| Figure 1.16. (A) Updated testbed (B) Close-up of the simulated operating area. (C) Bent tip pipette during cannulation (D) Sclera model with constrained instrument entry point and grasper tool [39].   | 25 |
| Figure 1.17. Using the MIST system (Mentice Medical Simulation AB, Gothenburg, Sweden) for training and assessment of psychomotor skills for minimally invasive surgery [119].   | 28 |
| Figure 1.18. The “Cutting” task on the LapSim virtual reality simulator [120].   | 29 |

|   |    |
|---|----|
| Figure 1.19. The “Dissection” task on the LapSim virtual reality laparoscopic simulator [120].  | 29 |
| Figure 1.20. Surgical virtual environment including micro-tools and guidance information. The eyelids have been pulled back as they are during actual surgery. Superimposed on the image is additional information to guide the surgeon. The broken line around the cornea shows a planned cutting path [108].    | 30 |
| Figure 1.21. VR simulation of steps of vitreous surgery: (a) Simulation of vitreous opacity; (b) Insertion of active instrument with simulation of piecemeal removal of the opacity under direct illumination; (c) Insertion of passive instrument; (d) Removal of vitreous opacity with endo-illumination [100]. | 31 |
| Figure 1.22. 3D reconstruction images of the blood vessels by open scene graph [125].   | 32 |
| Figure 1.23. Simulation of catheter inserting into the vessel model [125].  | 33 |
| Figure 1.24. Use of synthetic models. A resident uses a synthetic model to practice breast reconstruction at new York university langone health [127].  | 35 |
| Figure 1.25. The practice eye model for membrane peeling [135].   | 35 |
| Figure 1.26. Stereolithograph of human Skull. A. Virtual model of the skull. B. Physical 3D model [115].  | 38 |
| Figure 1.27. A 3D printed cardiac model with a congenital defect [144,145].   | 40 |
| Figure 1.28. Four example models for surgical simulation. Colored model is preferred to white or light beige-colored model. Slightly dark color improves the perception of complex surface anatomy [146].   | 40 |
| Figure 1.29. Scenes of surgical procedures on the models. A, Arterial switch operation in complete transposition of the great arteries. B, Norwood operation in hypoplastic left heart syndrome with aortic   |    |

- atresia [149]. LCA, Left coronary artery; RA, right atrium; RV, right ventricle; SVC, superior vena cava. 41
- Figure 1.30. 3D printed model for kidney with tumor anatomy. Comparative views of the CT scan at the nephrographic phase (**a** axial, **b** coronal and **c** sagittal planes) and corresponding views of the physical model (**d** superior and median view, **e** median and anterior view, **f** lateral view). An inferior polar cyst is also displayed on this model (translucent yellow). The cubes show the 3D printed model orientation in space [147]. 42
- Figure 1.31. A 3D printed kidney model using flexible material as the kidney's main cortex showing the relative position of the renal tumor with respect to the renal artery, vein, and collecting system [148]. 44
- Figure 1.32. The 3-D printed donor organ kidney replicas allowed for the creation of translucent models showing the visceral organs, vessels, and other details [149]. 44
- Figure 1.33. (A) 3-D structure of basilar tip artery with giant aneurysm reconstructed with CT angiography. (B) An in vitro patient-tailored biological model of human cerebral artery with vasculature-like thin uniform membranous configuration [163]. 47
- Figure 1.34. Main steps to manufacture PDMS in vitro models of human artery vessels [164]. 48
- Figure 1.35. Steps taken in producing a three dimensionally printed aneurysm [135]. 49
- Figure 1.36. Manufacturing process of patient-specific vessel simulator. (a) Data is obtained by CT and converted to an STL file. (b) The STL file is exported and the acrylonitrile butadiene styrene (ABS) vascular model is printed using the 3D printer. (c) The ABS solid model and supports are removed with nippers. The surface is

|   |    |
|---|----|
| smoothed by dipping into ABS solvent and then dried. (d) The solid ABS model is coated with liquid silicone. (e) The ABS is dissolved in acetone after the silicone solidifies. (f) The silicone vessel is connected to a circulation pump and the simulation is performed. (g) The surface of the ABS vessel model is smoothed by ABS solvent. Left: Before dipping in the ABS solvent, Right: After dipping in the ABS solvent [166]. | 50 |
| Figure 1.37. Endo Vascular Evaluator surgical simulator [159].  | 51 |
| Figure 1.38. Concept of multiscale fabrication for transparent microvessel models [161].  | 53 |
| Figure 1.39. The fabricated circulation model [161].  | 53 |
| Figure 1.40. Artificial retinal vein model: (a) 60 $\mu\text{m}$ (pitch 200 $\mu\text{m}$ ); (b) 90 $\mu\text{m}$ (pitch 200 $\mu\text{m}$ ) [162].   | 54 |
| Figure 1.41 The experimental set-ups for manual and robotic microcannulation : (a) for manual operation; (b) for robotic operation (b1, master manipulator; b2, slave manipulator) [162].   | 54 |
| Figure 1.42. Eye model: (a) sectional view; (b) fabricated model [162].   | 55 |
| Figure 1.43. Outline of the dissertation.   | 59 |
| Figure 2.1. Bionic Humanoid: Concept of whole body surgery training system.   | 62 |
| Figure 2.2. Modular structure of Bionic Humanoid.   | 62 |
| Figure 2.3. Modular structure of head part.   | 63 |
| Figure 2.4. The first prototype of Bionic Humanoid.   | 64 |
| Figure 2.5. Surgical practice eye kit introduced by Kitaro WetLab.  | 66 |
| Figure 2.6. Surgical practice eye developed by BIONIKO, Aventura, FL, USA[161].   | 66 |
| Figure 2.7. Modular structure of Bionic Eye   | 67 |
| Figure 2.8. Eye surgery training simulator (Bionic-EyE)   | 68 |
| Figure 2.9 Benchmark of eye surgery simulator   | 68 |



|   |    |
|---|----|
| Figure 2.10 Optical-microscope photograph of retinal vessels [169].   | 69 |
| Figure 2.11 Conceptual image of retinal vessel model on curved surface: a overview of model, b side view showing line A-A', and c close-up of side view[169].   | 70 |
| Figure 2.12. Photographs of fabricated model: a overview, b cross-sectional view cut along line A-A', and c enlarged image of cross-sectional view [169].   | 70 |
| Figure 2.13. Results of microcannulation simulation: photographs of retinal vessel model (a) before and (b) after puncture of retinal vessel by micropipette. These photographs were acquired by using an eye-surgery microscope [169].   | 71 |
| Figure 2.14. Photographs of the artificial ILM peeling task with an artificial eye mode [170].  | 73 |
| Figure 3.1. Concept of simulating capillary vessels and arterioles with models.   | 77 |
| Figure 3.2. Basic structure of 3D microchannel.   | 78 |
| Figure 3.3. Cause of rough surface by a femtosecond laser exposure (a) Femtosecond laser scanning process (b) Cross-section of the photoresist after scanning   | 81 |
| Figure 3.4. Mechanism for producing smooth mold surface when using chemically amplified resist. (a) Acid generation after femtosecond laser exposure. (b) Acid diffusion during post-exposure bake.   | 81 |
| Figure 3.5. Microvessel model fabrication using photolithography.   | 84 |
| Figure 3.6. Measurement of scanning line width and thickness during femtosecond laser exposure. (a) Design concept for microfluid device. (b) Top view SEM image fabricated 3D mold. (C) Relationship between scanning speed and line width and thickness by femtosecond laser exposure. Inset illustrates ratio of each pair |    |

|  |     |
|--|-----|
| of line width dimensions, and dashed line represents theoretical ratio by the two-photon laser method, $\ln 2/2 \approx 0.59$ .  | 87  |
| Figure 3.7. Microchannel model fabrication process using FMEEx.  | 89  |
| Figure 3.8. Images of the microchannel fabricated using classical photolithography. (a) PDMS base model with microchannel. (b) Optical microscope image of microchannel. (c) Cross-section of microchannel.  | 91  |
| Figure 3.9. Measurement of microchannel depth. (a) Full thickness profiles of the designed and fabricated microchannels. Position zero is the inclination starting point. (b) Distributions of deviations of fabricated depth calculated by subtracting each fabricated value from the design. | 91  |
| Figure 3.10. A CAD image design of 3D microfluidic devices for replication of microscopic vessel fabricated using FMEEx.   | 92  |
| Figure 3.11. SEM images of the mold fabricated using FMEEx: (a) Low magnification. (b) High magnification with chemically amplified resist (KMPR). (c) High magnification with standard resist (PMER).   | 93  |
| Figure 3.12. (a) Microscopic image of a PDMS microchannel mold fabricated using FMEEx (b) Cross-section of the microchannel at section A-A'.   | 94  |
| Figure 3.13. Schematic drawing of cross-sections of microchannels fabricated using femtosecond laser exposure and classical photolithography   | 100 |
| Figure 4.1. Schematic image of angle structure at corneal limbus and flow of aqueous humour in a human eye.  | 107 |
| Figure 4.2. Concept of a glaucoma model for training on inside-out (ab interno) surgery.   | 107 |

|  |     |
|--|-----|
| Figure 4.3. (a1) Anatomy of limbus area of human eye; (a2) Design and dimensions of eye model with 3D microchannel as artificial SC; (b) Fabrication process of the eye model with SC; (c) Fabricated eye model made from PDMS; (d) Cross-sectional image of fabricated SC structure of the eye model. | 110 |
| Figure 4.4. Fabrication process of an artificial trabecular meshwork (TM) adhered inside an artificial sclera.   | 112 |
| Figure 4.5. Sectional images of the fabricated eye model. (a) Cross-sectional image of the whole eye model. (b) High-magnification image of the angle for the tube structure of the SC covered with artificial TM.   | 115 |
| Figure 4.6. Relationship between the concentration of PVC solution and thickness of fabricated artificial trabecular meshwork.   | 116 |
| Figure 4.7. Stress–strain behavior of trabecular meshwork model. Numbers indicate the weight ratio of the PVC/DEHP mixture.  | 117 |
| Figure 4.8. Elastic modulus and fracture strain of various concentrations of PVC/DEHP  | 118 |
| Figure 4.9. Photographs of the eye model installed on the Bionic-EyE™ for simulation of micro invasive glaucoma surgery.   | 120 |
| Figure 4.10. Photographs from the training of the micro-invasive glaucoma surgery with a microhook.  | 120 |

## LIST OF TABLES

|  |     |
|--|-----|
| Table 1.1 : Advantages and disadvantages of robot-assisted surgery versus conventional surgery [26].   | 4   |
| Table 3.1 : Comparison between the femtosecond laser and photolithography fabrication methods.   | 100 |
| Table 4.1 : Benchmark of fabrication methods to fabricate the artificial trabecular meshwork for a glaucoma model                            | 109 |
| Table 4.2 : Mechanical properties of PDMS and PVC/DEHP used in this study to replicate sclera and trabecular meshwork tissues, respectively. | 118 |





# CHAPTER 1

## Introduction

### 1.1 Surgical training

Surgery is a major part of health care systems and is linked with increased life expectancy. Surgical operation has a significant role in dealing with a wide spectrum of diseases for the mitigation of human pain. Moreover, surgery is required at all ages; from infants with natural abnormalities to the elderly with cataracts [1]. As a result, the number of operations that takes place every year worldwide is large and continue to grow. Therefore, the development of understanding and the skills, required for performing a surgery, is crucial for the success of the surgery. To do so, intensive training program for surgeons on the target surgery is required.

Surgical skills training has heavily been depend on apprenticeship model using patients as teaching cases [2–4]. The procedures and techniques of any kind of surgery have traditionally been learned via an apprenticeship program, in which “see one, do one, teach one!” has been the aphorism of practical skills training. Surgical skills learned through a mentor's method, which includes watching, then supporting mentors, before being allowed to operate under supervision. As the novice’s experience develop, he can finally work independently. Obviously, apprenticeship model provides the potential

for medical doctors to understand the nature of surgery. This method of training produced highly skilled surgeons for a number of generations. However, surgical training with this model is associated with increased complication rates [5–16] and worse patient outcomes [17,18] . Many factors propose that surgical skills training, with the above-mentioned method, may not be the ideal method to advance the novice surgeons' skills. Firstly, due to the increased awareness of patient safety, reduced working hours and financial constraints in health care organizations, evolving of the operations techniques, a host of challenges have been arisen, mainly associated with steeper learning curves [19]. Secondly, evolving of the operations techniques, the expand usage of laparoscopy, endoscopy, and robotics, and the rapid spread of using minimally invasive techniques in the surgery, make this model to present a challenge for trainees to obtain the required level of mastery with these complicated techniques. Finally, legal and ethical issues about learning on the human have become a major concern.

There is a growing understanding that a vast part of the learning curve of surgical procedures does not necessarily need practising on patients and that it is even better to train on a model first. Thus, alternative methods for training novices to earn surgical skills and for evaluation of medical devices are highly required. The alternative surgical simulation systems allow training of surgeons and evaluation of robotics systems in a safe environment before entering the operative room. In the following sections, we will, firstly, discuss the advancement of robotics systems that involved in the surgery, particularly in the eye surgery, and make the training of surgeons with the traditional method, apprenticeship, strenuous. Secondly, we will discuss the alternative methods of the surgical simulation systems with advantages and disadvantages for each method.



## 1.2 Surgical robotics systems

However, as a form of entertainment, robotics was introduced, it gradually became used in different fields of science. This field influenced medicine, particularly in the operating room. Surgery and robotics have been combined to create a new kind of surgical operating room [20–23]. Through enhancing the ability of surgeons to conduct different surgical procedures, robotic systems offered great changes to medical or surgical processes [24]. Additionally, robotics systems underpin the precision, stability, and dexterity of the surgeons through several ways. For instance, tools with greater degree of freedom reinforce the capacity of the surgeon to manipulate tissues and organs. Furthermore, the tremor of surgeons can be balanced by correct in hardware and software filters in end effector movement. In fact, robotic technologies confer surgeons with a relaxed and convenient operating position as they do not have to stand throughout the surgery as in the conventional surgery [25]. Table 1.1 describes the advantages and disadvantages of a robot-assisted operation compared to conventional operation [26].

The application of robotics systems to surgery was a result of the advances and growth of medical technology during the last few decades. The first surgical application of robotics technology was presented in 1985. A modified industrial robot was used to guide a needle for biopsy with 0.05 mm accuracy [27–29]. Then, the surgical robotics system, which named Robodoc (Integrated Surgical Systems), was introduced for the use in hip replacement surgery as shown in [figure 1.1](#) [30]. The next breakthrough of robotic system for the surgery was in 1994 when the Automated Endoscopic System for Optimal Positioning 1000 (AESOP 1000) became the first laparoscopic camera

holder as shown in figure 1.2 [31]. Over the above, the idea of telerobotic was introduced to robotics surgery. With this system, the surgeon sits on console which at a distance from the robot that operates on the patient [32–34]. The field of telerobotic grew up and the idea of integrating this technology with the field of laparoscopic surgery was completely realised [35]. [Figure 1.3](#) shows a telerobotic laparoscopic cholecystectomy using the da vinci telerobotic surgical system [34].

Table 1.1 : Advantages and disadvantages of robot-assisted surgery versus conventional surgery [26].

|             | Conventional operation                          | Robot-assisted operation                           |
|-------------|---|--|
| Limitations | Limited geometric accuracy                      | No judgment  |
|             | Limited sterility                               | Unable to use qualitative information              |
|             | Susceptible to radiation and infection          | Absence of haptic sensation                        |
|             | Limited ability to use quantitative information | More studies needed                                |
|             | Limited dexterity outside natural scale         | Expensive  |
|             | Prone to tremor and fatigue                     | Technology in flux                                 |
| Advantages  | Good judgment                                   | Good geometric accuracy                            |
|             | Able to use qualitative information             | May be sterilized                                  |
|             | Rudimentary haptic abilities                    | Resistant to radiation and infection               |
|             | Can integrate extensive and diverse information | Can use diverse sensors in control<br>Scale motion |
|             | Strong hand–eye coordination                    | Stable and untiring                                |
|             | Dexterous<br>Flexible and adaptable             |  |



Figure 1.1. Robodoc surgical system. The surgeon's console is shown on the left and the robot arm tower on the right [30].



Figure 1.2. Automated Endoscopic System for Optimal Positioning 1000 (AESOP 1000) [31].



Figure 1.3. Simulated setup of the operating room for a telerobotic laparoscopic cholecystectomy using the da vinci telerobotic surgical system[34].

One of the advantages of robotic surgery is the scale that the surgery can be done at. Previously, it was not possible to involve smaller movement in the surgery because of the limit scope of actions of the surgeons. Currently, with the advances in robotic surgery, it is possible to complete more complex surgical tasks using robotics.

Types of surgical robotics can be classified in different ways such as classification based on manipulator design, level of autonomy, intending operating environment, or targeted anatomy/technique [24]. In this study we are concerning with the eye surgeries, therefore we will focus on the recent advances of robotic systems for ophthalmic surgery.

The development of operating microscope and precision micro instruments has been pivotal in the evolution of microsurgery. However, the potential of microsurgery is limited by abundant reasons. For instance, it is mainly depending on the surgeon's dexterity. Second, microsurgery requires that the surgeon spends long hours in the same relatively fixed posture. This immobility can be tiring during long, complex procedures and can adversely affect the surgeon's technical performance. Therefore, development of microsurgical robotics to assist surgeons in performing microsurgery, particularly ocular surgeries, is a growing field of research. Because of the advances in materials, computers, sensor technology, and miniature components, practical surgical robots become feasible. To underpin the surgeon's dexterity and manoeuvrability in the deep surgical field, ample microsurgical robotics systems have been developed to assist surgeons with the microsurgical procedures [3,36–39], [40–43]. This minimizes the surgeon's movement at the tissue level and tempers any incorrect movement associate with inexperience or fatigue [41].

Vitreoretinal surgery considers one of the most technically difficult eye surgeries. Fine and accurate motion is demanded to manipulate extremely delicate tissue within the small and constrained area of the eye. Some of the main technical limitations are insufficient spatial resolution and depth perception of microstructures to identify tissue planes, imprecise movements during micromanipulation of tissue due to physiological tremor, and lack of force sensing since the movements required for dissection are below the surgeon's sensory threshold. Robotic eye surgery could improve the surgical techniques of the accomplished vitreoretinal surgeon. Therefore, many researchers have worked to introduce robotic systems for ophthalmic surgery, particularly in vitreoretinal surgery. For instance, Kumar et al. explained the first steps in the development of a robotic assistant for microsurgery and other precise manipulation tasks [38]. Also, Mitchell et al. introduced a steady-hand system for retinal surgery as shown in [figure 1.4](#) [37,39,44]. Mitchell successfully, by using chicken embryos as eye phantoms, cannulate veins down to 80  $\mu\text{m}$  rapidly, reliably, and with marginal damage to the surrounding tissue as shown in [figure 1.5](#) and [figure 1.6](#) [39]. The system's drawback was that for different uses of ophthalmological surgery, the workspace was small.

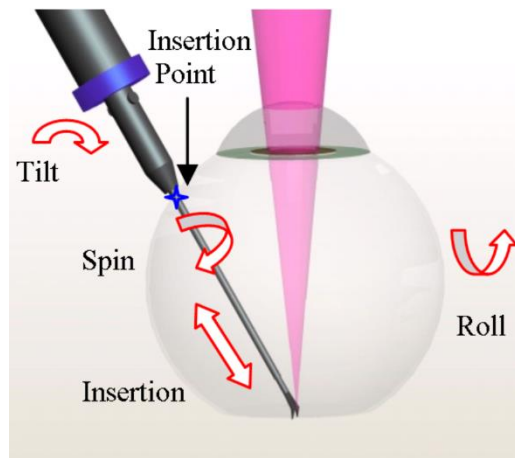


Figure 1.4 . DOF for retinal surgery tool [39]

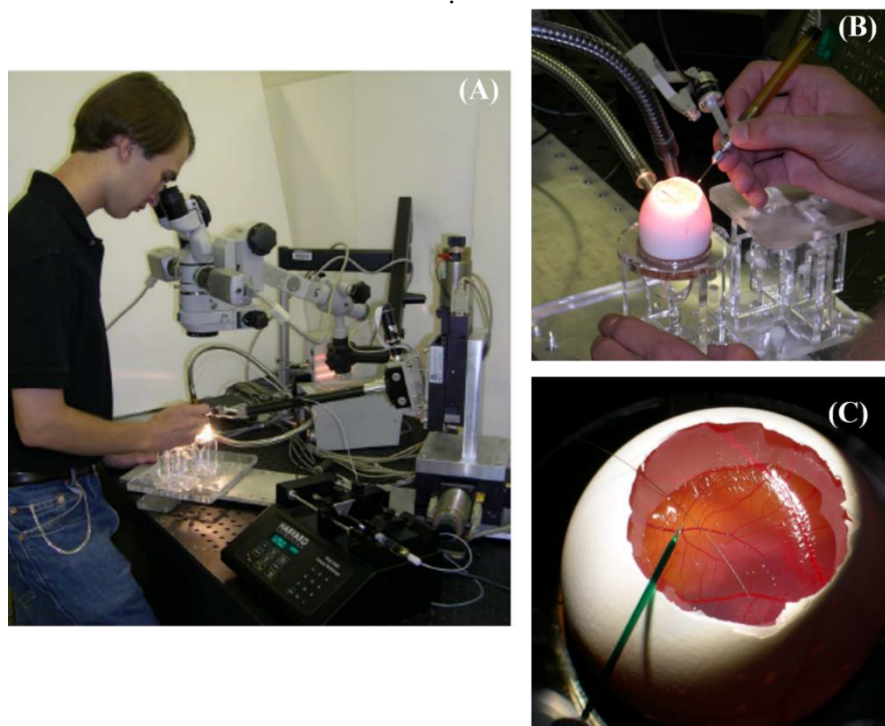


Figure 1.5. (A) The new steady-hand manipulator for retinal surgery during a CAM vein cannulation. (B) The tool holder and micro-injection tool during a cannulation. (C) Chicken embryo with a micro-pipette [39].

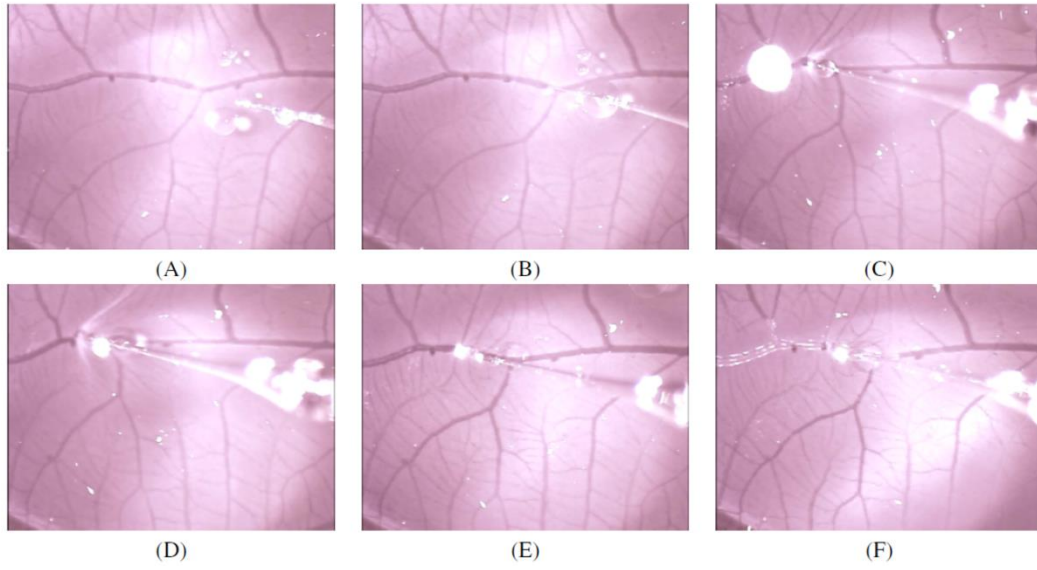


Figure 1.6. Successive images of a cannulation taken through a microscope: (A) tip is positioned near target vein. (B) tip is touching target vein. (C) tip is pushed against target vein. (D) tip is pulled up using hooking motion. (E) tip is pulled back to allow vein to undistort. (F) tip has not been moved; vein is filled with clear marker [39].



Yoshiki et al. developed a new master–slave robotic microsurgical system, as shown in [figure 1.7](#), that makes eye doctors able to perform different types of microsurgeries including ophthalmological, neurosurgical, and reconstructive surgical applications with large workspace [45]. In an ex vivo experiment, microcannulation was performed and a 30  $\mu\text{m}$  diameter micropipette was successfully inserted into retinal vessels of pig eyes with diameters of 70, 90 and 110  $\mu\text{m}$  ([figure 1.8](#)), showing good system performance ([figure 1.9](#)). With the proposed master–slave robotic system, a surgeon manages the slave units by operating the master manipulators while being provided with a 3D microscopic view from a high-definition monitor.

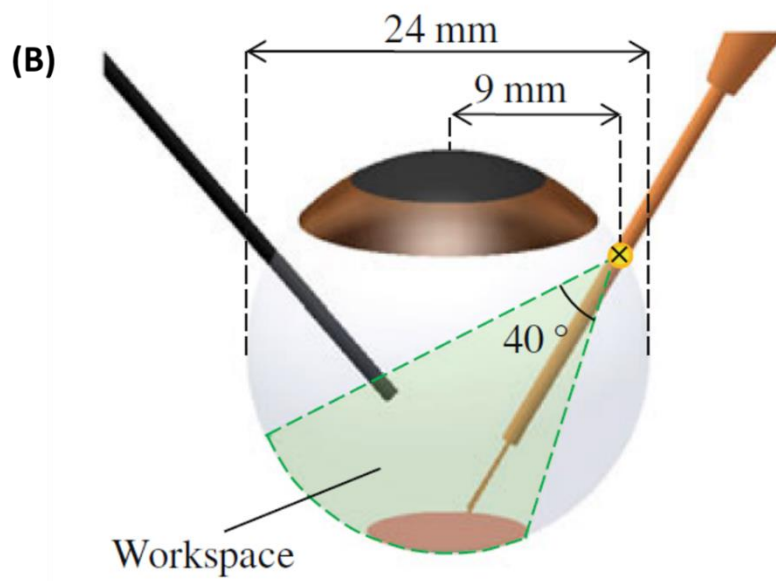
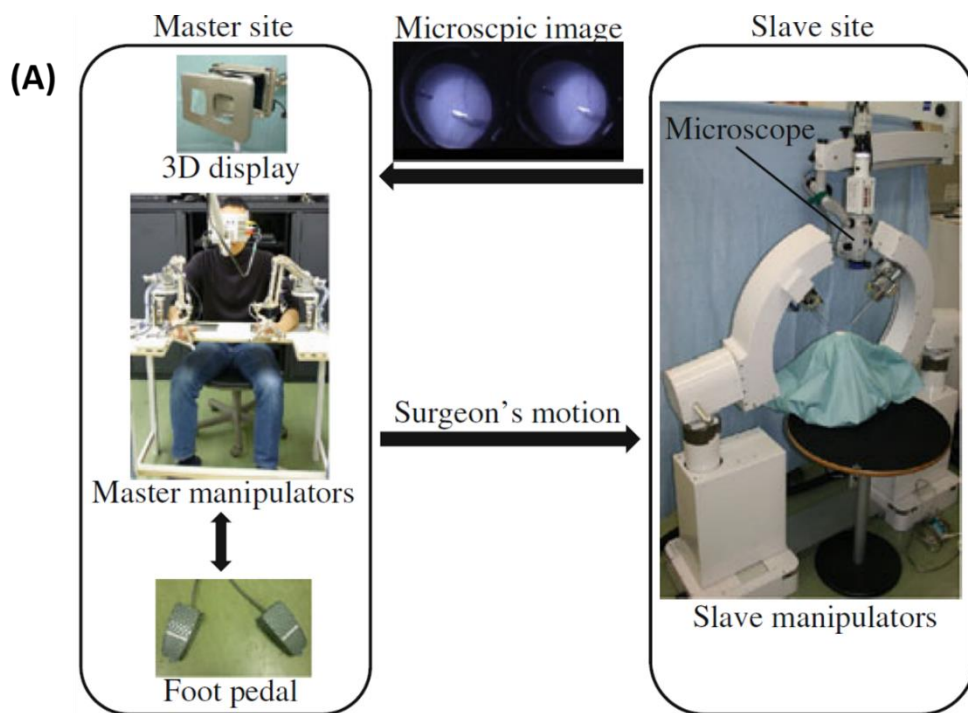


Figure 1.7. (A) system overview (B) Workspace [45].

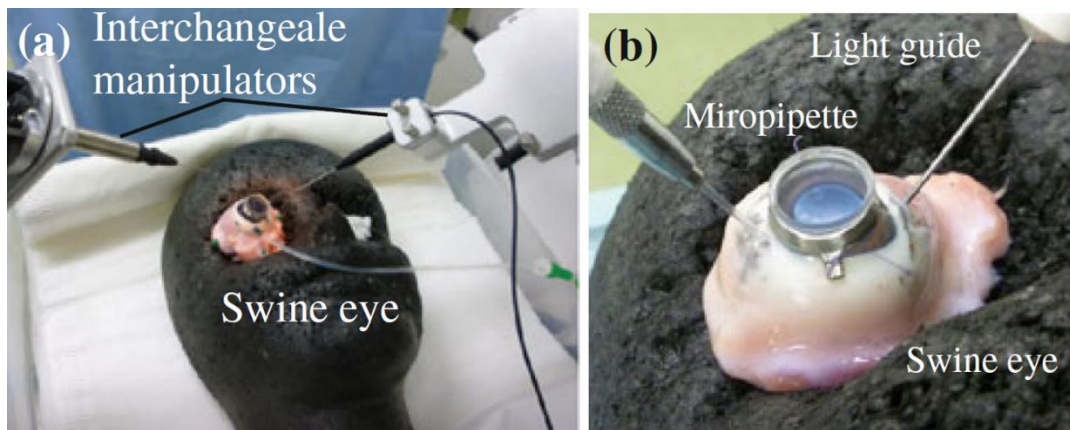


Figure 1.8. Ex vivo experiment: (a) experimental setup, (b) insertion of surgical tools into the eye [45].

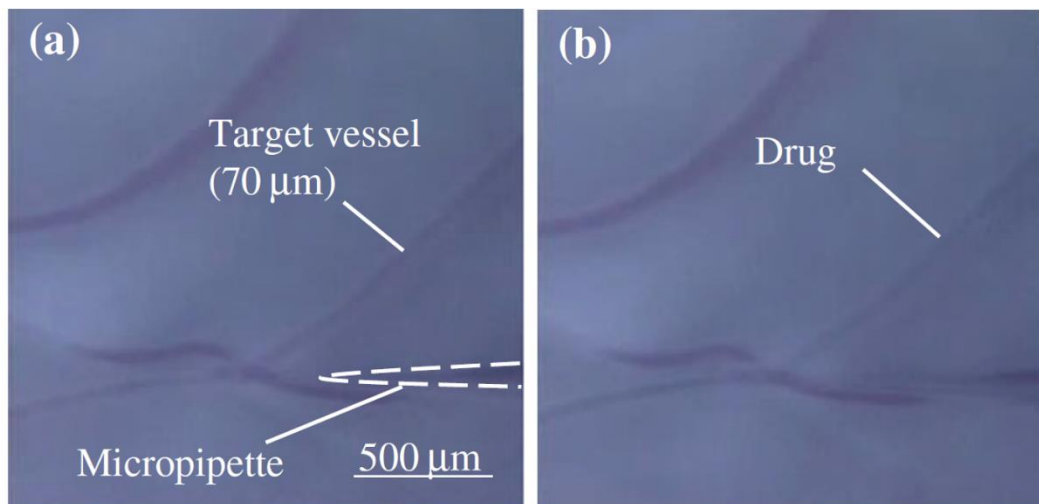


Figure 1.9. Result of microcannulation: a insertion of the tip, b drug being injected and replacing the blood [45].

Advances in materials science and micro-nanofabrication are significantly reinforcing the growth and progression of small-scale robots. Micro robots that are capable of navigation through complex environments such as human microvessels have emerged as a promising tool for vascular diseases. Ocular microrobots have the ability to change the way in which we remedy a variety of diseases at the anterior and the posterior segments of the eye.

In order to further the advantages of minimally invasive ophthalmic surgery, several researchers are developing smart miniature tools or robot-assisted devices that assist in ocular surgery and help overcome the limits of human performance due to their high precision. For the time being, micro robots can perform a number of tasks at small scales such as minimally invasive diagnostics, targeted drug delivery, and localized surgery ([figure 1.10A](#)) [46–51]. Recently, Kim et al. presented submillimeter-scale ferromagnetic soft continuum robots that can navigate through highly constrained environments based on active, omnidirectional steering upon magnetic actuation ([figure 1.10B](#)). Kim successfully developed the micro robot which has the capability of navigation through sinuous cerebrovascular with multiple aneurysms. The micro robot could enable a number of minimally invasive interventional procedures that are currently unavailable with existing techniques. In particular, the ability to access to hard-to-reach areas such as distal neurovasculature in a minimally invasive manner.

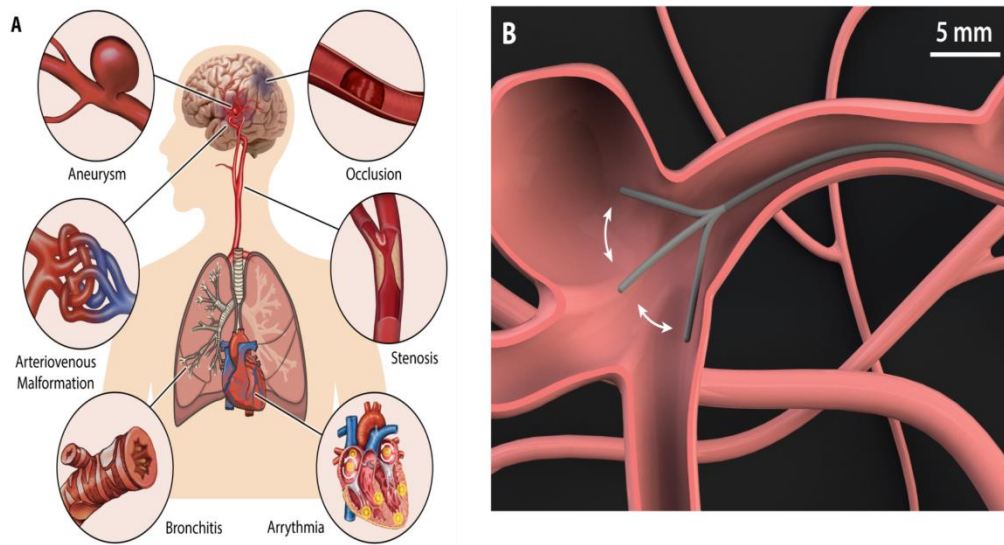


Figure 1.10. (A) Pathologic conditions in hard-to-reach areas across the human body where small-scale soft continuum robots with active steering and navigating capabilities have utility. (B) Illustration of the active steerability of a submillimeter-scale soft continuum robot navigating a complex vasculature with an aneurysm [51].

Now, the question is, how surgeons get well trained on different types of the precise surgeries, such as eye surgeries, which performed on tiny objects such as human microvessels, and how robotics systems are validated for using as assistant tools for surgeons in the operative room. Certainly, we cannot use these systems directly with actual patients for training the surgeons how they can use them or even for evaluation of its performance and accuracy. Therefore, similar to the high necessity for training the surgeons on performing different kinds of surgeries especially the most difficult and precise ones like eye surgeries, we need also to validate the surgical robotics system that involve in the surgery. Microsurgical robotics systems, which handle and manipulate tiny objects like human microvessels, need intense training and validation program. Abundant types of surgery simulation systems, which can be used for training surgeons on performing the surgery as well as evaluation of the robotics systems that used to assist the surgeons, have been developed. In the following sections we will discuss in details the different types of the training simulation systems.

### 1.3 Surgical simulation

Simulation has become widely accepted as a supplementary way of training. We can define the simulation as technique used to replace real experiences with guided experiences, often immersive in nature, that replicate substantial aspects of the factual world in a fully interactive manner [52]. Simulator devices are used as substitutes for real objects to educate individuals by imitating conditions in practical life [53]. Within this purpose and due to changes occur to the healthcare systems, a world of surgical simulation systems has arisen. The advantages of surgical simulation have been well established based on a full examination into its application as a surgical training modality [54–58]. The objective of surgical simulation systems is to permit the novice surgeons or even fully trained surgeons to earn the critical skills of a surgery outside the operation room and in a safe environment. Moreover, due to the rapid evolving of medical devices and the necessity for surgeons to become proficient with these technologies in shortened period of time, there has been an increasing demand for surgical training systems. The most conspicuous attribute of the simulation system is that it permits, among the many attributes of simulation, realization and repeated practice in a setting that boosts permission to fail and the chance to learn from one's mistakes. Additionally, the skills acquired from simulation-based training are directly transferred to the operative room. Therefore, to provide the finest quality care to patients, it is vital that surgeons are trained to the highest measures. Therefore, myriad of surgical simulation systems have been developed. In the next section we will discuss in details different types of surgical simulation system particularly for eye surgeries.

## 1.4 Classification of surgical simulation

Nowadays, wide range of surgical simulation devices and models exist. Surgical simulators can be classified based on the technology being used [59,60] or according to the varying complexity of the skill being simulated [61] as shown in [figure 1.11](#) [62]. Currently, a host of hospitals and medical schools have developed laboratory-based technical skills training courses where learners from a range of disciplines can practice their skills [63]. Surgical simulation allows the novices surgeons for the repetitive practice of the surgical procedures to allow them to develop their skills before get in touch with actual patients. Models of surgical simulation may be low or high fidelity, indicating the degree to which models are imitated to reality [64–67]. High fidelity is not always favoured to lower fidelity because this is dependent on the type of surgery and the level of the trainee. The degree of fidelity should correspond to the type of target surgery and training level. For example, a surgeon can get similar or higher skills for performing a kind of surgery by using a simple type of simulator whereas this is not the case with another type of surgery training that required high level of fidelity for the simulator. Therefore, despite the level of fidelity of the imitator, it can be very useful if it used in alignment with the training program goals. In the following subsections we will discuss the different forms of simulation models.



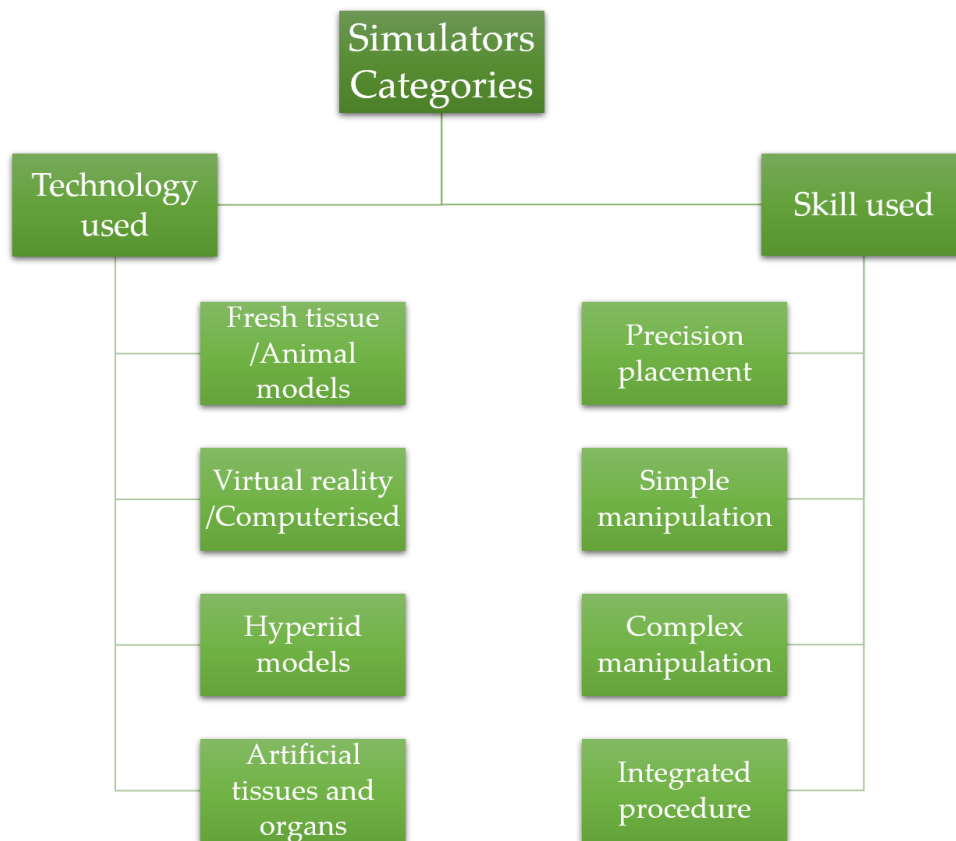


Figure 1.11. The various simulator categories [62].

### 1.4.1 Cadaveric models

Learning new surgical procedures and maintaining skills requires practice. A system that closely mimics the feel of a living human organ/tissue and also does not put patients at risk, for the purpose of practicing, is in high demand. Surgical simulation with cadaveric models consider the gold standard, before surgery on real patient, for surgical skills training [68]. This is because cadaveric models mostly mimic the anatomy of live patients. Cadaveric models used widely and appear popular with trainees [69–71]. However, this type of simulation is using dead tissues and thus cannot faithfully imitate all physiological conditions. Certain cadaveric surgical tissues create models of high-fidelity for vascular, microvascular and trauma surgery [72–75]. For instance, cadaveric tissue have, by utilized pressurized systems, used to simulate circulation of blood through the cadaveric tissues as shown on [figure 1.12](#) [72]. Borirak-chanyavat et al. used a cadaveric eye model for practicing different posterior and anterior segments eye surgeries as shown in [figure 1.13](#) [76]. Also, Sangita et al. presented an economical method for preparing cadaveric eyes for practicing anterior chamber angle surgical techniques [77]. He used the model for practicing technique of ab interno trabeculectomy using the trabectome system for treating open-angle glaucoma as shown in [figure 1.14](#). As well as various endoscopic and laparoscopic procedures, cadavers were used for training flap coverage techniques [78,79]. However, training using cadaveric models have limited availability because of practical and illegal difficulties of obtaining, storage, handling, and the logistics of surgical interventions that require significant funding to reproduce a relevant learning experience in an appropriate environment [68].

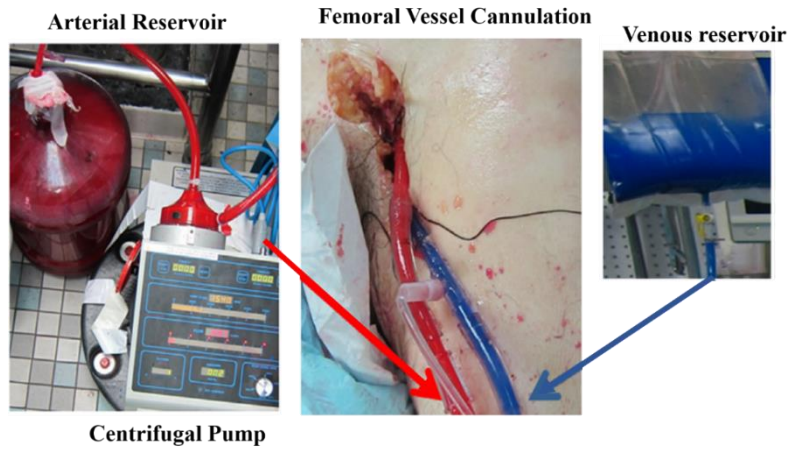


Figure 1.12. Pictorial demonstration of left femoral artery cannulation. Red and blue dyes are used for arterial and venous perfusion respectively. The arterial system is perfused using a centrifugal pump [72].

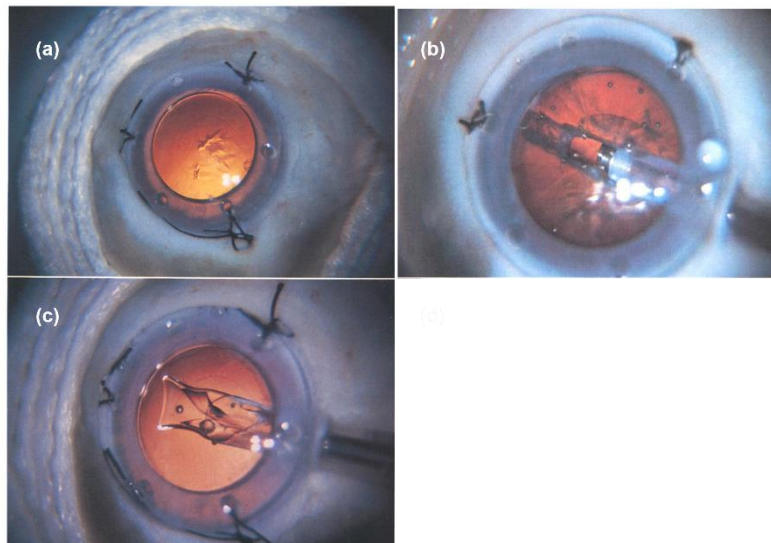


Figure 1.13. Practicing of different posterior and anterior segments eye surgeries with cadaveric eye model. (a). The continuous circular capsulorrhexis and a strong red reflex are evident. (b) A deep groove is phacoemulsified in the nucleus. (c) Injection of a foldable intraocular lens into the capsular bag. The capsulotomy margin can be clearly appreciated [76].



Figure 1.14. Trabectome (NeoMedix Inc, Tustin, California) handpiece approaching the trabecular meshwork viewed through a modified Swan-Jacobs gonioscopy lens in a prepared practice cadaveric eye [77].

### 1.4.2 Live animal models

Live animal surgery is an efficient type for the simulation of a surgery because they share several features of human surgeries. Live animals replicate the human surgery with high fidelity as they closely emulate the actual operative setting and provide non-patient environment which allow trainees to develop their skills required for the operative setting [80–83]. Because of the numerous benefits to working with live animals, animal models have been used extensively in ophthalmic surgery training [84–87] other forms of training, including endoscopic submucosal dissection, cholecystectomy and coronary bypass [88,89].

Porcine, canine, ovine, baboon, rat, and chicken embryos models are an examples of animals in use for training. Live rat models have been used for microsurgical skills training for many years [62,90] ([figure 1.15](#)). Chicken embryos often used in validation of robotics system assist surgeon in their task. [Figure 1.16](#) shows a chicken embryos used for validation of robot system for performing retinal microsurgery [39]. Ex vivo animal model is often used in surgical training, but provides simulation of lower-fidelity than live animals. Several research on the efficacy of these types of training have been performed and most have confirmed their use in enhancing technical skills and self-confidence [89,91,92]. The use of animals in medical research, however, has disadvantages. Firstly, the morphological differences between humans and animals' tissues. Secondly, surgical simulation using live animals needs access to large animal care facilities and veterinary personnel, which is costly [93].

Finally, animal models can be helpful for learning aseptic technique and suturing skills but less helpful for learning tissue handling, dissection, anaesthesia, or haemostasis [81].

Animal models provide accurate haptic feedback. However, the numbers of animals needed as well as cultural, and financial problems restrict their use as surgical simulation models. Additionally, ethical reservations have arisen over the use of animals as a model for surgical training. As a result, for instant, the UK prohibits the use of live animals for surgical simulation [88]. Thus, all above mentioned drawbacks, limit the use of live animal for surgical simulation for surgeons and robotics systems and lead out for finding other models for surgical simulation.



Figure 1.15. Microsurgical skills training using live rat model simulation [62].

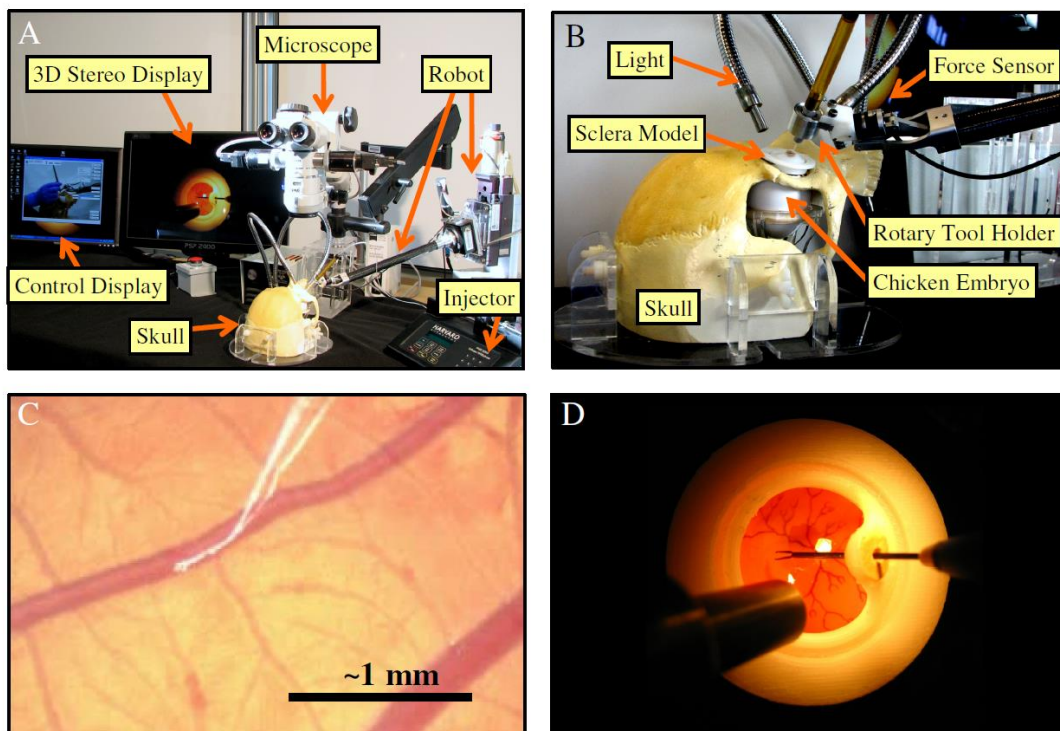


Figure 1.16. (A) Updated testbed (B) Close-up of the simulated operating area. (C) Bent tip pipette during cannulation (D) Sclera model with constrained instrument entry point and grasper tool [39].

### **1.4.3 Ex vivo animal tissue models**

Another form of surgical training is using anatomic sections or tissues from euthanized animals [94–96]. Such sections or tissues can be connected to synthetic frames that are designed to mimic human anatomy and can provide approximate haptic feedback. This kind of training system allows for organs to be prepared and frozen ready for use at a later time. While individual ex vivo models are limited in the variety of procedures for which they can be used, they may be useful as training tools for skills that require repetitive practice, as with some inanimate models [94]. The costs associated with this type of training are relatively low compared to live animal training, but employees are still expected to prepare the organs for simulation and to supervise and assess trainees [93]. Though data are beginning to emerge supporting the benefits of ex vivo stimulation, more evidence is needed to confirm that the use of this simulation model improves clinical outcomes [94]. Additionally, ex vivo models suffer from the same drawbacks that exist with live animal. Therefore, we still in need for alternative useful methods for surgical training and evaluation of the surgeons and assistant robotics systems.



#### 1.4.4 Virtual reality (computer-based) models

Virtual reality (VR) defined as the computer generated representation of an environment which allows sensory interaction thus giving the impression of actually being present [97–104]. Modern VR simulators produce realistic environments that capture minute anatomical details with high precision due to the power of computing and computer graphics [105]. Thus, VR imitators consider high fidelity models. The most appealing features of VR simulation is that it provides a real-time haptic feedback to trainees about their performance within the simulation, such as the time the users spent in completion of the task, the mistakes he did during the task, and the trainee's economy of movements [106,107]. Moreover, it lays a safe environment of training, and the possibility of repetition and practice. This makes it possible to map the performance of a trainee surgeon along the curriculum and define the attainment of dexterity. The goal is the acquisition of proficiency at early stage which result in reducing the learning curve with real patients.

Precious studies, which compare VR simulators with other simulators, have showed that they are useful in training novices in such procedures as eye surgery [41,108–111], upper endoscopy [93], haemostasis [112], flexible sigmoidoscopy [113,114] and colonoscopy [115,116]. Most of the technological emphasis in surgical VR simulators was on laparoscopic and endoscopic surgery, rather than open surgery [117,118]. The first commercially VR laparoscopic imitator was the minimally invasive surgical trainer-virtual reality system (MIST) [63]. With the MIST system, geometric shapes organs, that quite similar to those encountered in actual operations, generated for display on the screen and subsequently manipulated by the trainee as shown in [figure 1.17](#) [119]. Surgeons with VR systems can manipulate, clipped and cut tissues and can be incorporated into a recognizable simulation of Calot

triangle dissection, which bleeds and can respond to diathermy, as shown in [figure 1.18](#) and [figure 1.19](#) respectively [120].



Figure 1.17. Using the MIST system (Mentice Medical Simulation AB, Gothenburg, Sweden) for training and assessment of psychomotor skills for minimally invasive surgery [119].

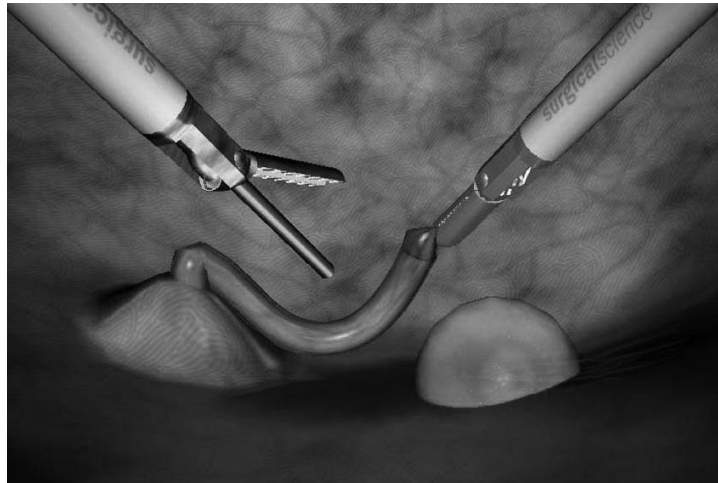


Figure 1.18. The “Cutting” task on the LapSim virtual reality simulator [120].

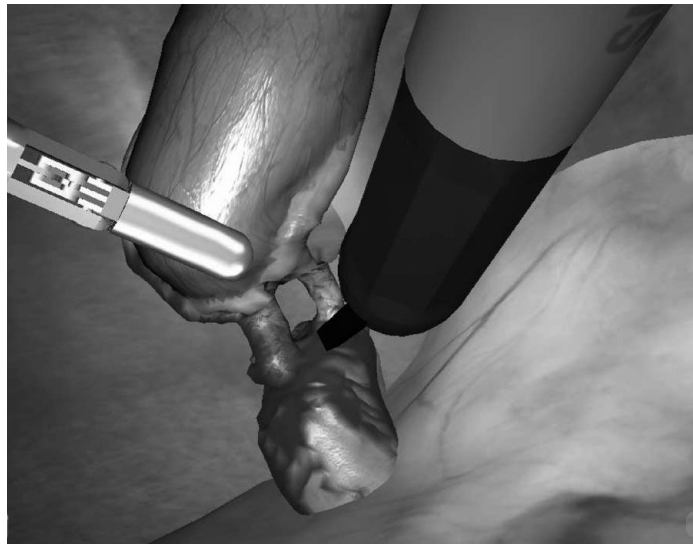


Figure 1.19. The “Dissection” task on the LapSim virtual reality laparoscopic simulator [120].

VR consider ideal model for training on surgeries which is complex. Ophthalmic surgery is one of the complex surgeries as it deals with a sensitive and small-scale size of tissues. Therefore, it needs high level of accuracy as any error during the surgery can result in irreversible damage. VR have been found to be superior for this kind of surgery [121]. VR system model of the eye and surrounding face within a virtual environment for use in eye surgical simulator has been developed, as shown in [figure 1.20](#), as a novel teaching method for surgeons without any risk to the patients [108]. Also, Verma et al. developed a VR system as a simulator for vitreoretinal surgery. Steps of vitreoretinal surgery successfully simulated with the developed system as shown in [figure 1.21](#) [100].

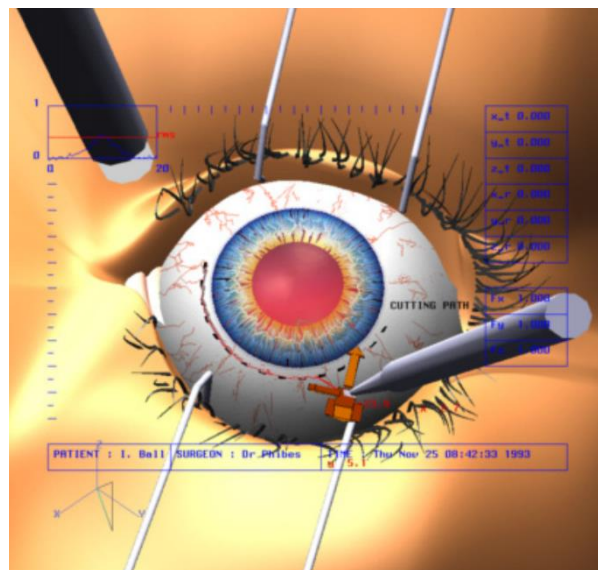


Figure 1.20. Surgical virtual environment including micro-tools and guidance information. The eyelids have been pulled back as they are during actual surgery. Superimposed on the image is additional information to guide the surgeon. The broken line around the cornea shows a planned cutting path [108].

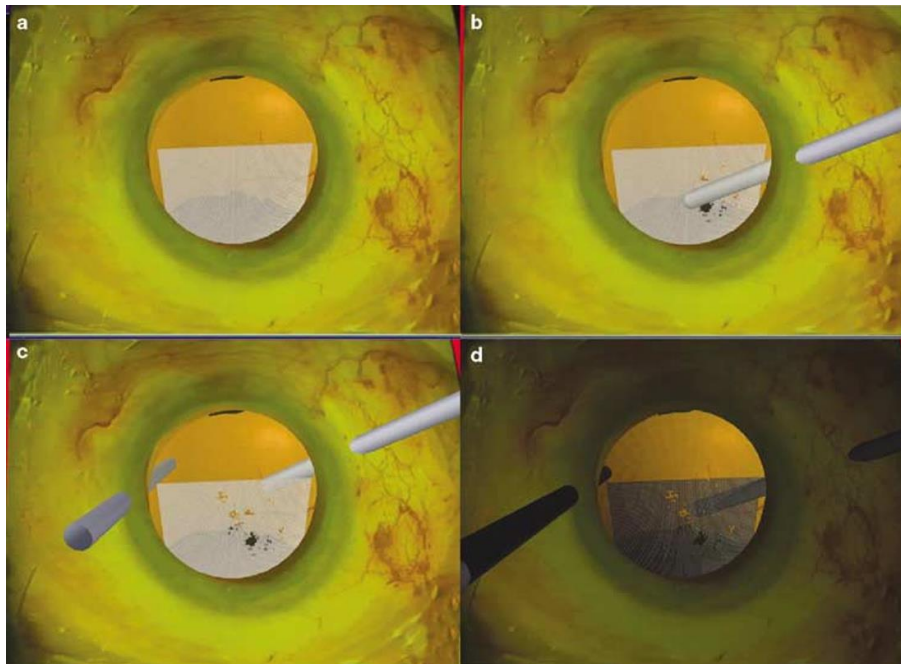


Figure 1.21. VR simulation of steps of vitreous surgery: (a) Simulation of vitreous opacity; (b) Insertion of active instrument with simulation of piecemeal removal of the opacity under direct illumination; (c) Insertion of passive instrument; (d) Removal of vitreous opacity with endo-illumination [100].

Human microvessels simulators which are a computer-based virtual reality simulators were introduced [122–125]. They developed VR system of 3D microvessel for the simulation of the minimally invasive surgery. The training system can provide the realistic virtual reality environment of microvessels according to patient's computed tomography images, in addition, allow unskilled doctors to drive a factual catheter for training courses directly and simulate surgeon's operating skills, insertion and rotation in real surgery. The 3D reconstruction images of the microvessels and the simulation of catheter inserting into the 3D vessel model are shown in [figure 1.22](#) and [figure 1.23](#) respectively [125].

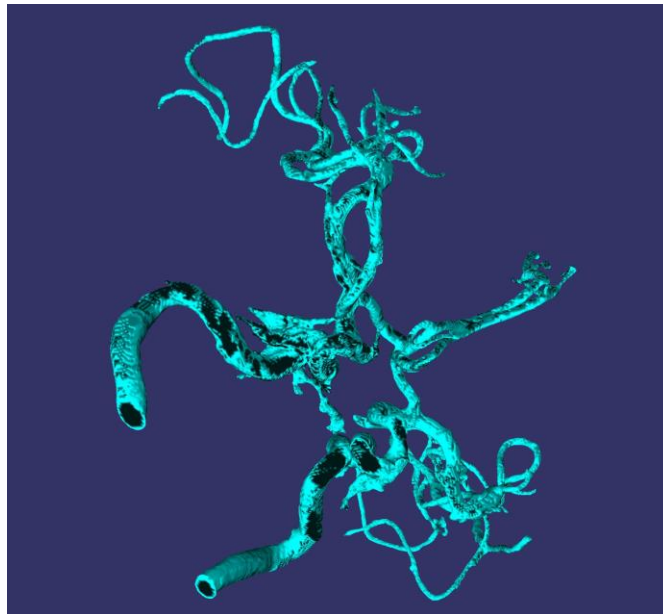


Figure 1.22. 3D reconstruction images of the blood vessels by open scene graph [125].

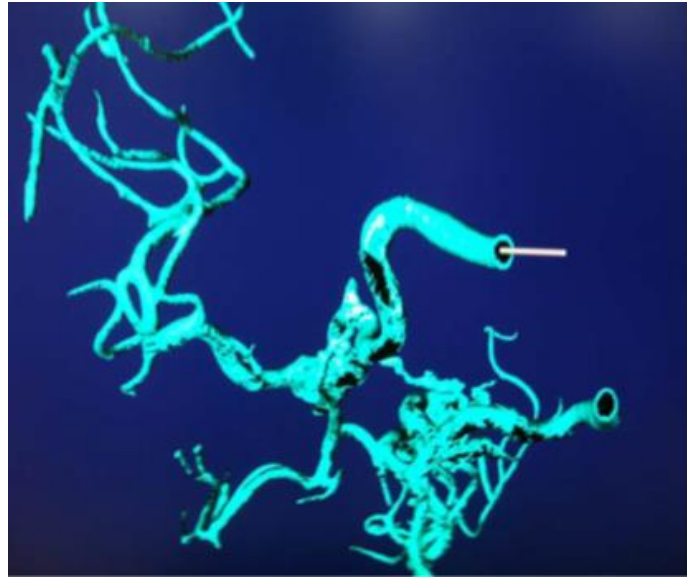


Figure 1.23. Simulation of catheter inserting into the vessel model [125].

In fact, VR offers a variety of benefits for surgeons. Surgeons can now use accurate recreations of individual patients' organs from high-resolution scanning data to practise patient specific operations within a virtual environment. However, it has some disadvantages. The key drawbacks of VR simulations entail high costs, lack of force-feedback, and minimal realism of some types of simulation [126]. Furthermore, VR simulators are not sufficient to assess new medical devices. This is because without the collection of large amounts of data, the effects of new medical technologies on the human body cannot be completely replicated. More the above, these simulations need expensive devices that are prone to technical failure and require regular calibration and maintenance. VR simulators are therefore not suitable for medical techniques assessment.

### 1.4.5 Artificial models

Simulation using physical objects made by synthetic materials to simulate tissues can offer medical doctors an opportunity to practice procedural steps and simultaneously obtain experience in the handling and manipulation of surgical tools ([figure 1.24](#) shows an example for the use of a synthetic models) [127]. Physical simulation models are used to create different organs and enable a trainee to perform specific tasks and procedures [93]. The artificial model has several advantages to other surgical simulators such as reproducing haptics of the actual surgery environment, no ethical problem, elaboration of structures and properties to the target organ. The progression of the artificial organ models was remarkable, and a lot of surgical simulators with the artificial organ were developed and commercialized [128–133]. For example, for eye surgery simulators, Mohan et al. developed a cost-effective, reusable practice eye model for epiretinal membrane peeling as shown in [figure 1.25](#) [134].

Artificial model has ample advantages such as it can be physically touched, enabling the user to learn the essential sensations of touch or texture. Moreover, selection of fitting materials allows the simulator to be sterilized and facilitates the reproduction of the effects of medical equipment on the human body. Thus, mock-up simulators can be used in actual operating rooms to train surgeons and assess the performance of assistant robotics systems.





Figure 1.24. Use of synthetic models. A resident uses a synthetic model to practice breast reconstruction at new York university langone health [127].



Figure 1.25. The practice eye model for membrane peeling [135].

#### 1.4.6 Summary

Surgical simulation-based training is appealing in the field of surgical training because it does not require the use of patients for skills practice, and is less reliant on supervising surgeons' time. Since the early 1990s, surgical simulation technologies have brought enormous change from mannequins and plastic bench-top sets to 3D printing and patient-specific VR systems. High demands on surgical training programs led to the review and use of alternative alternatives to training. Therefore, surgical simulators today are more realistic, collaborative, and versatile than in the past. The majority of models used for surgical training programs include synthetic models, virtual reality, live animals, and human cadavers, to simulate living human tissue and anatomy. Human cadavers are most closely approximate reality. However, the cost of the models and limited availability limit their use. Also, the use of living animals has many disadvantages such as the ethical concerns, high cost, and the necessity for specialized facilities. On the other hand, artificial models, made by synthetic materials, are cost effective, safe, reproducible, portable, and readily available. Thus, using of artificial models, for purpose of surgical training or evaluation of medical tools, considered as an ideal alternative method. In this thesis, we mainly focused on fabrication techniques and methods for artificial models of microscopic vessels which can contribute in the development of microvessels treatment and can be used as surgical simulator for training surgeons on different types of surgeries, especially the difficult kind of surgeries such as eye surgeries, or evaluation of medical devices.

## 1.5 Recent development of artificial surgical simulator

A host of studies reported the development of the surgical simulators and the majority of the fabricated models were fabricated based on stereolithography, FDM, or inkjet 3D printing technologies [135–140]. For example, the human skull, which consider a complex geometry and cannot be easily constructed in a physical model using cutting manufacturing methods, was fabricated by stereolithography, one of the 3D printing technologies, as shown in [figure 1.26](#) [132]. The fabricated 3D models provide a better understanding of the anatomy, facilitate the pre-surgical simulation and improve the education of trainees [141].

Artificial models are not used solely in the pre-surgical phase. They can also be used in real surgery, during which, 3D models are utilized to guide the surgeons through the operation, confirming accuracy and quality of the results. Previous reports examined the potential of using 3D printing models of the patient for planning and rehearsing the target surgery [142,143]. They were endeavoring to simplify and enhance the accuracy of the practice of stereotactic surgery, a minimally invasive form of surgical intervention which uses 3D coordinates to locate specific targets and perform them on an operation such as removal, implantation or injection. They found significant advantages in using 3D printing models in terms of speed, simplicity, accuracy, and versatility but with the extra cost and time that required for the fabrication of the models. In the following subsections we will discuss the development and progress artificial eye surgical simulators equipped with 3D microchannel, particularly 3D microchannel that simulates human vessel, developed by different fabrication techniques, for different types of surgeries, such as eye

surgeries, and the limitations in the models due to the current limitations in the used fabrication technique.

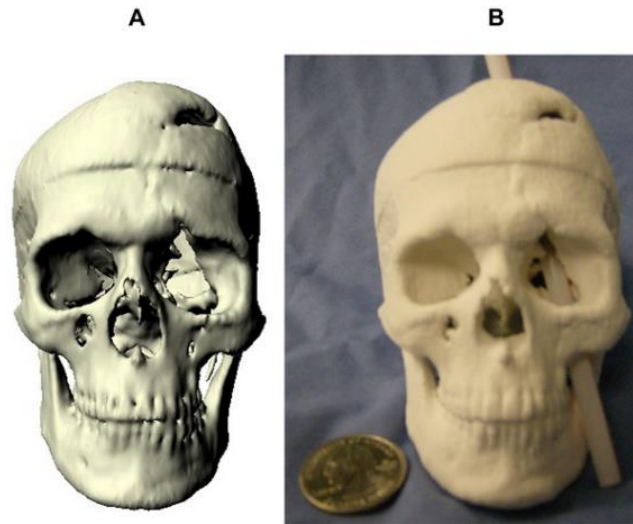


Figure 1.26. Stereolithograph of human Skull. A. Virtual model of the skull. B. Physical 3D model [115].

### 1.5.1 Surgical simulator for cardiac applications

Recently, Yoo et al. introduced a cardiac model with congenital heart disease by using 3D printing technology [144]. The developed models were used number of professional and novice surgeons to perform the target surgical procedures ([figure 1.27a](#)). Kiraly et al. provided another example of a versatile hollow heart model with a congenital defect ([figure 1.27 b,c](#)) [145]. The surgeons used the developed model to direct the arch repair surgical method at each stage of the procedure ([figure 1.27 b](#)). The patient surgery ([figure 1.27c](#)) was conducted after preoperative training on the 3D printed model, resulting in increased patient safety and, eventually, the probability of a positive outcome of the surgery. Yoo et al. also developed congenital heart surgery model with 3D printing models [146]. The model made from flexible rubber-like materials. [Figure 1.28](#) and [figure 1.29](#) show the printed model and series of surgical procedures on the model respectively.

All responders that tested the above-mentioned models place a feedback that the models are helpful in improving the surgical skills required for the target surgery. However, they also reported that the consistency and elasticity of the models' material were different from those of the human tissues. Therefore, further improvements and solutions, for mimicking the demeanor of the materials of the artificial models with human tissues, are required.

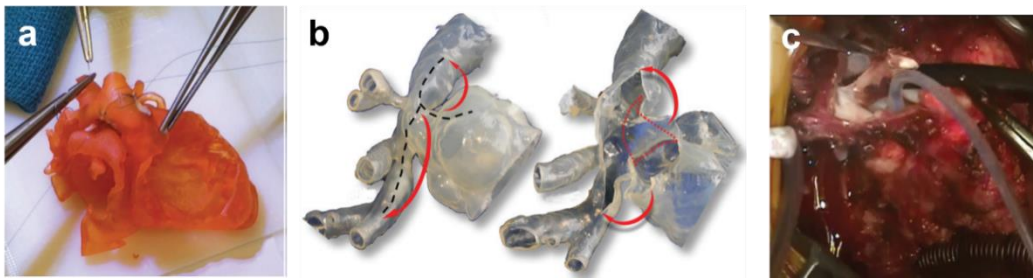


Figure 1.27. A 3D printed cardiac model with a congenital defect [144,145].

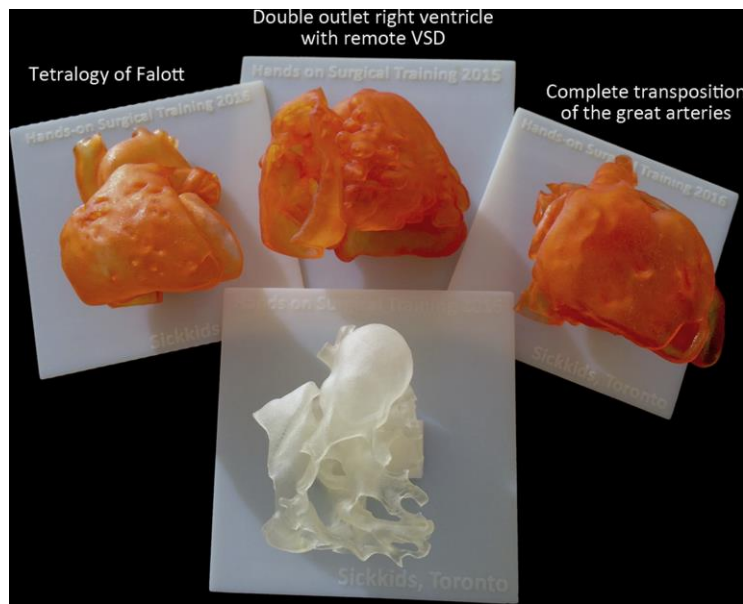


Figure 1.28. Four example models for surgical simulation. Colored model is preferred to white or light beige-colored model. Slightly dark color improves the perception of complex surface anatomy [146].

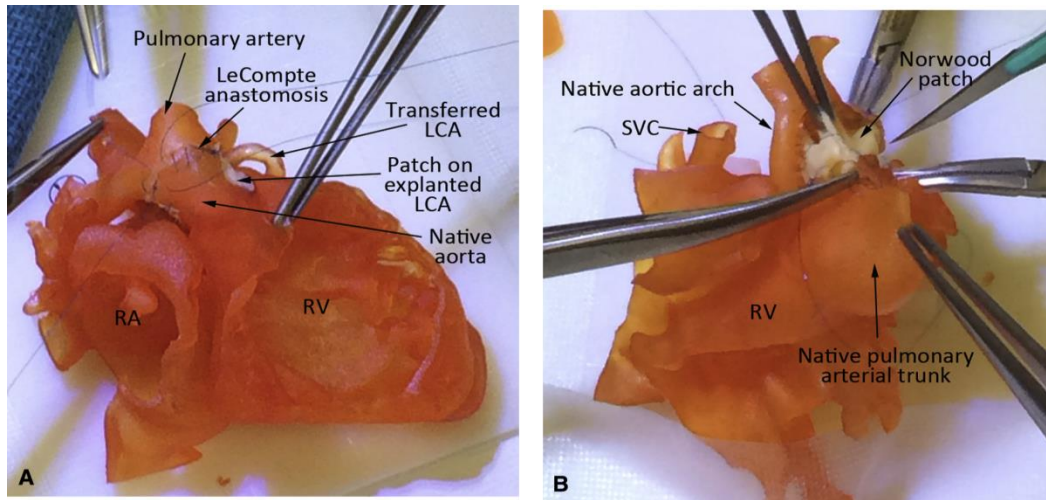


Figure 1.29. Scenes of surgical procedures on the models. A, Arterial switch operation in complete transposition of the great arteries. B, Norwood operation in hypoplastic left heart syndrome with aortic atresia [149]. LCA, Left coronary artery; RA, right atrium; RV, right ventricle; SVC, superior vena cava.

### 1.5.2 Surgical simulator for urology applications

In the field of urology, Bernhard et al. used also 3D printing technology to fabricate 3D physical model of kidney and tumour anatomy, as shown in [figure 1.30](#), as a useful tool for patient education [147]. The proposed model demonstrated an improvement in the knowledge and understanding of pre-surgical kidney tumor and the surgery for patients. This was the first experience with 3D printing models for improving the knowledge for the patients about their diseases.

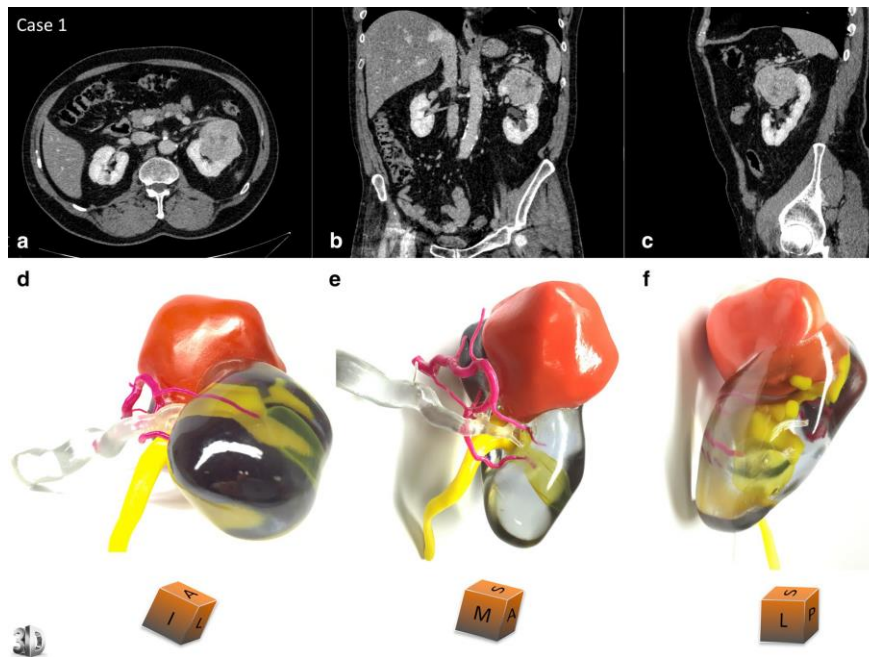


Figure 1.30. 3D printed model for kidney with tumor anatomy. Comparative views of the CT scan at the nephrographic phase (**a** axial, **b** coronal and **c** sagittal planes) and corresponding views of the physical model (**d** superior and median view, **e** median and anterior view, **f** lateral view). An inferior polar cyst is also displayed on this model (translucent yellow). The cubes show the 3D printed model orientation in space [147].



Wake et al. 3D printed a patient-specific, cancerous kidney model with detailed anatomy using a transparent flexible material for the application of urological oncology [148]. Such tumor-sected kidney models allowed surgeons to determine the nature of the tumor and its spatial relationship with other parts of the organ, allowing operational preparation for partial nephrectomy or ablative therapy. In addition, the model was used in the case of realistic surgery to assist surgeons in choosing a partial nephrectomy solution as well as resection guidance during surgery. Through the PolyJet printing process, Kusaka et al. also printed a kidney graft and pelvic cavity model using the tango family of photopolymers with different colors as shown in [figure 1.32](#) [149]. The model has been applied successfully for preoperative planning and accurate simulation of the kidney transplant surgical procedure. The main disadvantage of the fabricated models is, as we mentioned previously, the difference of the mechanical characteristics of materials, used in fabrication of the models, with the mechanical properties of human tissues.

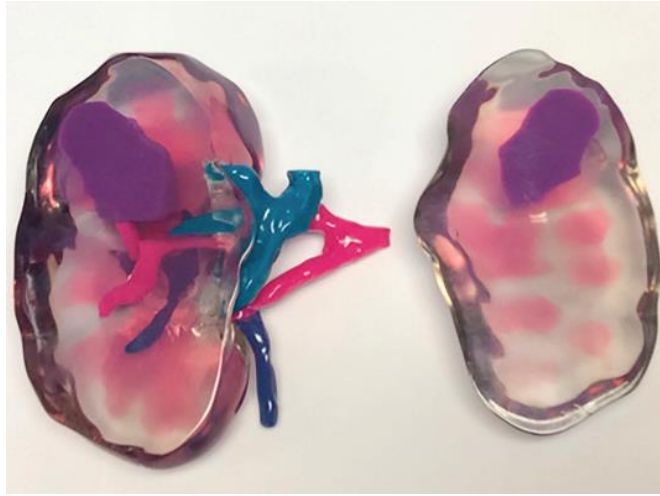


Figure 1.31. A 3D printed kidney model using flexible material as the kidney's main cortex showing the relative position of the renal tumor with respect to the renal artery, vein, and collecting system [148].



Figure 1.32. The 3-D printed donor organ kidney replicas allowed for the creation of translucent models showing the visceral organs, vessels, and other details [149].

### **1.5.3 Surgical simulator of vascular system**

The vascular system is a system that intermediate the transfer of solutes, such as metabolites, waste products and signals, and cells, such as leukocytes, through the body. These living pipes have a central role in the regulation of metabolic activity, development, healing, immune response and the progression of many diseases. Vascular diseases, which comprise any condition that affects the circulatory system such as cardiovascular, and cerebrovascular diseases, are the second highest cause of death worldwide. For therapy of human vascular disease, there are researches of surgeries on human vessels through thin devices called catheters. Catheters are medical devices that can be inserted in the body to treat diseases or perform a surgical procedure, are vary in size and used on treatment of variety of diseases. However, the small diameter of human vessels, such as retinal vessels and capillary vessels, makes the procedure, of using catheters or similar devices, arduous. Furthermore, the length and flexibility of catheters, as well as their limited number of degrees of freedom, may severely lessen the surgeon's visual and tactile perception when manipulating these tools during the treatment. Therefore, to solve this problem, many researches from the other approaches proposed such as surgical simulators for rehearsal, practice and evaluation of real surgical operation and for evaluation of medical tools as well. Thus, development of reliable models of the normal and pathological vascular system, which work as surgical simulator of human vessel, is highly demanded to allow practicing and evaluation of real operation as well as in vitro research activities such as development and evaluation of new vascular imaging and endovascular therapeutical methods.

Emulating human vessel is of considerable interest for emerging applications including tissue engineering [150–153], organ printing [154,155], microfluidics [156,157], and biomedical devices [158]. Numerous studies have been discussed the fabrication techniques for fabrication of simulators for various types of human vessels which can be a valuable tool for a vast range of applications, such as diagnoses, surgical training prior to practical operation and experimental investigations [159–162]. Traditionally, the superior training environments on which to learn the anatomic–pathologic and therapeutic techniques have been animals or actual patients. Due to ethic problems and individuals’ differences between human and animal’s tissues, the development of alternative models are required.

Several studies have been published discussing the different types of human vessel simulators made from artificial materials simulating endovascular intervention. For large scale vessels, i.e. mm scale, such as the coronary artery, cerebral arteries, and carotid arteries, with the benefit of rapid prototyping technology, an in vitro model of the human cerebral arteries based on CT images, for the simulation of endovascular intervention, presented as shown in [figure 1.33](#) [163]. The model made of soft and transparent silicone elastomer calibrated in shape and curvatures to mimic the human vasculature and has a physical property quite similar to the actual vascular tissue.

Queijo et al. also through the rapid prototyping technique known as tridimensional printing combined with polydimensiloxane casting technique made a polydimensiloxane anatomically a carotid arteries model with and

without aneurysm [164]. [Figure 1.34](#) shows the main steps to make human artery model. Queijo et al. proposed this model to be a promising tool to perform in vitro blood flow studies through anatomically realistic replica of a human carotid artery with and without aneurisms.

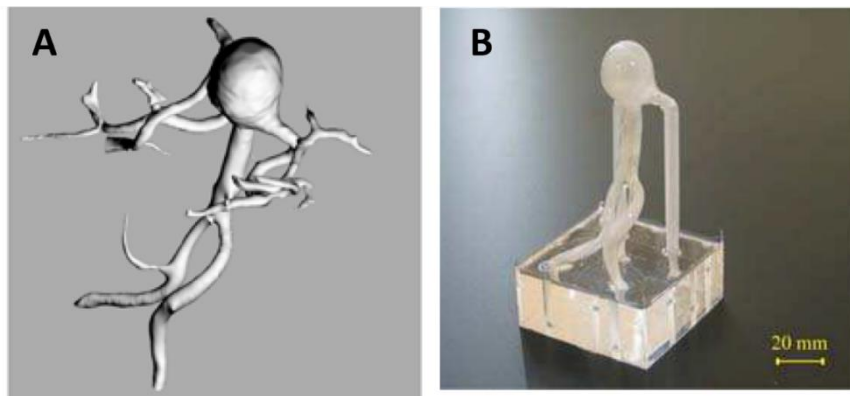


Figure 1.33. (A) 3-D structure of basilar tip artery with giant aneurysm reconstructed with CT angiography. (B) An in vitro patient-tailored biological model of human cerebral artery with vasculature-like thin uniform membranous configuration [163].

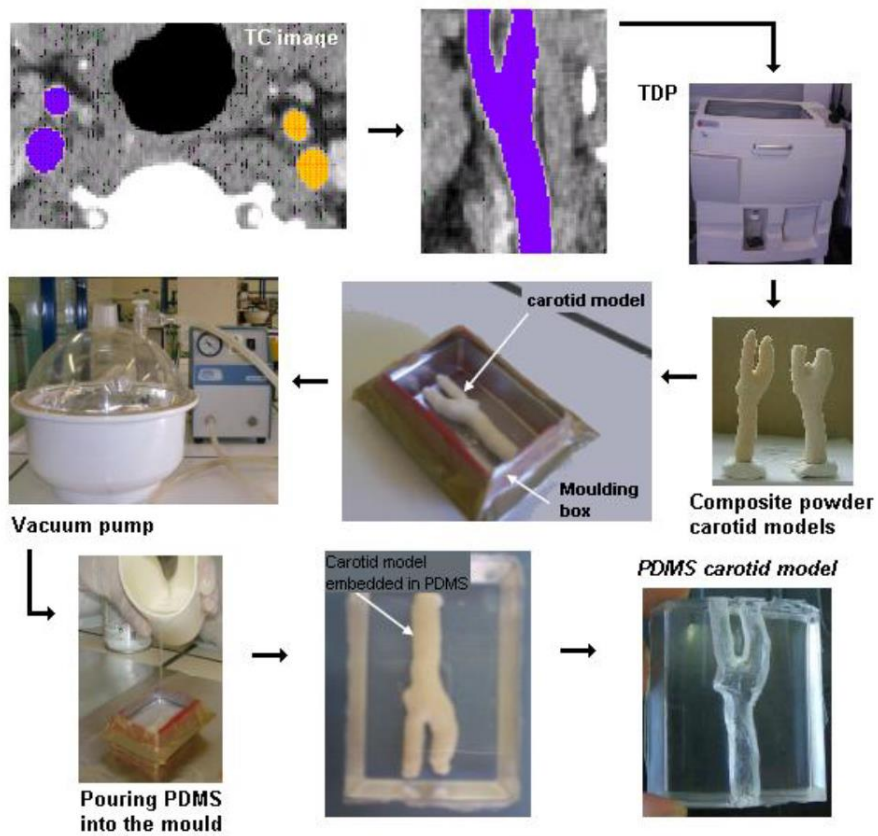


Figure 1.34. Main steps to manufacture PDMS in vitro models of human artery vessels [164].

For the simulation of minimally invasive intervention of aortic aneurysm, Torres et al. developed an endovascular aneurysm repair (EVAR) simulation system using 3D printed aneurysms. The proposed model used for training vascular surgery residents on EVAR to investigate the impact of the training on the real surgery performance [165]. By using 3D printing technology EVAR simulation system developed and the process of 3D printing of the model is shown in figure 1.35 [135]. Kaneko et al. also produced patient-specific vascular replicas for endovascular simulation using fast, a low-cost method [166]. The fabrication process of the model with low cost desktop 3D printer is shown at figure 1.36.

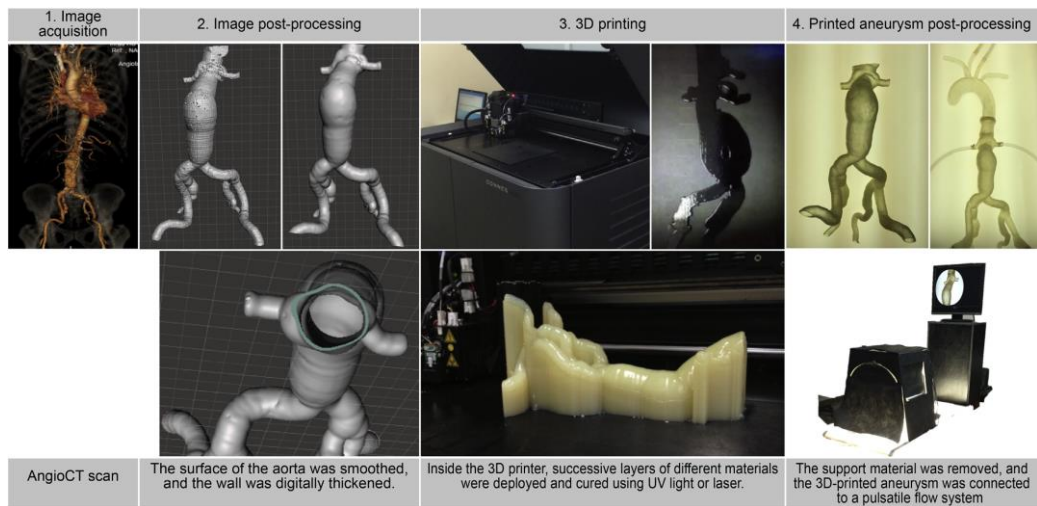


Figure 1.35. Steps taken in producing a three dimensionally printed aneurysm [135].

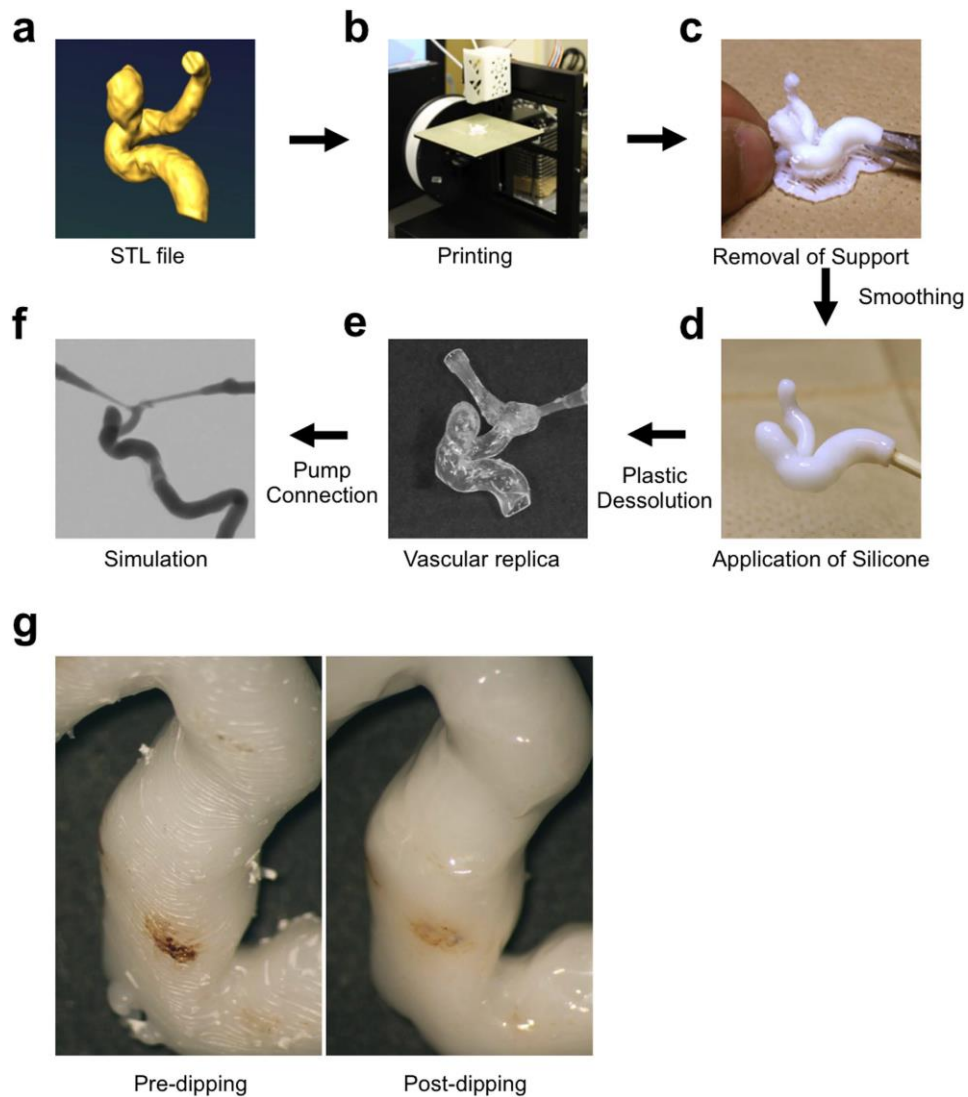


Figure 1.36. Manufacturing process of patient-specific vessel simulator. (a) Data is obtained by CT and converted to an STL file. (b) The STL file is exported and the acrylonitrile butadiene styrene (ABS) vascular model is printed using the 3D printer. (c) The ABS solid model and supports are removed with nippers. The surface is smoothed by dipping into ABS solvent and then dried. (d) The solid ABS model is coated with liquid silicone. (e) The ABS is dissolved in acetone after the silicone solidifies. (f) The silicone vessel is connected to a circulation pump and the simulation is performed. (g) The surface of the ABS vessel model is smoothed by ABS solvent. Left: Before dipping in the ABS solvent, Right: After dipping in the ABS solvent [166].



For a fine small human microvessel model with diameter 500  $\mu\text{m}$ , S. Ikeda et al. proposed a surgical simulator (Endo Vascular Evaluator) having 3D microvessels models that are tailor-made using ink-jet rapid prototyping with wax as shown in figure 1.37 [159]. However, it is very laborious to fabricate 3D microchannel, which simulate human microvessel, with diameter smaller than 500  $\mu\text{m}$  due to the brittleness of wax.

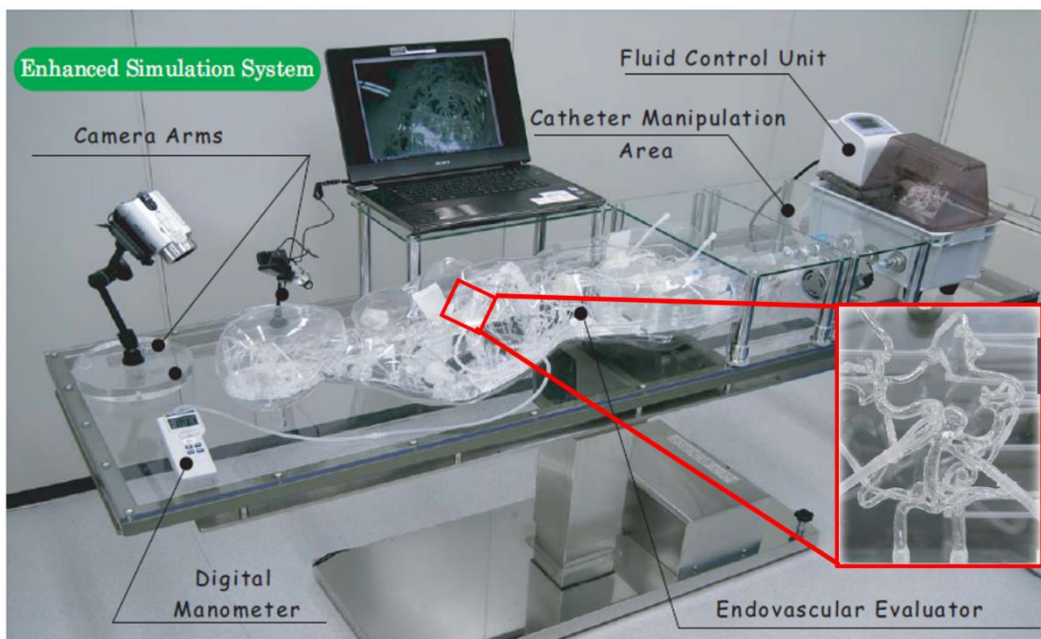


Figure 1.37. Endo Vascular Evaluator surgical simulator [159].

3D printing technology enables us from making 3D model of human microvessel model as training model for different type of minimally invasive intervention with reasonable price comparing to the cost of VR systems and provide the surgeons with the physical sensation and touch of the model which was also not available with VR systems [167,168]. However, the methods used for fabrication of 3D microchannel that represent human micorvessel have difficulties in fabrication of human vessels with smaller sizes, such as retinal microvessels ( $\leq 100 \mu\text{m}$ ) or such as the size of capillary vessels ( $\leq 10 \mu\text{m}$ ). Therefore, 3D models that represent narrower vessel models are needed.

For a fine small human microvessel model with small diameter ( $\leq 10 \mu\text{m}$ ), T. Nakano et al. fabricated a 3D microchannel that mimics a fine microvessel with sizes up to about  $10 \mu\text{m}$  using photolithography techniques and polymers molding [161]. Nakano et al. proposed multiscale fabrication methods for microvessels models as described in [figure 1.38](#). Overexposure, reflow, grayscale lithography, and ink-jet rapid prototyping using a layer stack molding machine were the fabrication methods for the blood vessel models. Micorvessel models with diameter size of  $10 \mu\text{m}$  are fabricated by the overexposure method, whereas arteriole models with  $20\text{--}100 \mu\text{m}$  in diameter and arteriole models with diameter of  $100\text{--}500 \mu\text{m}$  were fabricated with reflow and grayscale lithography methods respectively. The fabricated multiscale microvessel model is shown at [figure 1.39](#). Tanaka et al. also used photolithography techniques to develop a 3D microchannel that simulate

retinal veins and used as surgical simulator for microcannulation surgery [162]. The fabricated 3D microchannel, which is shown in [figure 1.40](#), placed on the bottom of an eye model, which is shown in [figure 1.41](#), to represent the retinal vein that have a diameter range of 60-90  $\mu\text{m}$  for assessment of manual and robotic microcannulation for eye surgery as shown in [figure 1.42](#).

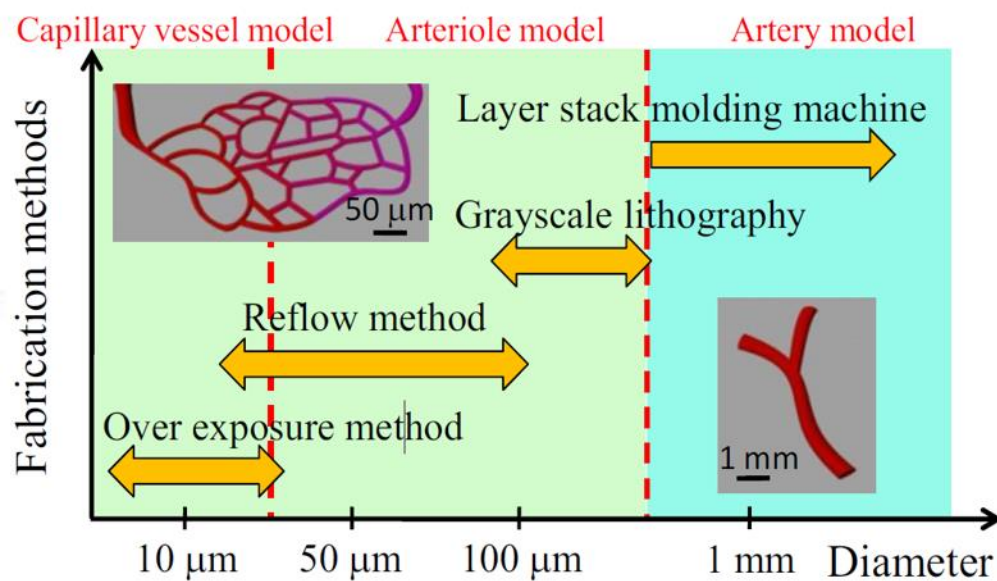


Figure 1.38. Concept of multiscale fabrication for transparent microvessel models [161].

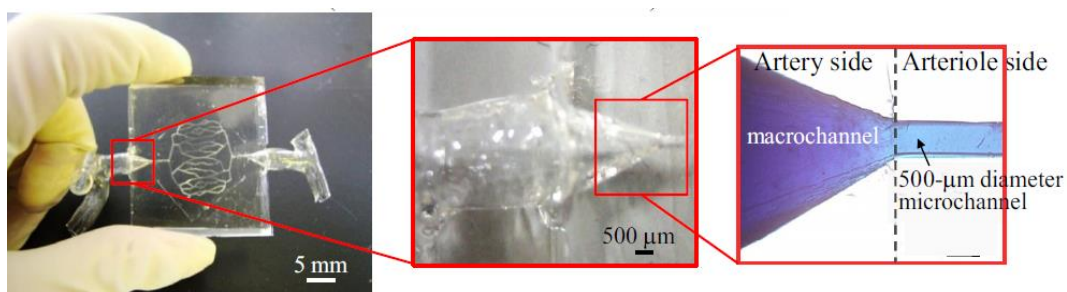


Figure 1.39. The fabricated circulation model [161].

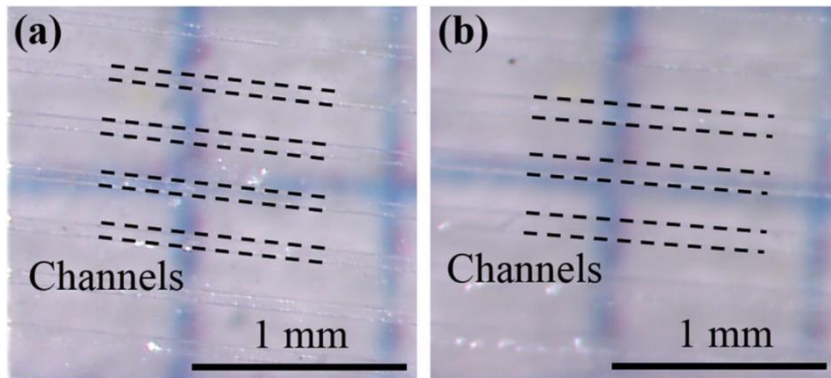


Figure 1.40. Artificial retinal vein model: (a) 60  $\mu\text{m}$  (pitch 200  $\mu\text{m}$ ); (b) 90  $\mu\text{m}$  (pitch 200  $\mu\text{m}$ ) [162].

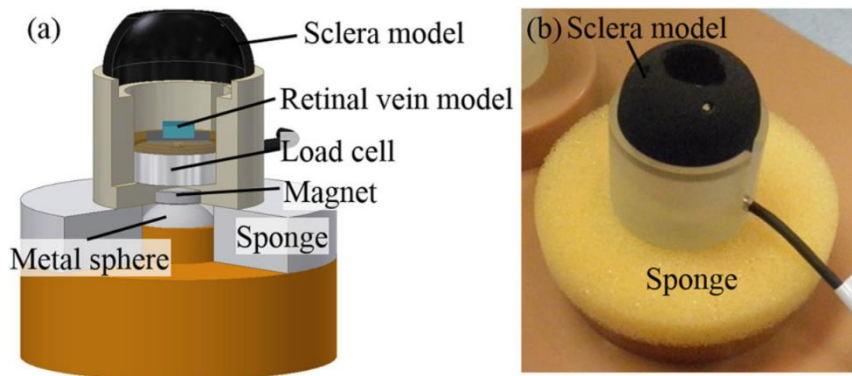


Figure 1.41 The experimental set-ups for manual and robotic microcannulation : (a) for manual operation; (b) for robotic operation (b1, master manipulator; b2, slave manipulator) [162].

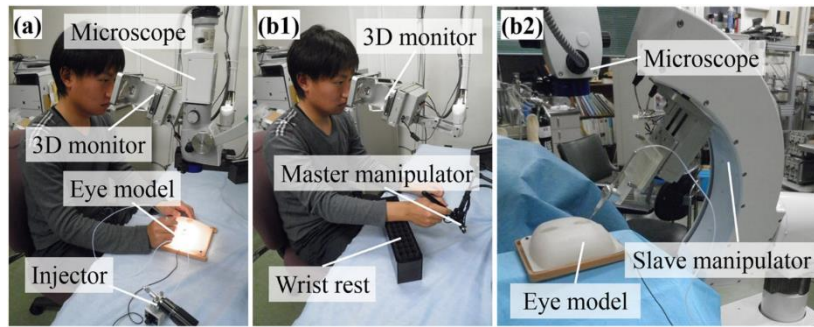


Figure 1.42. Eye model: (a) sectional view; (b) fabricated model [162].

Although the proposed method, photolithography, to fabricate human microvessel models has sufficient resolution to make it possible to achieve human microvessel model with diameter size of 10  $\mu\text{m}$ , the model is still limited to two-dimensional structure. In reality, human microvessels are 3D structure, therefore to mimic the true human microvessel we need further development of the current models to make them in 3D structure. In this study, one of our aims is to propose different methods for fabrication of 3D microvessel models, with adequate size resolution to mimic the human microvessels. The proposed 3D microchannel, which represent human microvessel, could be used as surgical simulator for human microvessel for training surgeons on different type of surgeries such as eye surgeries and also could be used for other application such as microfluidics device for biomedical applications.

#### 1.5.4 Summary

Artificial 3D models have been beneficial for surgical planning and rehearsal. However, the models still suffer from many disadvantages such as: (1) the developed models have been made from materials with mechanical characteristics, such as stiffness and hardness, are different from mechanical characteristics of factual organs/tissues. To give surgeons and trainees the same sensation they encountered in tasks such as suturing, severing, and dissecting in real surgery, artificial models should mimic the actual organs/tissues in their mechanical characteristics. Additionally, due to the differences between artificial and real organs/tissues in their mechanical properties, we cannot use these models to predict the physical demeanor of the organs/tissues throughout surgical handling, including deformation and reaction forces. (2) The current artificial model also lacks of embedded devices that could provide a feedback form the artificial models, such as the applied force to the synthetic model, to the surgeons. This feature is important to aid in evaluation of the performed tasks from the trainees.

For the human microvessel models, above the mentioned disadvantages, the current models, which simulate human vessel, at the small scale (smaller than 10  $\mu\text{m}$ ) are still limited to 2D structures. However, human microvessels are 3D structures. Therefore, rapid fabrication methods, that can be used to fabricate microvessel models in 3D structure with materials mimic the mechanical properties of the target section of human vessels, are highly required.

## **1.6 Thesis overview**

### **1.6.1 Research objectives**

As we described above, surgical simulator is a pivotal tool for training unexperienced and even expert doctors for different sort of surgeries and for evaluation of medical equipment as well. However, the current synthetic models lack several properties such as anatomical fidelity and repeatability, in addition methods used for fabrication of artificial models suffer from several disadvantages such as complexity and expensive of the process. In this research we aim to propose simple fabrication methods for fabrication of 3D microchannel, which simulate human microvessel, and can be used for a variety of applications such as surgical training model or evaluation of medical devices. Additionally, we developed an eye model, consists of 3D microchannel that represent human micro tube named schlemm's canal, sclera with clear cornea, and trabecular meshwork as a surgical training simulator for glaucoma surgery.

### **1.6.2 Outline of the dissertation**

This dissertation consists of five chapters as illustrated in [figure 1.43](#).

**Chapter 1** gives the background and motivation for this study and describe the aims of the research. We also discuss the recent developments and progress of artificial surgical training simulators, particularly eye and vascular surgical simulators, made from synthetic materials, and the different technologies and fabrication techniques used for fabrication of these models with their advantages and limitations.

**Chapter 2** discusses the concept of eye surgical training simulator with previous achievements that made by our group and our target goals in this study

**Chapter 3** demonstrates the fabrication methods used to fabricate 3D microchannel that mimic human microvessel and work as surgical training simulator for different kind of surgeries. In this chapter, we proposed two different methods for fabrication of 3D microchannel. First, we proposed fabrication method for creation of 3D microchannel which has rectangular cross section. Secondly, we proposed another method for fabrication of 3D microchannel with circular cross section. Based on the target surgery or application, we can choose between the two methods for the fabrication for the model of the 3D microchannel.

**Chapter 4** demonstrates an eye model that was fabricated as surgical training simulator for the glaucoma surgery. An eye model consists of a sclera with a clear cornea and 3D microchannel, which represent SC, and TM was built. The methods that used for fabrication of the model are versatile because they replicate anatomical details with submillimeter resolution and permit a wide range of materials to be used.

**Chapter 5** summarizes our findings and discusses the future directions of our research.



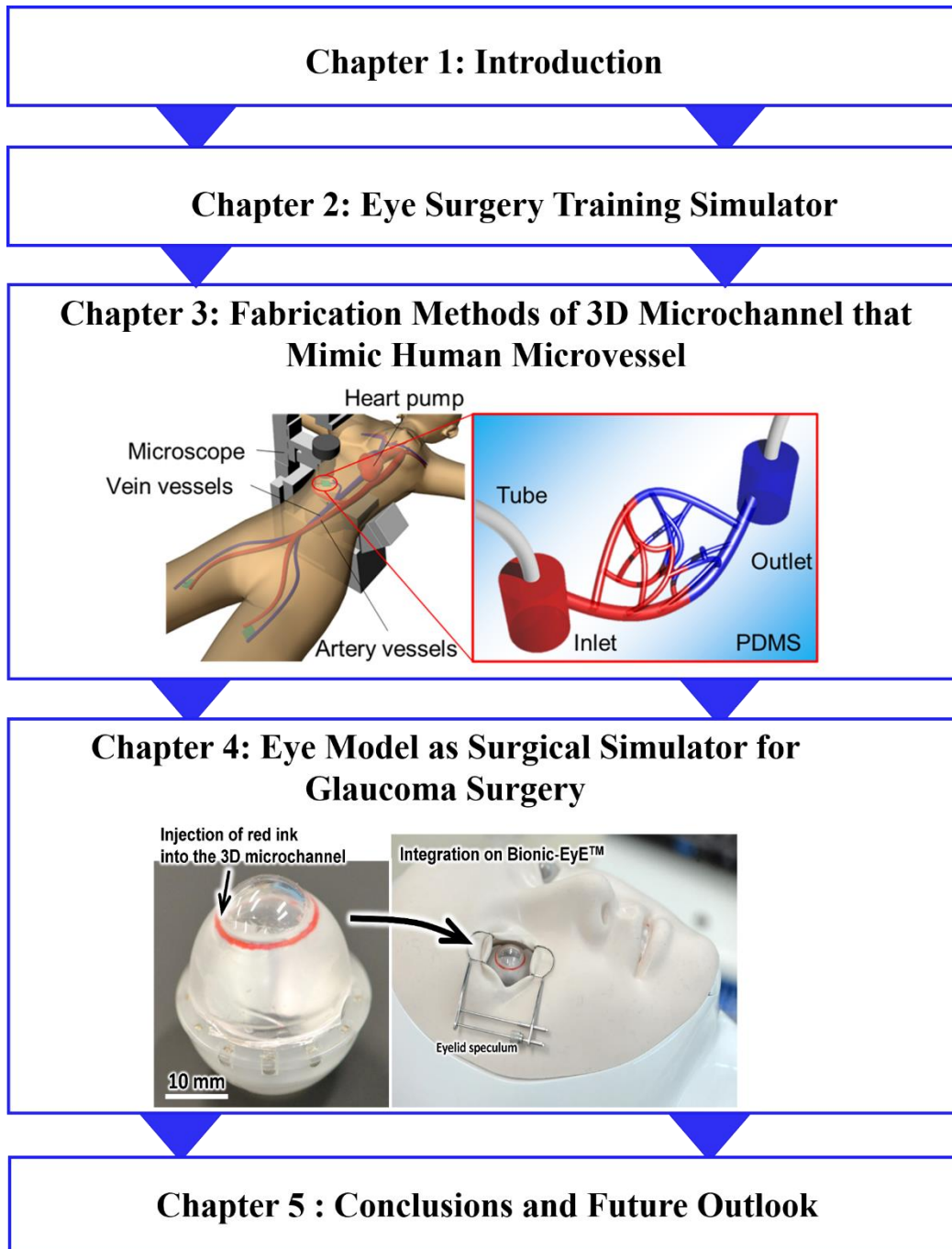


Figure 1.43. Outline of the dissertation.

## CHAPTER 2

### Eye Surgery Training Simulator

#### 2.1 Introduction

Surgeons are like pilots, as both undergo immense training before starting work in the real environment. While pilots have simulators that allow them to spend hours of training in a realistic environment and consequently reducing flight accidents, there really is no lifelike equivalent for surgeons. Therefore, provide an opportunity for surgeons to practice full procedures of surgeries and to keep their skills sharp and learn new surgical technologies is highly demand. Thus, an elaborate patients simulators is necessary. Our group aim to introduce an elaborate human model, we gave it the name 'Bionic Humanoid' which is a well-mimicked human model that can be utilized as surgical training simulator for many different types of surgeries and can be used for evaluation of medical equipment as well.

## 2.2 Bionic Humanoid

We proposed the Bionic humanoid, as shown in [figure 2.1](#), which is a well- mimicked human model consists of many artificial organs such as eye, brain, bone, vascular system, and so on, as a surgical training simulator for training novice surgeons or even experts to earn the skills needed for a target surgery. Bionic humanoid is expected to mimic shape and physical properties of a human, and is also integrated with sensors for quantitative evaluation of surgeon skills to serve as a substitute for humans and test animals. To do so, bionic humanoid needs to satisfy a certain specifications such as anatomical fidelity, shape, and physical properties. The current development process we designated for bionic humanoid is, first, measurement of the shape or physical properties of human body. Then, integration of artificial material, sensor, actuator, and user interface. Finally, evaluation by medical doctors.

[Figure 2.2](#) shows the modular structure of bionic humanoid. The main parts include head, bone, skin, and vascular system. For the head part, [figure 2.3](#) shows the modular structure of this part that includes skullcap, brain, blood vessel, nasal septum, and eye modules.

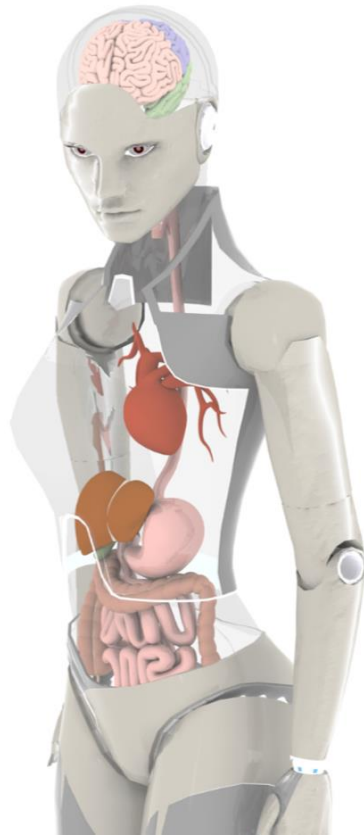


Figure 2.1. Bionic Humanoid: Concept of whole body surgery training system.

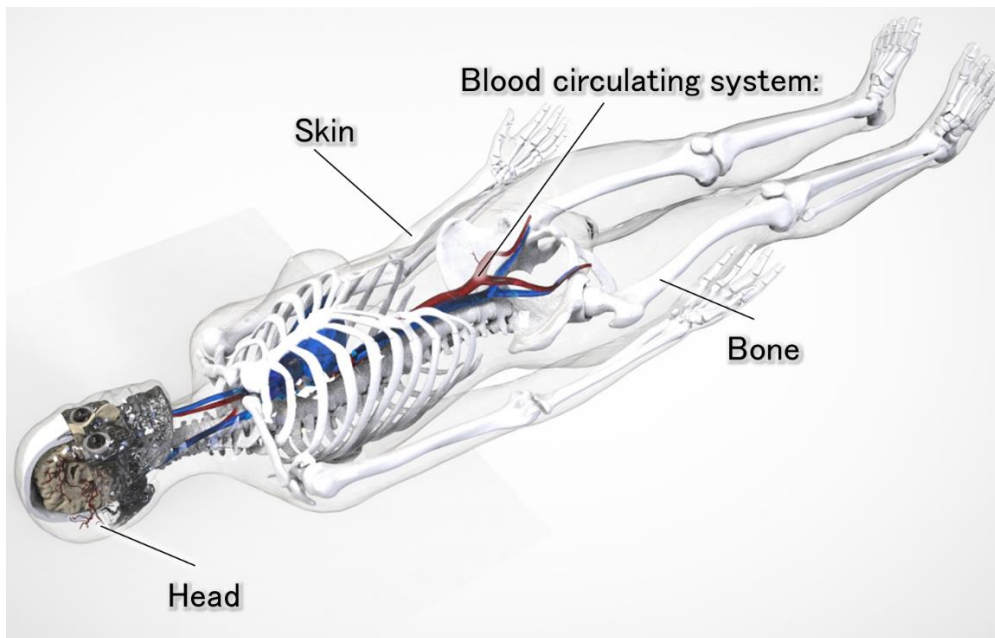


Figure 2.2. Modular structure of Bionic Humanoid.

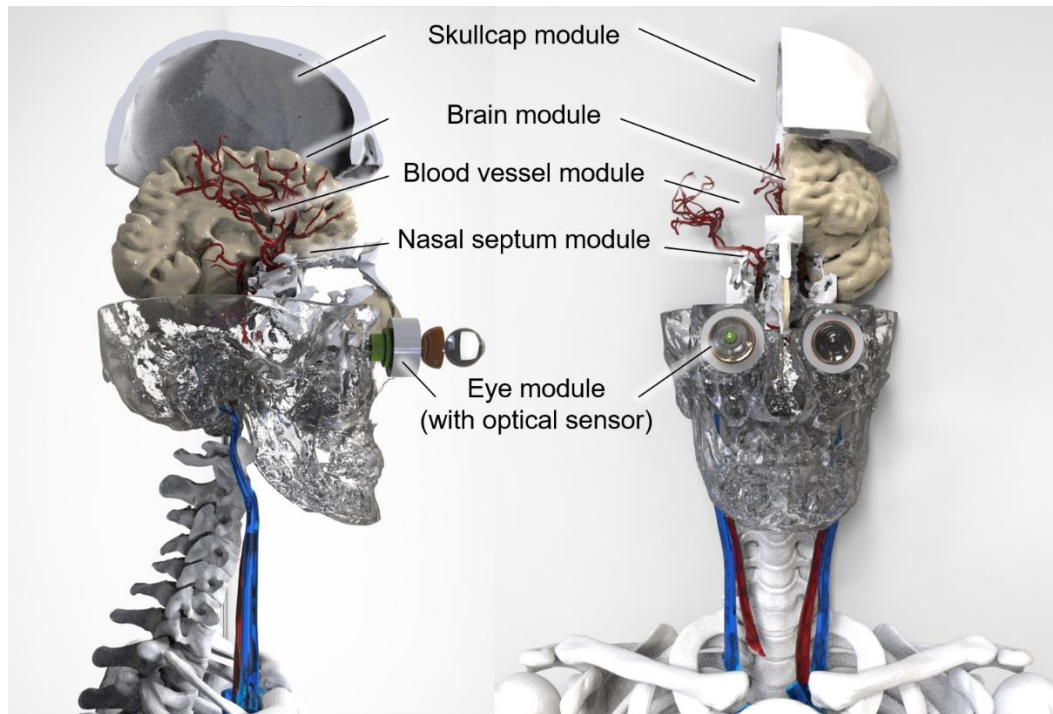


Figure 2.3. Modular structure of head part.

Bionic humanoid can be used, for example, to quantify the requirements of medical doctors, assess surgical skills, replicate physical constraints for the development of a medical device, development of medical implant, and provide novice surgeons with training opportunities. In surgical training, our proposed model is a promising new tool which offers an alternative to an animal and therefore can avoid the ethical problems in case of the animal model, and encourage to the quantitative surgical training with high reproducibility.

[Figure 2.4](#) shows the first prototype of bionic humanoid developed by our group. As we can see and described above that bionic humanoid consists of several modules such as skin, circulating system, bone, brain, and eye

modules. In this study, we chiefly focus on eye module. We propose an eye surgery simulator which is a training surgery tool for ophthalmologists on different kind of eye surgeries.



Figure 2.4. The first prototype of Bionic Humanoid.

### 2.3 Eye surgery training simulator

The human eye one of the most delicate structure in the human body. Ophthalmic surgeons need years of training and continues practice to carefully and successfully manipulate the tissues. Tool motions and forces used in these procedures are extremely small. Therefore, development of surgical skills is important and assist surgeons with surgery in live patients in the operating room. Currently, there are several eye surgery models that novice or even expert surgeons used to practice different type of eye surgeries. For example, Kitaro WetLab (Frontier Vision Co., Ltd., Hyogo, Japan) introduced eye surgery training model, as shown in [figure 2.5](#), for teaching and practicing basic phaco surgery and complex cataract cases. The model has been developed for beginner and intermediate ophthalmologists to improve their surgical skills for complex cases in cataract surgery.

Another model-based surgical simulator was introduced by Bioniko (BIONIKO, Aventura, FL, USA) called Bioniko ophthalmic surgery [161]. The Bioniko ophthalmic surgery model is a synthetic model of the anterior and posterior structures of the eye, and is assembled from two parts: an orbit model and a rhexis model as shown in [figure 2.6](#). The model used as surgical training model for a variety of surgeries ad tasks such as trabeculectomy, suture a corneal graft to a host, and rhexis without breaking the wound.

However eye surgery simulators have been developed such as the previous mentioned models, these simulation systems typically are often fabricated from hard plastics with material properties that are very different from the target organ. In other words, this means that surgeons will not have the same sense of real organ that they encounter in real operation.



Figure 2.5. Surgical practice eye kit introduced by Kitaro WetLab.

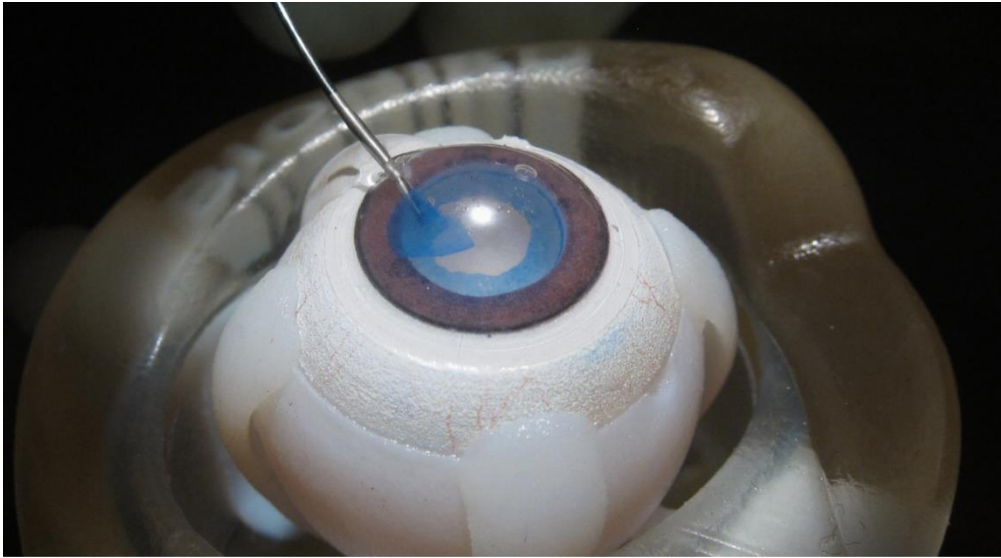


Figure 2.6. Surgical practice eye developed by BIONIKO, Aventura, FL, USA[161].



Based on the concept of bionic humanoid, we established a brand-new eye surgery simulator for ophthalmology called Bionic-EyE. [Figure 2.7](#) shows the modular structure of bionic eye. We target to introduce this model as surgical training model to eye doctors for a variety of eye surgeries to gain the needed skills to perform the target surgery. The eye surgery simulator basically consists of anterior and posterior segments as shown in [figure 2.8](#) and based on the target surgery we update the model with the needed tissues that are necessary for the surgery. [Figure 2.9](#) shows the benchmark of eye surgery simulator that clarify the kind of surgeries that we succeeded in making our model suitable for, and the new target surgeries.



Figure 2.7. Modular structure of Bionic Eye

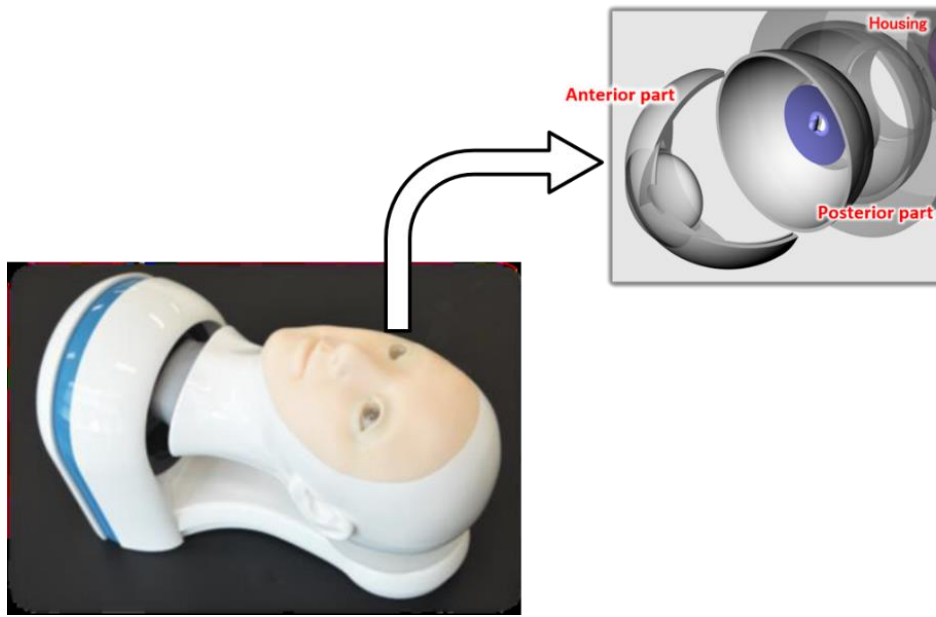


Figure 2.8. Eye surgery training simulator (Bionic-EyE)






| References          | Kitaro  | Bioniko   | Phake-i   | Jacrs  | Bionic-EyE  |
|---------------------|---|---|---|--|---|
|                     |  |  |  |  |  |
| (Anterior) Cataract | ○<br>CCC, Phaco   | ○<br>CCC, Phaco   | ○<br>CCC, Phaco   | ○<br>CCC, Phaco  | —   |
| (Anterior) Glaucoma | —   | ○<br>Trabeculectomy   | —   | —  | Trabeculotomy<br>Trabeculectomy   |
| (posterior) Retinal | —   | ○<br>• ERM peeling<br>• ILM peeling   | ○<br>• ERM peeling<br>• ILM peeling   | —  | ○<br>• ILM peeling<br>• microcanulation<br>• Retinal sensor                           |
| Eye rotation        | ○<br>28 degree  | ×<br>NA   | ×<br>NA   | —  | ○<br>45 degree  |
| materials           | ○<br>Artificial   | ○<br>Artificial   | ○<br>Artificial   | ×<br>(Pocine)  | ○<br>Artificial   |

Figure 2.9 Benchmark of eye surgery simulator

Firstly, our group has introduced the Bionic-EyE as surgery training model for microrcannulation. Recently, as a new treatment for retinal vein occlusion, microcannulation, has been used in eye surgery. Retinal vein occlusion is a disease of the retinal vein leads to fundal hemorrhage, which may cause blindness. Microcannulation is a treatment to approach the retina by inserting a micropipette from the surface of the eye, injecting thrombolytic drugs directly into the lesion. Hayakawa et al. fabricated a blood vessel model that simulates retinal blood vessel at the posterior segment of the eye model for the simulation of microcannulation surgery [169]. Figure 2.10 and 2.11 show the optical image-microscope of retinal vessels and conceptual image of retinal vessel model on curved surface respectively. Figure 2.12 shows the fabricated retinal blood vessel model. By using the fabricated vessel on the fundus part of the eye, Hayakawa succeeded in simulating the puncture and injection processes of microcannulation as shown in [figure 2.13](#).

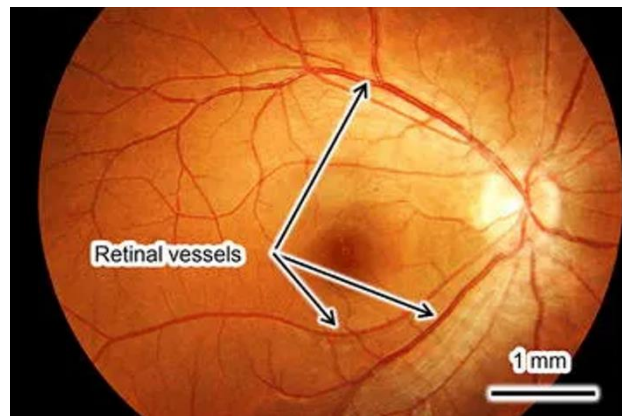


Figure 2.10 Optical-microscope photograph of retinal vessels [169].

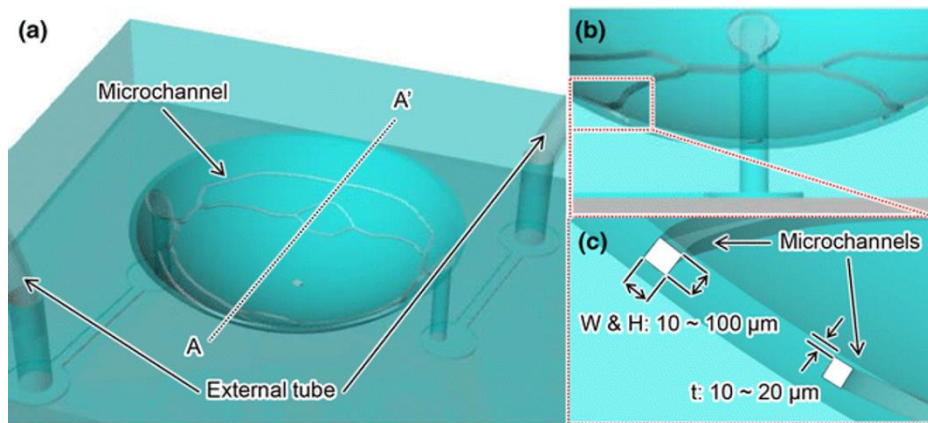


Figure 2.11 Conceptual image of retinal vessel model on curved surface: (a) overview of model, (b) side view showing line A-A', and c close-up of side view[169].

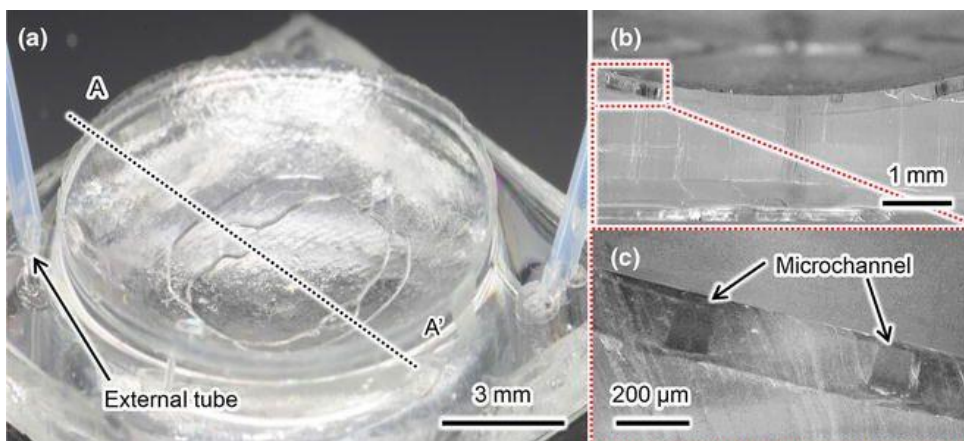


Figure 2.12. Photographs of fabricated model: (a) overview, (b) cross-sectional view cut along line A-A', and (c) enlarged image of cross-sectional view [169].

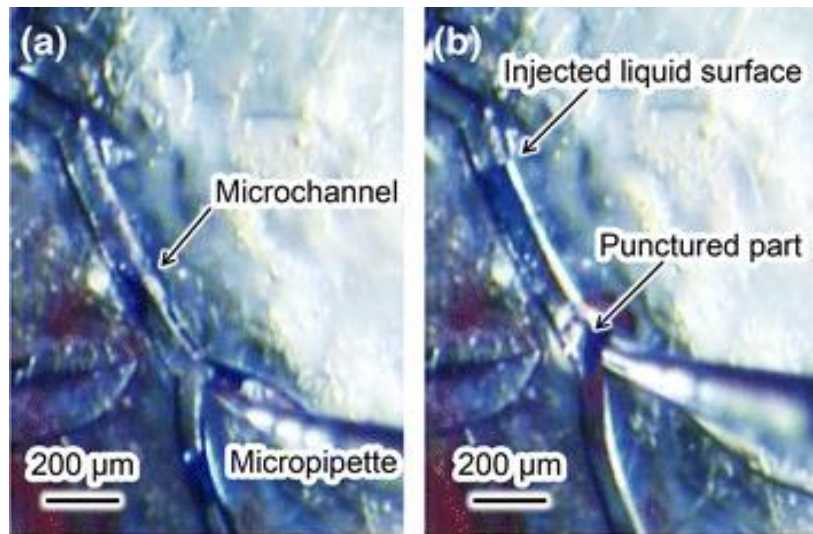


Figure 2.13. Results of microcannulation simulation: photographs of retinal vessel model (a) before and (b) after puncture of retinal vessel by micropipette. These photographs were acquired by using an eye-surgery microscope [169].

Then, our group updated the model to be suitable for another kind of eye surgery which is peeling of inner limiting membrane (ILM), superficial layer of the retina. Peeling of ILM surgery is a treatment for a foveal defect that located at the center of the macula, which can induce the retinal tears and rhegmatogenous retinal detachments. Omata et al. successfully introduced a novel ocular surgery simulator for peeling of inner limiting membrane using bionic eye [170]. The model for this surgery consists of eye-ball part and fundus part. The fundus part has an artificial retina and ILM for training the ILM peeling task using micro forceps. Artificial ILM was fabricated with chemically-crosslinked poly(vinyl alcohol) on artificial retina and sclera with polydimethylsiloxane; then, he succeed in integrating an eye-ball model with fundus part having artificial ILM in to the Bionic-EyE, and it was realized to demonstrate surgical training by eye doctors as shown in [figure 2.14](#).

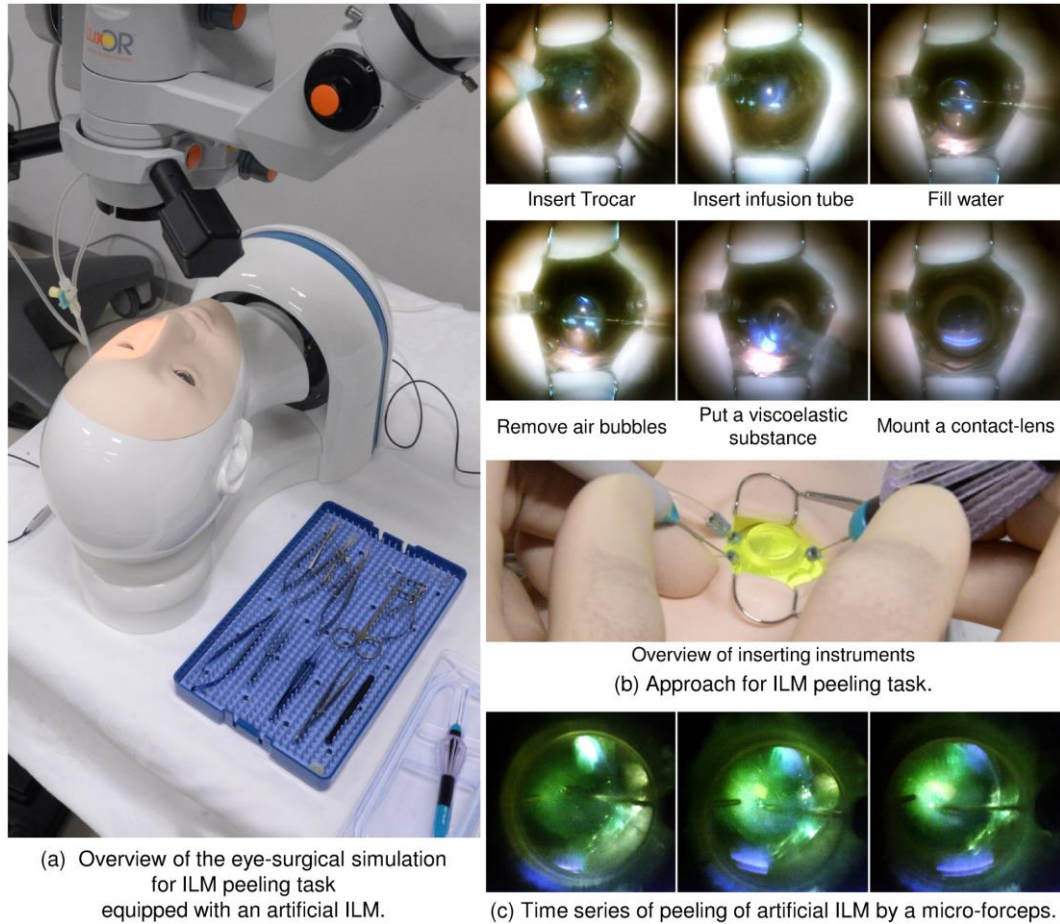


Figure 2.14. Photographs of the artificial ILM peeling task with an artificial eye mode [170].

In the current study, we aim firstly to introduce two fabrication methods of blood vessels (<15  $\mu\text{m}$ ) that could simulate the natural structure of capillary vessel at the fundus segment of the eye, but not limited to this area. We also can use the proposed methods of fabrication to develop capillary vessel model at different places of human body such as superficial layer of the mucosa of the colon. Additionally, the fabricated vessel can be used for evaluation of medical equipment such as evaluation of the endoscopic imaging system. Secondly, we aim also to update our bionic eye using simple and rapid fabrication techniques to fabricate the necessary tissues to make it suitable as eye surgical simulator for glaucoma surgery.

## 2.4 Summary

Human body model, consists of several organs such as eye, brain, bone, circulatory system, and so on, that mimics shape and physical properties of real one has been introduced. For eye module, we developed an eye surgery simulator for training eye doctors on several types of eye surgeries. The model currently can be used for simulation of microcannulation and peeling of ILM surgeries. In this study, we aim to update the bionic eye, using simple fabrication techniques, with the necessary tissues such as microvessels, trabecular meshwork, and schlemm's canal to make it useful tool for training eye doctors on glaucoma surgery as we will discuss in the next chapters.



## CHAPTER 3

# Fabrication Methods of 3D Microchannel that Mimic Human Microvessel

### 3.1 Introduction

Recently developed medical technologies including operating techniques, through blood vessels, and medical equipment are developing rapidly and diversifying. Therefore, medical doctors need to learn these technologies with only short-term training. Moreover, development and evaluations of medical equipment, such as endoscopic imaging system, need to conduct in a short time as well. We explained in details, in previous chapters, the limitations of using human, animal, or virtual reality as a models of blood vessel for practice and rehearsal intravascular surgery and for the development of new medical instruments, such as catheters, and concluded that the synthetic models are the promising alternative tools.

The benefit of a physical simulation model is that it can be manipulated directly, allowing the user to learn the necessary touch or feel sensations. Prototype simulators use highly reproducible individual samples due to well-controlled manufacturing methods. Blood flow can also be imitating by flowing a fluid in the vessel models by connecting them to external tubes and pumps. In addition, the selection of appropriate materials enables the device to be sterilized and allows the replication on the human body of the effects of medical equipment. Therefore, mock-up simulators can be used to test the performance of medical equipment in actual operating rooms.

Numerous methods have been suggested for the manufacture of mock-up simulators, such as stereolithography, ink-jet rapid prototyping, and photolithography. While stereolithography is applicable to the manufacture of molds, creating hollow structures is difficult. S. Ikeda et al. proposed a surgical simulator having 3D blood vessel models that are tailor-made using ink-jet rapid prototyping with wax [159,171]. However, it is very hard to fabricate microchannel with diameters smaller than 500  $\mu\text{m}$  because of the brittleness of wax.

Recently, 3D printing technologies have begun to make it possible to fabricate a high-resolution microchannel of about 50  $\mu\text{m}$  in diameter [172,173]. However, even smaller microchannels 10  $\mu\text{m}$  in diameter are needed in order to simulate a bionic capillary vessel environment with realistic diameters and branching structures by applying a micro-nano fabrication technique, as shown in [figure 3.1](#). Photolithography-based fabrication techniques can be applied to fabricate models of smaller vessels. T. Nakano et al. fabricated a microchannel that mimics a fine blood vessel with sizes up to about 10  $\mu\text{m}$  using photolithography techniques and polymer molding [161]. Although photolithography offers sufficient resolution for the blood vessel model, it can only be applied to two-dimensional (2D) structures. Two-dimensional simulators can be connected to conventional artery models to simulate an arteriole network and blood circulation within it. However, these simulators are limited to two dimensions even though the real vessel is 3D. A capillary vessel simulator, proposed to surgery training, evaluation of medical equipment or test hypothesis concerning microvasculature and its connection with circulating cells, should replicate 3D structure of in vivo capillary vessel. In this study, therefore, we aim firstly to propose two fabrication methods for

3D biological simulation models using microchannels to mimic capillary vessels and arterioles.

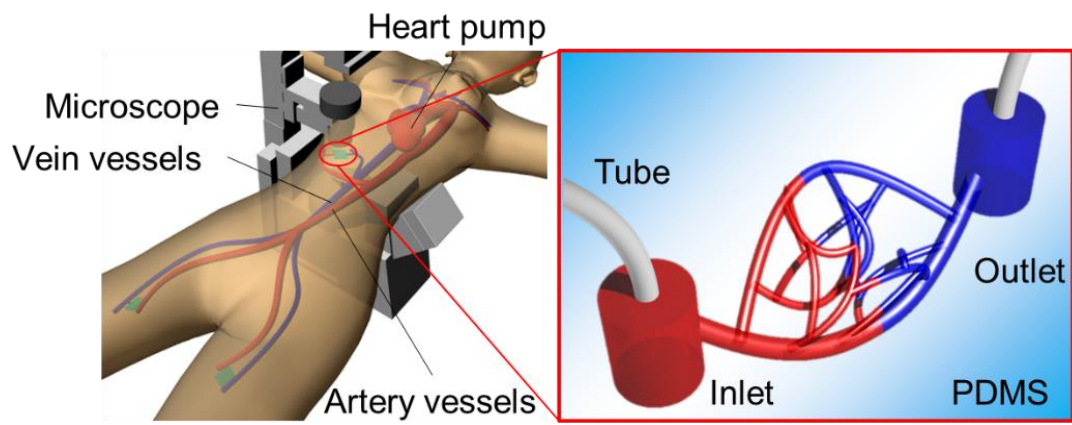


Figure 3.1. Concept of simulating capillary vessels and arterioles with models.

### 3.2 Microfluidic channel design and concept

We designed microchannels for mimicking blood vessels, such as colonic and intraocular retinal microvascular vessels, with two connection ports as inlet and outlet for the fluid flow. We simplified the shape of complex actual blood vessel as shown in [figure 3.2](#). We developed two fabrication methods for 3D capillary vessels: (1) photolithography with transfer to a 3D-printed model and (2) femtosecond laser and mask hybrid exposure.

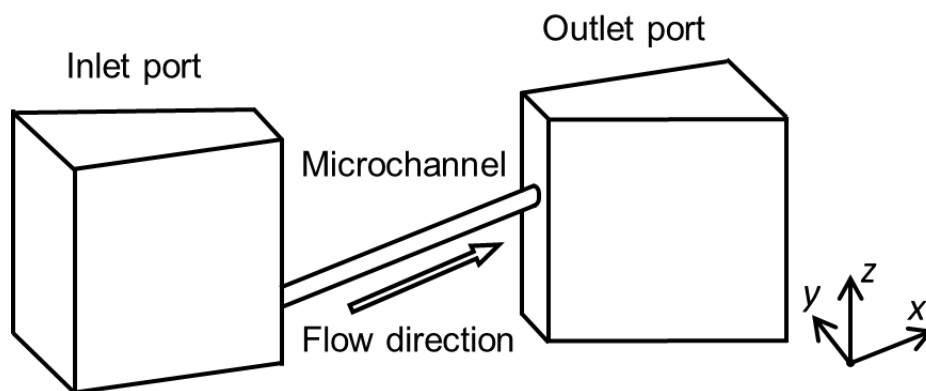


Figure 3.2. Basic structure of 3D microchannel.

### 3.2.1 Photolithography method

Photolithography is a fundamental technology for fabricating microchannels, and a high resolution of 1  $\mu\text{m}$  is easily attained [174,175]. Photolithography has been used for fabricating arteriole capillary vessel models [150]. However, this process is not suitable for fabricating 3D models, as it is limited to one flat plane. To achieve a 3D model with photolithography, we propose using photolithography to fabricate a 2D microchannel and then use PDMS (Sylpot 184, Dow Corning Toray Co., Ltd., Tokyo, Japan) molding and the water transfer printing technique to transfer the 2D microfluidic channel to a 3D printed model. First, we fabricate the microchannel on a PDMS sheet by laser lithography and PDMS molding. Next, this thin PDMS sheet is transferred to an angled 3D-printed model, which can be created in any desired shape using 3D printing technology. Third, to make the final surface of the microfluidic device flat, we put the model into a mold, pour PDMS, and remove the excess PDMS by squeegeeing. The result is a 3D microchannel formed at different depths that can be easily controlled. Additionally, the microchannel can be connected to external tubes via the connection ports, as shown in [figure 3.2](#), allowing liquid to flow through the microchannel for mimicking blood flow.

### 3.2.2 Femtosecond laser exposure method

Here we propose a method for fabricating a model with a cross-section close to circular, similar to that of a real blood vessel. During femtosecond laser exposure, the region of the sphere at the focal position of the laser is exposed as shown in [figure 3.3](#). Although it is processed into a 3D shape by repeating laser scanning, surface roughness occurs due to the scan line width and scanning interval. If the minimum line width is alleviated by decreasing the laser power or increasing the scanning speed, the surface roughness would be reduced. However, when the scanning interval diminishes, the time required for scanning increases. Therefore, we propose to take advantage of the acid diffusion phenomenon by using a chemically amplified resist.

Photoresists are materials that enable fine processing due to changes in the solubility of the region irradiated with light. Chemically amplified resists are a mainstream material for semiconductor fabrication. This material comprises a base polymer, dissolution inhibitor (for positive type resists – negative types use a scrubbing agent), and an acid generator. The acid generated by the exposure is diffused in a post-exposure heating step, that is, the post-exposure bake (PEB), and new acid is generated continuously by acid catalyst reaction; in the positive type, the exposure dissolves a dissolution inhibitor, and in the negative type, the exposure accelerates a crosslinking reaction to form a pattern. Therefore, compared with conventional resist, it is possible to form materials with a small exposure dose [176]. This acid-diffusion distance affects resist sensitivity and pattern shape. When the diffusion distance is too long, the resolution decreases because the catalytic reaction of the acid reaches the unexposed region. The diffusion distance of acid is influenced by the residual amount of solvent in the photoresist and the PEB temperature and duration [177–179]. Chen Q et al. effectively used acid-

diffusion phenomena and succeeded in producing a smooth shape with the chemically amplified resist SU-8 [180]. Here, we propose to make effective use of long-range acid diffusion. The photoresist used is a positive photoresist with high reliability (KMPR, MicroChem Corp., MA, USA). After exposing the chemically amplified resist to a femtosecond laser to generate acid (figure 3.4a), we actively induce acid long-range diffusion during PEB (figure 3.4b). We propose using this concept to make a mold of a fine blood vessel with a smooth surface.

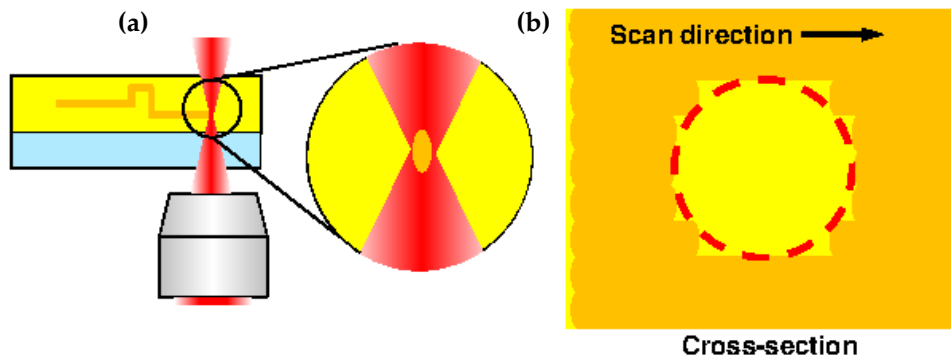


Figure 3.3. Cause of rough surface by a femtosecond laser exposure (a) Femtosecond laser scanning process (b) Cross-section of the photoresist after scanning

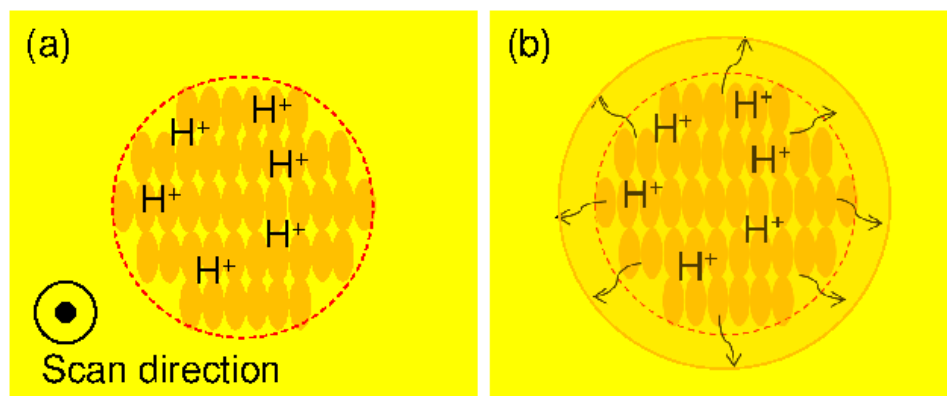


Figure 3.4. Mechanism for producing smooth mold surface when using chemically amplified resist. (a) Acid generation after femtosecond laser exposure. (b) Acid diffusion during post-exposure bake.

### 3.3 Fabrication methods

#### 3.3.1 Photolithography exposure method

To fabricate a microchannel structure on an angled surface, we hydraulically transferred the PDMS pattern, which had the microchannel, to an angled 3D-printed model. Water transfer printing is generally used for printing on curved surfaces [181]. A printed film was floated on water, and the model was pressed onto the surface of the film so that the pattern was uniformly applied to the angled surface. With water transfer printing process, we realized a fine microchannel with size of  $\approx 15 \mu\text{m}$  on an angled surface, which is strenuous to achieve with conventional fabrication techniques.

The fabrication process steps are summarized below. The step numbers correspond to the numbers in [figure 3.5](#).

1. Laser lithography (MA-6, SUSS Micro Tec KK, Kanagawa, Japan) was used to form a pattern in SU-8 photoresist (Nippon Kayaku Co. Ltd) on a silicon surface. The exposure time is 9.7 sec. The mold was heated using a hot plate at  $65^\circ \text{C}$  for 1 min,  $95^\circ \text{C}$  for 3 min. Then, the part was developed with PM thinner for 120 sec and rinsed with 2-propanol for 60 sec. This pattern was used as a mold for the microchannels, and the size of the microchannels could be locally controlled by adjusting the exposure conditions.
2. Spinning coat (2000 rpm for 30sec) was used to apply Lift-off resist (LOR) (Nippon Kayaku Co. Ltd.) then bake on hotplate for 10 min at  $95^\circ \text{C}$ . Spin coat PDMS (3000 rpm for 30 sec) (Silpot 184, Dow Corning Toray Co. Ltd., Tokyo, Japan) over LOR onto a glass substrate, then bake on hotplate for 10 min at  $95^\circ \text{C}$ .



3. The SU-8 mold was pushed onto the spin-coated PDMS and the ensemble was heated to 85°C for 10 min with a hot plate.
4. The LOR was dissolved with ethanol to free the PDMS sheet from the substrate.
5. A PDMS base was created using a 3D printer (EDEN250, Stratasys Ltd, MN, USA).
6. The PDMS sheet and base were treated with O<sub>2</sub> plasma to activate their surfaces for bonding, and the PDMS sheet was transferred to the PDMS base.
7. Holes were punched into the connection channel to connect external tubes from the bottom side of the model.
8. A thin sheet of PDMS was created by spin-coating to serve as a cover layer for the channel.
9. The thin PDMS sheet placed over the PDMS sheet containing the microchannel.
10. PDMS was poured and squeezed to form a slab over the angled surface.
11. The assembled PDMS model baked in the oven for 20 min at 85° C, and the mold was removed.

In this fabrication process, a 15- $\mu\text{m}$ -wide microchannel could be fabricated by using laser photolithography (step 1 in [figure 3.5](#)). The patterning on an oblique structure was done using water transfer printing (steps 5 and 6). Furthermore, the thickness of the cover layer was controlled by changing the spin-coating conditions (step 8). To confer the microfluidic device a flat surface, we put the model in the mold, poured PDMS, and squeezed out the excess PDMS (steps 10 to 11). The cross-section of the microvessel model is rectangular because the cross-section of the patterned

photoresist is rectangular. Previously we fabricated a vessel model with semicircular cross-sections using a reflow process with the patterned photoresist [161].

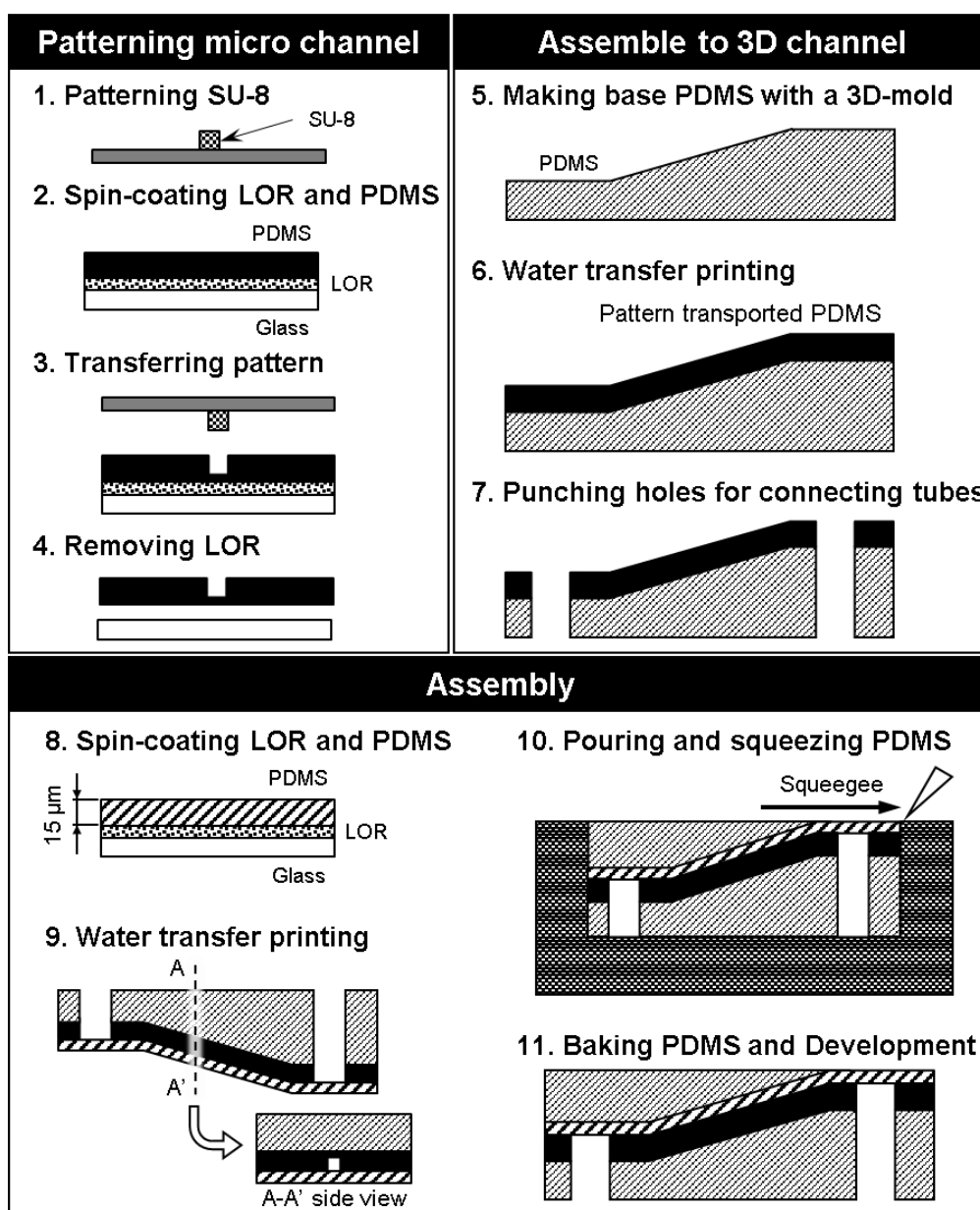


Figure 3.5. Microvessel model fabrication using photolithography.

### **3.3.2 Femtosecond laser and mask hybrid exposure (FMEx)**

Microvessels have been fabricated using semicircular photoresist patterns and light-cured resin, but the cross-sections of the fabricated channels were semicircular [161,182]. Therefore, these processes are not suitable for fabricating fine blood vessel models. So, to fabricate a capillary vessel and arteriole simulator with submicrometer resolution and circular cross-section, we used a new 3D exposure method, specifically, two-photon absorption exposure by a femtosecond laser. However, since it takes a long time, this method is not suitable for exposing millimeter-scale areas. The typical microfluidic area used for the inlet or outlet port of the simulator is relatively large, that is, at millimeter-scale. Therefore, these large areas were exposed using a mask aligner. The femtosecond laser exposure makes it possible to fabricate a part of the millimeter-scale structure with submicrometer resolution in three dimensions.

#### **2.3.2.1 Femtosecond laser exposure system**

We used a purpose-build femtosecond laser system [183]. This system uses a Ti:sapphire laser with a wavelength of 780 nm and pulse width of 140 fs (Chameleon XR-SK, Coherent, Inc., Glasgow, UK). The laser was focused using an objective lens with a numerical aperture of 1.40, magnification of 100 $\times$ , and working distance of 130  $\mu$ m (UPLSAPO 100XO, Olympus, Tokyo, Japan). Positioning of the sample was performed using a piezo stage (P-563 3 CD, Physik Instrumente Japan Co. Ltd., Tokyo, Japan). The positioning resolution was 4 nm, and the movable range was 300  $\mu$ m in each direction (x, y, and z). A Karl Suss MJB3 mask aligner (MA-6, SUSS Micro Tec KK, Kanagawa, Japan) was used during fabrication. As in previous research [184], we used the negative photoresist KMPR (Nippon Kayaku Co., Ltd., Tokyo, Japan) and the

positive photoresist PMER P-LA900PM (Tokyo Ohka Kogyo Co., Ltd.) as a negative control to fabricate capillary vessel simulators.

### 3.3.2.2 Line width processing

As a preliminary experiment, we measured the minimum line width that could be processed when a PDMS block was exposed using the femtosecond laser, as shown in [figure 3.6](#). We varied the scanning exposure conditions to form various line patterns with the scanning laser, as shown in [figure 3.6a](#). The processed line pattern was observed using scanning electron microscopy (SEM; SPG-724, JEOL, Tokyo, Japan), and the width of the line pattern in the x-axis direction was measured. From the image ([figure 3.6b](#)), obtained obliquely at 45°, the z-axis position estimates the width in the axial direction. The scanning line width was measured using a 100× objective lens, with the laser power set to 3 mW. The scanning speed was increased from 1 to 500 μm/s in the y direction. The obtained measurements are shown in [figure 3.6c](#). At 160 μm/s, the minimum possible line width was 250 nm in the x-axis direction and 490 nm in the z-axis direction. When the scanning speed was higher than 160 μm/s, the resist was not sufficiently exposed, and it was difficult to form the pattern, as shown by the top feature in [figure 3.6b](#). The line width diminished with increasing scanning speed, and the mean ratio between widths in the x and z directions was 0.54 with a standard deviation of ±0.04. This approximates the theoretical number of the two-photon method,  $\sqrt{\ln(2)/2} \approx 0.59$  [185,186]. Therefore, we could confirm that our fabrication technique with the femtosecond laser exposure had a reproducible resolution for line width of  $500 \pm 100$  nm and  $240 \pm 70$  nm in the z- and x-axis directions, respectively.

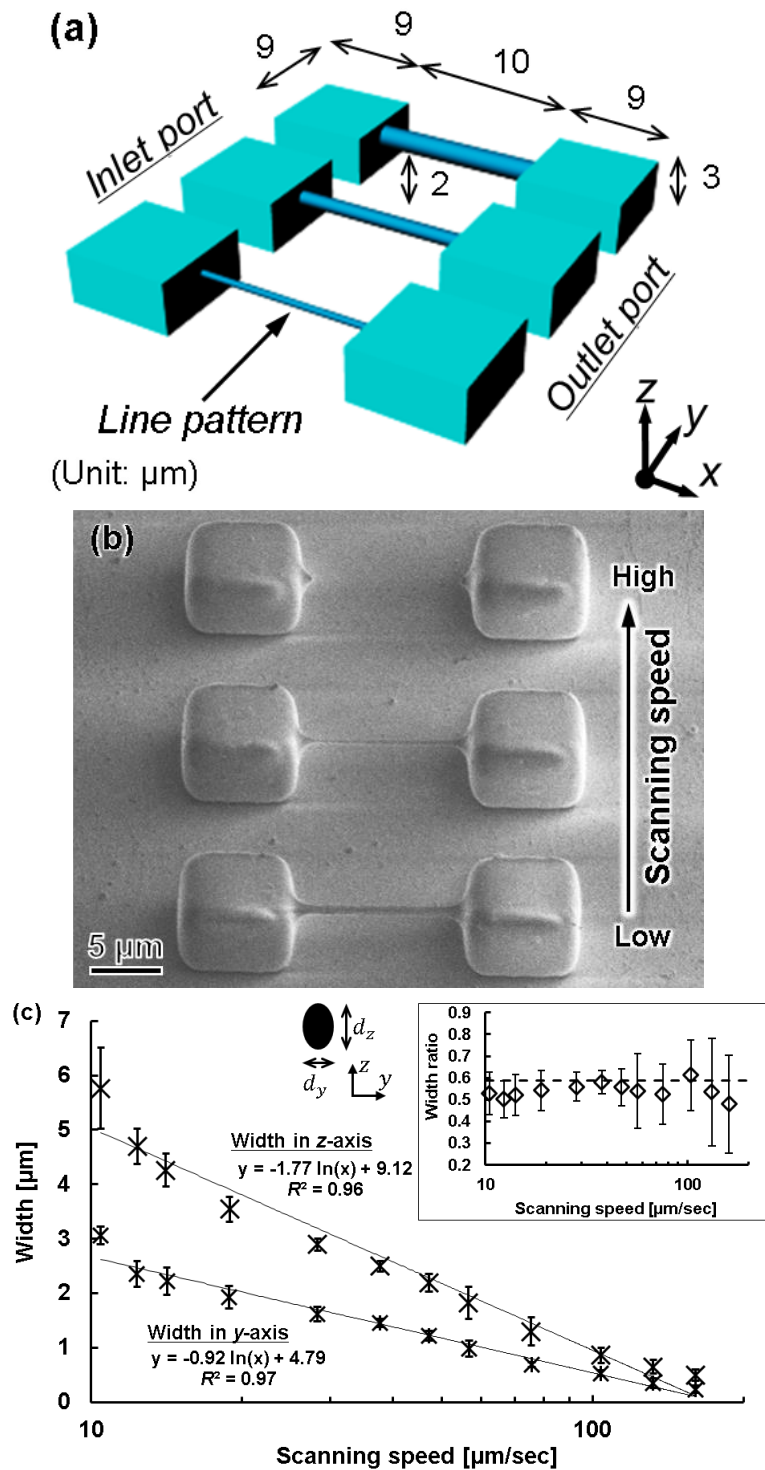


Figure 3.6. Measurement of scanning line width and thickness during femtosecond laser exposure. (a) Design concept for microfluidic device. (b) Top view SEM image fabricated 3D mold. (c) Relationship between scanning speed and line width and thickness by femtosecond laser exposure. Inset illustrates ratio of each pair of line width dimensions, and dashed line represents theoretical ratio by the two-photon laser method,  $\sqrt{\ln(2)/2} \approx 0.59$ .

### 3.3.2.3 Experimental procedure for FMEx

[Figure 3.7](#) shows the process for fabricating a 3D capillary vessel simulator, which is summarized as follows (as before, step numbers correspond to those in the figure):

1. A 20- $\mu\text{m}$ -thick film of KMPR or PMER was formed by spin-coating and pre-baking on a hot plate at 100°C for 30 min.
2. A fine 3D microchannel was formed by femtosecond laser exposure.
3. The connection port, which introduces the liquid flow path, was exposed using the mask aligner.
4. The mold was heated using a hot plate at 65°C for 1 min, 95°C for 3 min, and 65°C for 1 min. Then, the part was developed with PM thinner and rinsed with 2-propanol.
5. After replacing the mold with t-butyl alcohol, it was dried with a vacuum dryer and the pattern was transferred by pouring PDMS into the mold.
6. Remover PG was applied to remove the KMPR or PMER resist and form a hollow structure.
7. The finished microchannel was bonded to a glass substrate with plasma treatment.

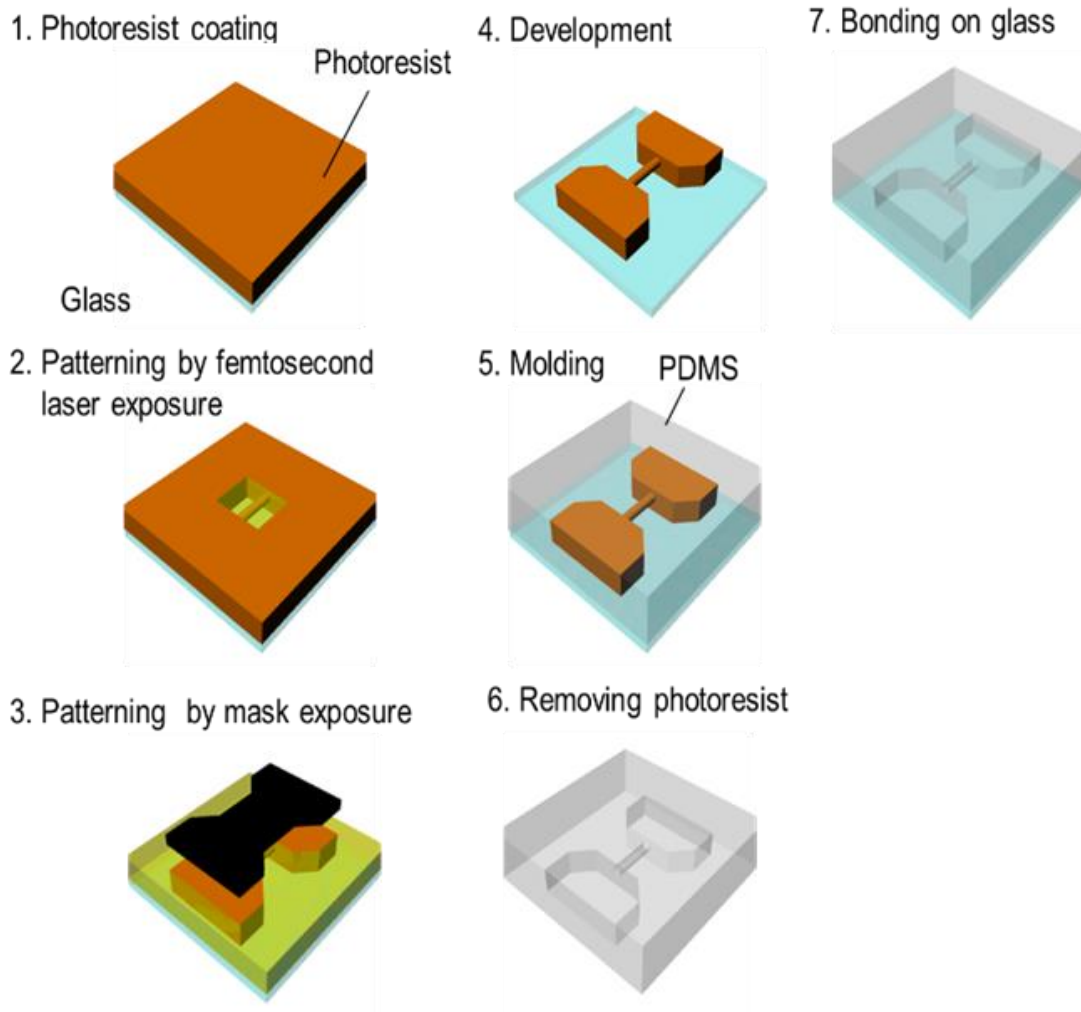


Figure 3.7. Microchannel model fabrication process using FMEEx.

## 3.4 Experimental results

### 3.4.1 Photolithography method

[Figure 3.8](#) shows a fabricated 3D microchannel in a PDMS block for modeling a microvessel. The channel was neither broken nor collapsed after the water transfer printing process, as shown in figure 3.8b. The cross-section of the fabricated vessel model was square, as shown in figure 3.8c, because the cross-section of the patterned photoresist was square. As noted above, fabrication of a circular capillary vessel is quite complex using this exposure method [174,187], so the square cross-section was intentional.

We created microchannels with various depths and measured the depth of the microchannel at different positions. The fabricated model was sectioned at different locations. Then, by using optical microscope, we measured the depth of the microchannel at all sectioned locations, as shown in figure 3.8c. Details of the designed and measured microchannel depths are given in [figure 3.9](#). In addition, we tested the flow of liquid in the microchannel by injecting a colored liquid into it via external tubes connected to the ports. The injected liquid flowed through the channel without leakage, as shown in figure 3.8b



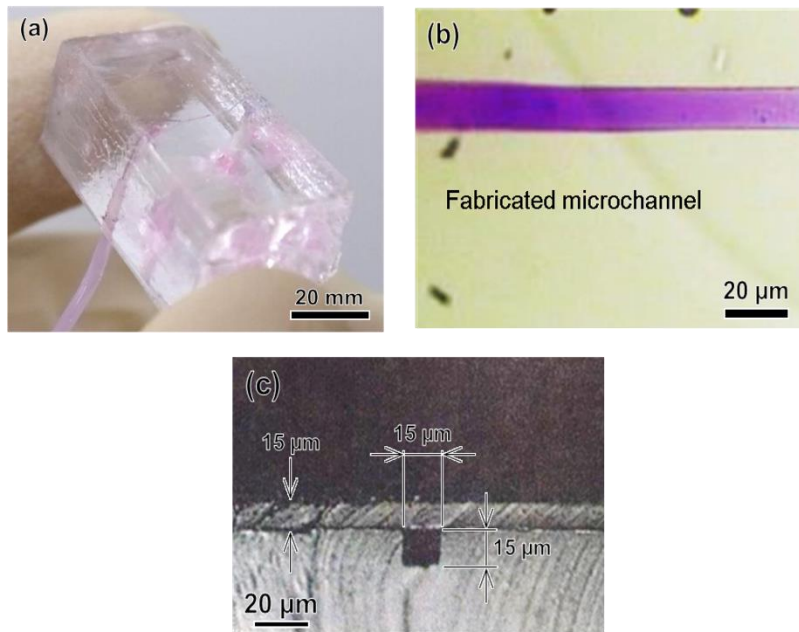


Figure 3.8. Images of the microchannel fabricated using classical photolithography. (a) PDMS base model with microchannel. (b) Optical microscope image of microchannel. (c) Cross-section of microchannel.

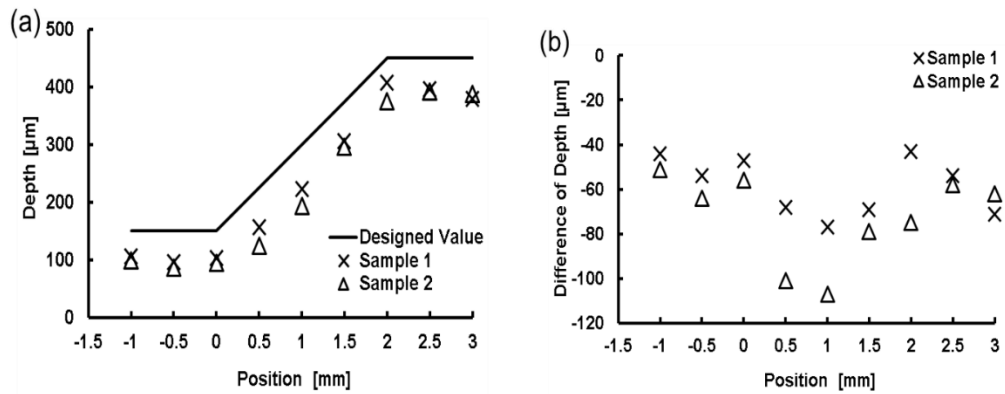


Figure 3.9. Measurement of microchannel depth. (a) Full thickness profiles of the designed and fabricated microchannels. Position zero is the inclination starting point. (b) Distributions of deviations of fabricated depth calculated by subtracting each fabricated value from the design.

### 3.4.2 FME<sub>x</sub> method

[Figure 3.10](#) shows a CAD image of our simple design for a 3D microfluidic channel. Processing conditions were a laser power of 3 mW, scanning speed of 50  $\mu\text{m/s}$ , scanning interval in y-axis direction of 0.99  $\mu\text{m}$ , and scanning interval in the z-axis direction of 1.83  $\mu\text{m}$ . SEM images of the produced mold are shown in [figure 3.11](#). Figure 3.11b is a 2,700 $\times$  enlargement of the mold prepared with KMPR resist, which we compared with a mold prepared with a standard PMER positive resist (figure 3.11c). The KMPR resist fabricated a microchannel with a smoother surface compared to the surface prepared with PMER. A cross-section of the microchannel formed with KMPR is shown in [figure 3.12](#). As defined by the length ratio between the z- axis and y-axis, the circularity of the channel using the FME<sub>x</sub> method was 0.95.

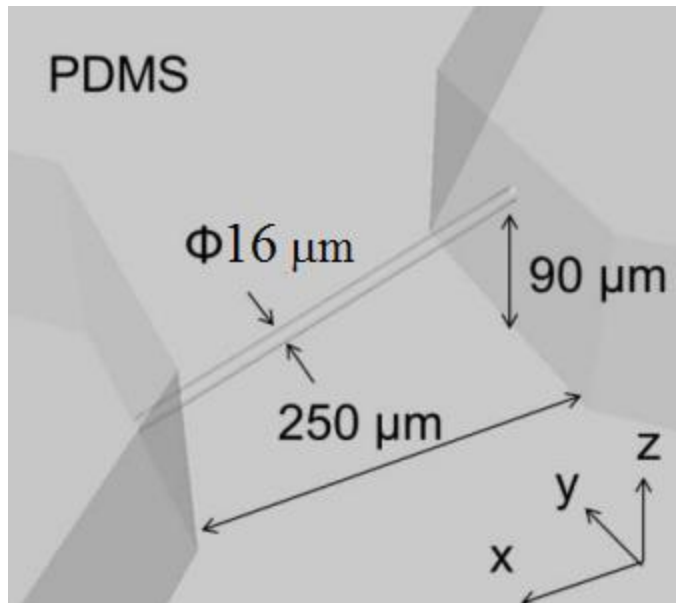


Figure 3.10. A CAD image design of 3D microfluidic devices for replication of microscopic vessel fabricated using FME<sub>x</sub>.

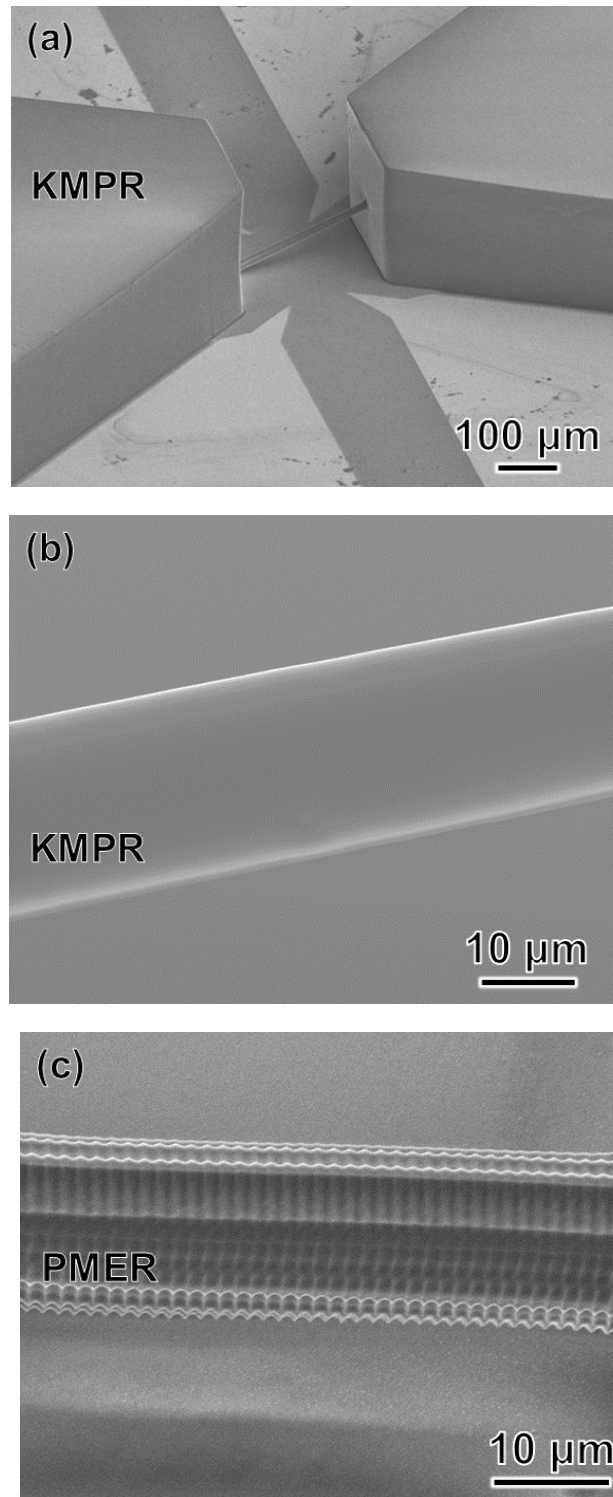


Figure 3.11. SEM images of the mold fabricated using FMEx: (a) Low magnification. (b) High magnification with chemically amplified resist (KMPR). (c) High magnification with standard resist (PMER).

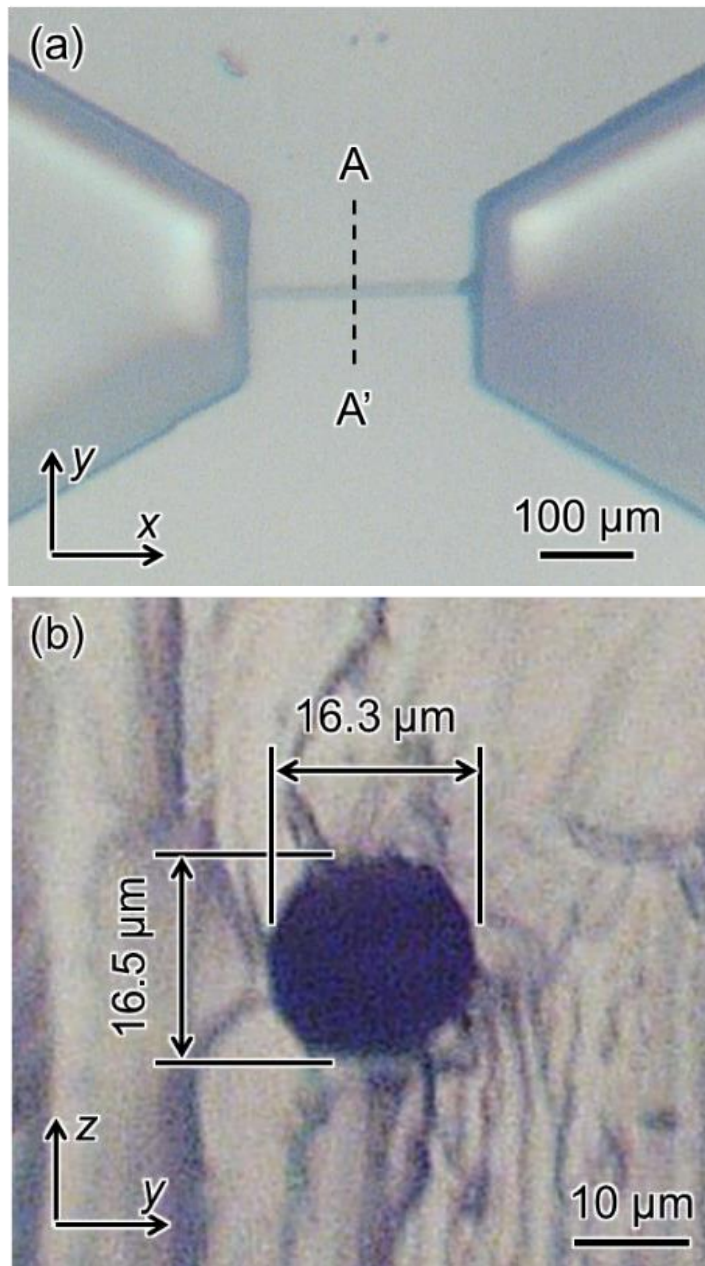


Figure 3.12. (a) Microscopic image of a PDMS microchannel mold fabricated using FME<sub>x</sub> (b) Cross-section of the microchannel at section A-A'.

### 3.5 Discussion

We developed two methods for fabricating 3D microfluidic devices having 3D microchannel that mimic human microvessel. First, we fabricated a microfluidic device using a conventional photolithography exposure method, which was limited to one plane, but with assistance of PDMS molding and water transfer printing, we succeeded in forming a 3D microvessel model with rectangular cross-section at various depths in a slab-shaped model. With water transfer printing and 3D-printed models (steps 9 to 11 in figure 3.5), we could easily control the depth of the microchannel to mimic the dimensions of a real microvessel. The photolithographic exposure method was a suitable choice for fabrication of a microfluidic device with millimeter scale, as the time needed for exposure was short. But to form a microchannel with a circular cross-section and smooth surface with this exposure method would be very complicated.

Second, we developed the FMEx method for fabricating 3D microchannel that simulate human capillary vessel, with a diameter smaller than 20  $\mu\text{m}$ . We employed the femtosecond laser exposure method to fabricate a millimeter-scale microchannel structure with submicrometer resolution in 3D. By comparing the microchannels in figures 3.11b and 3.11c, the latter of which was created by PMER, it can be seen that the FMEx method with KMPR resist produced a much smoother surface. This smooth surface could be produced independent of minimum line width during femtosecond laser exposure scanning (figure 3.11b). In addition, we compared our results with

conventional studies on circularity. The model was sectioned and a cross-section image was taken with an optical microscope, as shown in figure 3.12. In the previous research, a microvessel model with a diameter of about 15  $\mu\text{m}$  was produced by photolithography with overexposure, and it had a circularity of 0.84 [161]. The circularity produced by the FMEx method (figure 3.12b) was improved, with a circularity of 0.95. Therefore, this study demonstrated that the FMEx method is a superior 3D modeling technique compared with photolithography using standard photoresist.

In the fabrication of micrometer-scale channels ( $< 20 \mu\text{m}$  in diameter) for mimicking human microvessels, a crucial issue is how to connect an external tube to the microchannel for modeling microvessel flow. In our research, we made our microchannel design with two regions to provide inlet and outlet ports for fluid, as shown in figures 3.10–3.12. Although the total model size included a micrometer-scale channel and two millimeter-scale connecting regions, we were able to easily make holes at these regions to connect external tubes and flow fluid through the microchannel. According to the effect of different exposure methods on fabrication of a micrometer-scale channel, the mask exposure method was completed within a few minutes and it has the advantage of not being dependent on the exposure area.

The time of exposure was independent of model size and the time was short, up to few minutes. On the other hand, it is hard to fabricate a large-scale model with the FMEx method, as both the laser exposure and removal of the photoresist after molding in PDMS take a long time. In this study, we solved

the problem of port connection by integrating masking techniques from classical photolithography. By using the FME<sub>x</sub> method, we could forge a 3D microchannel that represent human capillary vessel a few hundred micrometers in length and equip it with inlet and outlet ports.

Let us consider the advantages and disadvantages of the methods of photolithography and FME<sub>x</sub>. [Table 3.1](#) shows a comparison between the two methods used to fabricate 3D microchannel that simulate human microvessels. Additionally, we present a schematic selection map of these fabrication methods in [figure 3.13](#). In cases where we need to fabricate 3D microvessel with a small size, fine surface, and circular cross-section, the FME<sub>x</sub> method is preferred. For simulating retinal microvessel surgery, such as microcannulation, with a model having large vessels >50 μm in diameter, square versus circular cross-section makes no considerable difference for surgeons [169]. Therefore, microvessels surgical simulator formed by the photolithography method would be sufficient during training surgeons on eye surgeries performed within retinal vessel, which located at the posterior part of the eye, such as microcannulation. Moreover, with surgery dealing with human vessel with diameter more than 100 μm, 3D printing models with the aid of polymer molding are sufficient techniques to make 3D microchannel simulate the target microvessel. For instance, for fabrication of microvesel such as schlemm's tube, which located on the anterior segment of the eye and has dimeter more than 100 μm we can easily fabricate this vessel by only 3D

printing models with the aid of polymer molding as we will discuss in details next chapter.

On the other hand, there is another need of simulation of microvessels <20  $\mu\text{m}$  in diameter in the superficial layer of the mucosa of colon, that are especially targeted for cancer diagnosis by using spectral endoscopy system [188]. In this case, both methods, photolithography and FME<sub>x</sub>, can be used to form a microvessel models having different depth from the surface. We used photolithography method in fabrication of microvessel simulator for evaluation of endoscopic imaging system [188].

Additionally, there is another need for evaluation of deformability of Red Blood Cell (RBC) for diagnosis of diseases. One approach for this evaluation is to measure the time of RBC passing through the simulated microvessel [189]. A capillary vessel simulator was used to flow in the simulated capillary vessel model with rectangular cross-section. By using FME<sub>x</sub> method, we can test and compare the 3D capillary vessel model with circular cross-section and diameter similar to the geometry of in vivo microvessel.

In the future, we will use the models developed by photolithography and FME<sub>x</sub> methods for quantitative examination of superficial capillary vessels, with the cooperation of medical experts. Additionally, we will use the model made by FME<sub>x</sub> for evaluation of RBC deformability. Thus, based on the application, we can choose the proper method from the two methods developed here for fabrication of 3D microchannel that simulate human



microvessel. Using our proposed methods, we can create multiscale transparent arteriole and capillary vessel models with rectangular and circular cross-sections of submicrometer to submillimeter diameter and lengths for evaluating practice and rehearsal of surgeon skills on different kind of surgeries, such as eye surgeries, and for developing new medical devices, such as spectrum endoscopy system, and for study hypotheses concerning to microvessel and its circulating cells.

Table 3.1 : Comparison between the femtosecond laser and photolithography fabrication methods.

| Method                                | Femtosecond laser exposure                  | Photolithography      |
|---------------------------------------|---|-----------------------|
| Dimension                             | 3D  | 3D                    |
| Microchannel width                    | Max. 20 $\mu\text{m}$                       | Over 10 $\mu\text{m}$ |
| Process time                          | Hours                                       | Seconds               |
| Cross-sectional shape of microchannel | Circular cross-section<br>Circularity: 0.95 | Rectangular           |
| Total time of fabrication             | Over 4 hours                                | Less than 2 hours     |

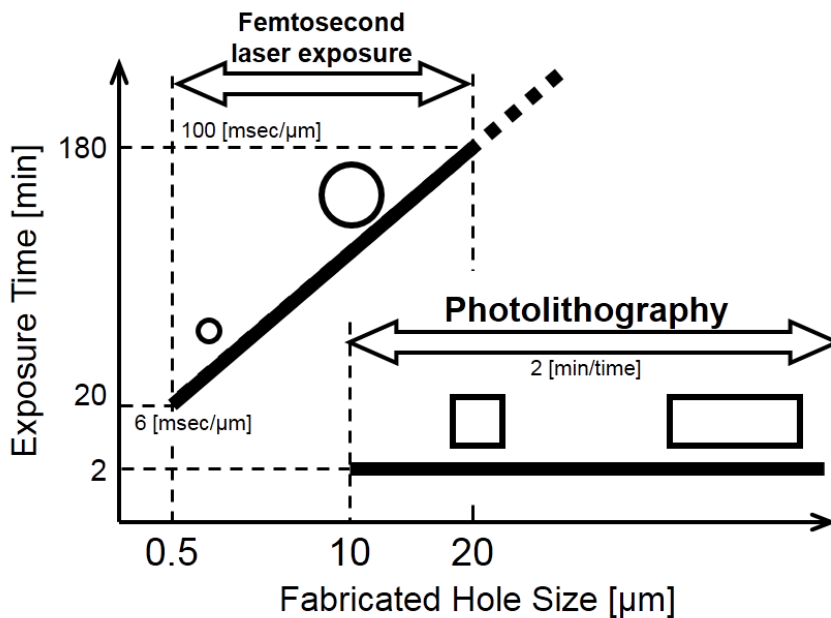


Figure 3.13. Schematic drawing of cross-sections of microchannels fabricated using femtosecond laser exposure and classical photolithography

### 3.6 Summary

We presented two fabrication methods of 3D microchannel that can be used as a model for capillary vessel were proposed. Based on the target surgery or application, we can decide which method is appropriate for the surgery or application. The first method, photolithography with the aid of 3D printing models, enabled us from creation of 3D microchannel, with rectangular cross section, over irregular surface with different depth. Second method, FMEx, can be used for creation of 3D microchannel with circular cross section. Both methods made it possible to fabricate a millimeter-scale 3D structure with a submicrometer resolution and achieve an easy injection of solution. This is because it was possible to fabricate typical microfluidic channels used for model inlet and outlet ports. Additionally, with the FMEx method, we employed an acid-diffusion effect using a chemically amplified resist to form a circular channel cross-section. The acid-diffusion effect made it realizable to fabricate a smooth surface independent of the laser scanning line width. The acid diffusion phenomenon was essential for achieving a model with a smooth surface and circular cross-section. With the proposed FMEx method, we can create complex 3D capillary vessel models that realistically mimic blood vessels. Our proposed methods can make a significant contribution to the medical field and forge an alternative to the use of animals for surgical training and method evaluation.

## CHAPTER 4

### Eye Model as Surgical Simulator for Glaucoma Surgery

#### 4.1 Introduction

To practice surgical procedures before they are used on patients, it is necessary to have access to artificial models [135]. Artificial models are particularly useful for eye surgery because miniaturized surgical devices are often used. Among eye pathologies, glaucoma is the second leading cause of blindness worldwide [190]. The disease has a prevalence of 3.54% in the adult population aged 40–80 years, and 64.3 million people are affected by it [190,191]. In the normal eye, there is a liquid, secreted from the ciliary body of the uvea, called aqueous humor. This liquid has a regular outflow path to keep the intraocular pressure (IOP) within the normal range, which is 20 mmHg or less. The aqueous humor provides a path between the crystalline lens and iris and flows to the angle structure. Then, it flows through the trabecular meshwork of the angle structure, reaches the Schlemm's canal (SC), and flows out to the veins [192]. In glaucoma, the drainage of aqueous humor into the SC is hindered, leading to an increase in IOP and subsequent damage to the optic nerve, resulting in a progressive loss of sight. Previous studies showed that the main source for the elevation in IOP is the resistance of the TM to the outflow of aqueous humor to the SC [193–197]. Lowering the IOP is the only uncontroversial therapeutic strategy for reducing the risk of glaucomatous progression [198]. The surgery is usually reserved for advanced stages of the

disease, when drugs and laser treatments fail to adequately mitigate the IOP to control it. Surgical therapy can be divided into external filtering procedures, such as trabeculotomy, and micro invasive glaucoma surgery (MIGS). The trabeculotomy, which is performed by incising the sclera, is a fundamental operation that has been done since long ago. On the other hand, MIGS has been proposed as a less invasive method in recent years [199–202]. There are 4 main approaches in lowering IOP by MIGS (1) increasing outflow via ablation of the trabecular meshwork (2) reducing aqueous humor production (3) increasing outflow via suprachoroidal pathways; and (4) creating a new subconjunctival pathway [202]. Dual blade Kahook (DBK), trbetome, and ab interno are the common medical instruments used for lowering IOP through ablation of TM.

Despite the used device in severing TM, MIGS is a complex surgery which involving many procedures such as advanced gonioscopy techniques and bimanual coordination [203,204]. Bimanual coordination, where one hand holds the goniolens and the other holds the device or inserter. To address the prevalence of glaucoma, an extensive training program that allows surgeons to earn a high degree of skill and an understanding of the principles of the operation is in high demand.

Several systems that simulate various kinds of eye surgery are already in use [205–207]. However, these simulation systems lack paramount anatomical details, such as the 3D microchannel, which represents the SC, over the spherical shape of the eye, which is necessary for the simulation of glaucoma surgery. The importance of creating SC structure, in the simulation systems, comes from that the target area of TM, which will be removed by surgeons, should be over the SC structure to make an access to the SC as a way for the aqueous humor to lower IOP. Surgeons determine the target area of

TM by identify the location of SC. Moreover, these simulation systems are often fabricated from materials whose mechanical properties are different from those of the target tissue. Consequently, for progression of the current surgical and education models, a fabrication method for the 3D microchannel over the spherical shape and materials with controllable properties are required. Additionally, fabrication of 3D microfluidic channels over complex shapes can contribute in making inroads in biological research. An important application of 3D microfluidic channel over complex shapes, that stimulate blood vessel, entails studies on blood flow, which requires 3D geometries with biocompatible materials. Moreover, 3D microfluidic channel allows us to realize accurate manipulation and analysis of fluids, cells, drug screening, and medical procedures [208,209].

A number of microfabrication techniques for 3D microchannels have been produced over the years for various types of applications. Photolithography is employed as a microfabrication technique for creating microchannels. Micromachining, soft lithography, and laser ablation are other techniques for fabricating microfluidic channels, which are used for large-scale replication and production [210]. However, those techniques suffer from a limited availability of biological materials.

In this research, we present a simple microfabrication technique that allows for the rapid construction of a 3D microchannel on a spherical shape. We applied this technique to fabricate a 3D microchannel that represents the SC structure on the inside surface of an eye model. Additionally, we used a blow-molding method to fabricate the thin membrane covering the microchannel, which represents the TM. We introduced this model as a surgical simulator for the inside-out (*ab interno*) approach which is a kind of MIGS. In the fabrication of the artificial eyeball and TM, we used materials

with controllable properties to mimic those of human tissues. Finally, by mounting this glaucoma model on an eye surgery simulator (bionic eye surgery evaluator: Bionic-EyE™) [170], a series of surgical exercises could be performed.

## 4.2 Materials and Methods

### 4.2.1 Design concept

A pivotal structure for ab interno surgery is the angle structure around the limbus cornea, which is shown in [figure 4.1](#). The SC is a microchannel with a width of about 500  $\mu\text{m}$ . The TM works as a filter during the flow of aqueous humour. A review of the surgical procedures of an ab interno approach using a microhook has been made [211]. [Figure 4.2](#) shows a schematic of an inside-out approach for ablation of the TM. First, the surgeon tries to recognize the location of the SC using a goniotomy lens over the cornea. Then, they make an incision at the cornea limbus position to insert the microhook. Finally, they commence to ablate part of the TM to allow the fluid inside the eye to exit through the SC, which lowers the IOP inside the eye. To perform such surgical exercises, we designed our eyeball model with an artificial sclera model, including a clear cornea part and 3D microchannel to represent the SC and TM, respectively.



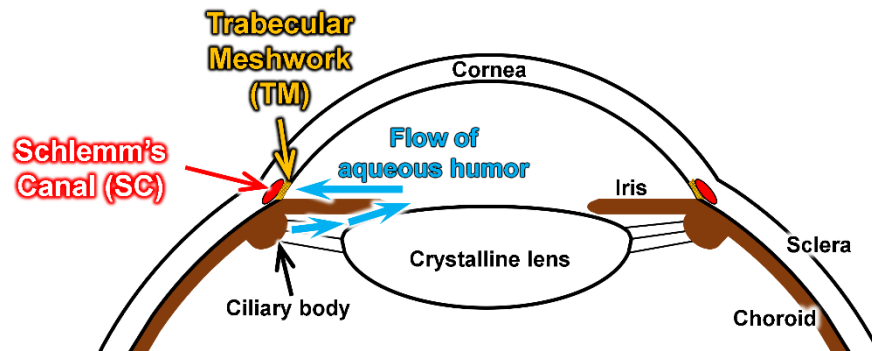


Figure 4.1. Schematic image of angle structure at corneal limbus and flow of aqueous humour in a human eye.

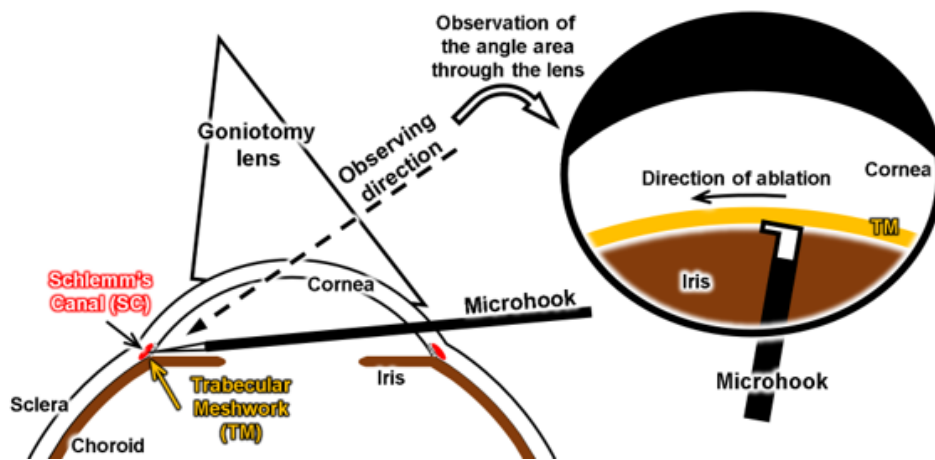


Figure 4.2. Concept of a glaucoma model for training on inside-out (ab interno) surgery.

Here, we discuss how to shape a 3D microchannel on the inner surface of a spherical shell that has a large curvature, representing an eyeball. By casting, we could easily mold the eyeball with a 3D microchannel, which works as an SC, on the curvature surface of the eyeball.


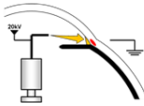
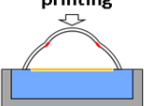
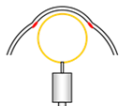
On the other hand, to fabricate an artificial TM with a thickness of 40 to 100  $\mu\text{m}$  on a casted eyeball that has the microchannel, several fabrication methods can be considered, as shown in [Table 4.1](#).

- Dip coating is a method of laminating a thin film onto the surface of a 3D object by immersing the object in a polymer solution. This method makes it somewhat easy to control the film thickness formed over the object. However, we cannot use it because the 3D microchannel on the eyeball, which represents the SC, will become clogged.
- Electrospinning is a method of laminating a thin film with a micron- or submicron-scaled fiber using an electrical force to draw charged threads of polymer solution. This method is expected to allow ample adjustment of the film thickness and have good reproducibility. However, one its major drawbacks is the difficulty in maintaining the groove structure of the SC.
- Hydraulic transfer printing [181] is a method of transferring a thin film over 3D objects. This is done by floating the printed film on water and pressing the 3D object onto the film. Therefore, it is easy to adjust the thickness of the laminated layer, and the reproducibility of the mechanical properties is high. It is also expected that maintaining the groove structure of the SC would be easy. However, this method is difficult to laminate on a concave surface such as the inside of an eyeball model.

- Blow molding is a widely used method in the molding of thin plastic containers. The main feature of this method is its high shape reproducibility even for concave shapes. This method is expected to be able to laminate the thin film covering the 3D microchannel without clogging it.

Therefore, in this study, an artificial TM, which is a lesion on glaucoma models, is achieved by the blow-molding method.

Table 4.1 : Benchmark of fabrication methods to fabricate the artificial trabecular meshwork for a glaucoma model

|  | Dip coating   | Electrospinning   | Hydraulic transfer printing  | Blow molding  |
|--|---|---|--|---|
| Uniformity of thickness                  |  |  |  |  |
| Reproducibility of mechanical properties |   | ✓   | ✓  | ✓   |
| Ease of maintenance of SC tube structure |   |   | ✓  | ✓   |
| Adequateness of thin film forming        |   |   |  | ✓   |

## 4.2.2 Fabrication of the eyeball model

[Figure 4.3](#) shows the design and fabrication process for the eyeball model used in this study, which has a sclera model with a clear cornea and a 3D microchannel, which represents the SC. The thickness of the sclera and cornea, resulted from the casting process, designed to be 1 mm and 0.5 mm respectively to be similar to real tissues. Eye-shape cast molds were made in a precision-machined, three-dimensional mold. Polydimethylsiloxane (PDMS; Sylpot 184; Dow Corning Toray Co. Ltd., Tokyo, Japan) was mixed using a commercial manufacturing process, degassed, and poured into the mold. The polymer was cured by placing the mold in an oven at 120°C for two hours, after which it was removed from the hard mold.

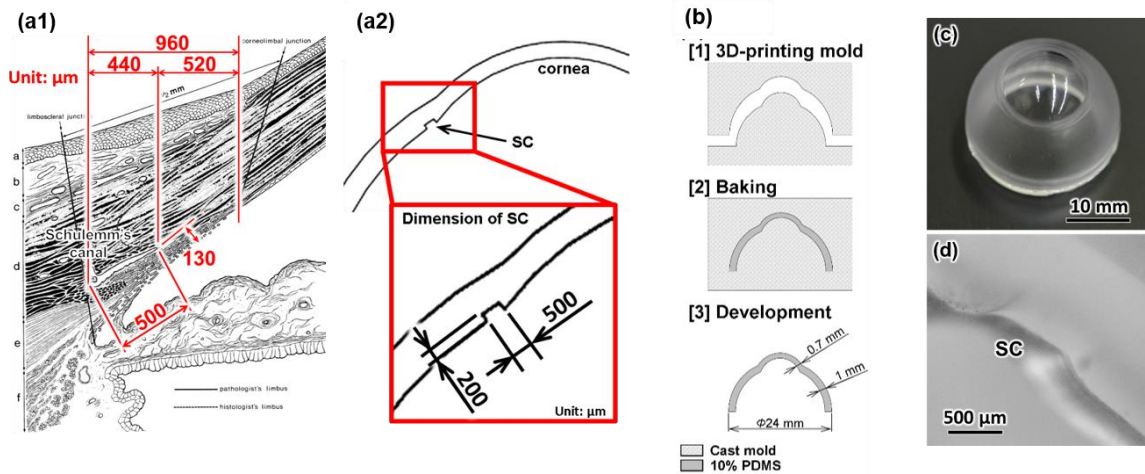


Figure 4.3. (a1) Anatomy of limbus area of human eye; (a2) Design and dimensions of eye model with 3D microchannel as artificial SC; (b) Fabrication process of the eye model with SC; (c) Fabricated eye model made from PDMS; (d) Cross-sectional image of fabricated SC structure of the eye model.

### 4.2.3 Fabrication of the TM

The human TM is a thin membrane with a thickness over wide range of values (40–132  $\mu\text{m}$ ) [212]. [Figure 4.4](#) shows the fabrication process of a TM using the blow-molding method. Polyvinyl chloride (PVC) (molecular weight 230,000, Sigma-Aldrich Co., St. Louis, USA) was the main polymer used in its fabrication. The PVC was dissolved, with a weight concentration of 30%, in a mixture of tetrahydrofuran (THF) (204-08745, Wako Pure Chemical Industries, Osaka, Japan) and N, N-dimethylformamide (DMF) (045-02916, Wako Pure Chemical Industries) (1:1), on hotplate at 95°C for five hours. A syringe with a nozzle diameter of 10 mm was used to create a balloon from the PVC solution. The tip of the nozzle was immersed into the solution, and then the syringe was fed manually until the balloon was formed over the eyeball model.

Plasticizers are compounds that are added to brittle polymers such as PVC. They are expected to reduce the elastic modulus, tensile strength, and hardness of the polymer, while at the same time increasing its flexibility and elongation at breaking [213]. Di-(2-ethylhexyl) phthalate (DEHP) is the most commonly used phthalate plasticizer for plasticizing PVC. To control the mechanical conduct of PVC so that it mimics human tissue, DEHP (022-10815, Wako Pure Chemical Industries, Osaka, Japan) was mixed with the PVC solution at various concentrations. Then, the mechanical behavior of each concentration was tested.

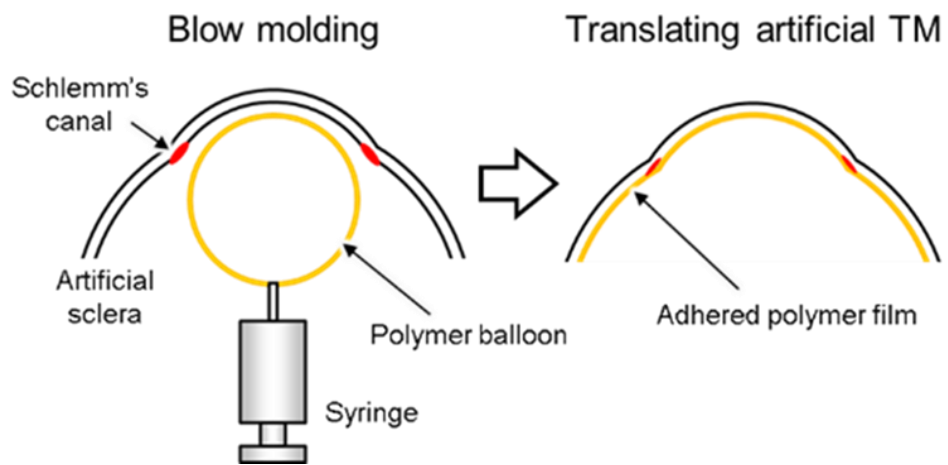


Figure 4.4. Fabrication process of an artificial trabecular meshwork (TM) adhered inside an artificial sclera.

#### 4.2.4 Measurement of the thickness and mechanical properties of TM

To measure the thickness of the fabricated artificial TM over the eyeball model, we sever the eye model and used an optical microscope.

Uniaxial tensile testing was performed to failure with ten specimens tested for each concentration of the fabricated TM. The test specimens were prepared by spin-coating PVC/DEHP solution over a PDMS sheet at room temperature and waiting ten minutes for evaporation of the solvent. The test specimens were cut from the PVC/DEHP membrane (2 mm wide at their narrowest point with a gage length of 25 mm) using a JIS 7-type, dumbbell-shaped template (JIS K 6251) to assure uniformity and isolate the failure point away from the grips. The thickness of each sample was measured using a laser microscope. The uniaxial tensile test was performed on each sample using a tabletop universal testing machine with a 50-N load cell (SHIMADZU) at an extension rate of 10 mm/min.

Polyvinyl chloride, a rubber-like material, has hyperelastic characteristics, showing a nonlinear relationship between the load and deformation. Many attempts have been made to theoretically reproduce the stress–strain curves obtained from experiments on the deformation of highly elastic rubber-like materials [214]. The elasticity (E) of the artificial TM was calculated based on Mooney-Rivlin model [214]. For the case of an incompressible Mooney–Rivlin material, such as the material used in the fabrication of TM, under uniaxial elongation, E is calculated as follow:

$$\sigma = \frac{1}{3}E \left( \lambda - \frac{1}{\lambda^2} \right),$$

where  $\sigma$  represents the uniaxial tensile stress and  $\lambda$  represents the strain ratio, which is defined as  $\lambda = 1 + \varepsilon$  with strain  $\varepsilon \geq 0$ , respectively.

## 4.3 Results

### 4.3.1 Eyeball model

[Figure 4.3c](#) shows the fabricated eyeball model made using PDMS. Polydimethylsiloxane is a popular polymer that has been used in building artificial organ models [215–217]. It has an elastic modulus of 1.32–2.97 MPa [218], very close to that of real sclera tissue (2 MPa) [219]. Moreover, PDMS shows excellent optical transparency. This facilitates a clear visualization of the SC through the cornea using a gonioscope during the surgery simulation. To clarify the structure of the microchannel, which represents the SC, we made a cross section of the eye model. [Figure 4.3d](#) shows the resulting cross-sectional images.

### 4.3.2 Fabrication results of the TM

To confirm the existence of the microchannel after forming the TM, we observed a cross section of the eyeball model. [Figure 4.5](#) shows the cross-sectional images of the eyeball model after the artificial TM was formed. An advantage of blow molding compared with other methods such as electrospinning and hydraulic transfer printing is the reproducibility of the method. Additionally, while using of electrospinning or hydraulic transfer printing methods impede us from getting microchannel without clogging, blowing method enables us to form the TM with maintaining the structure of the microchannel.



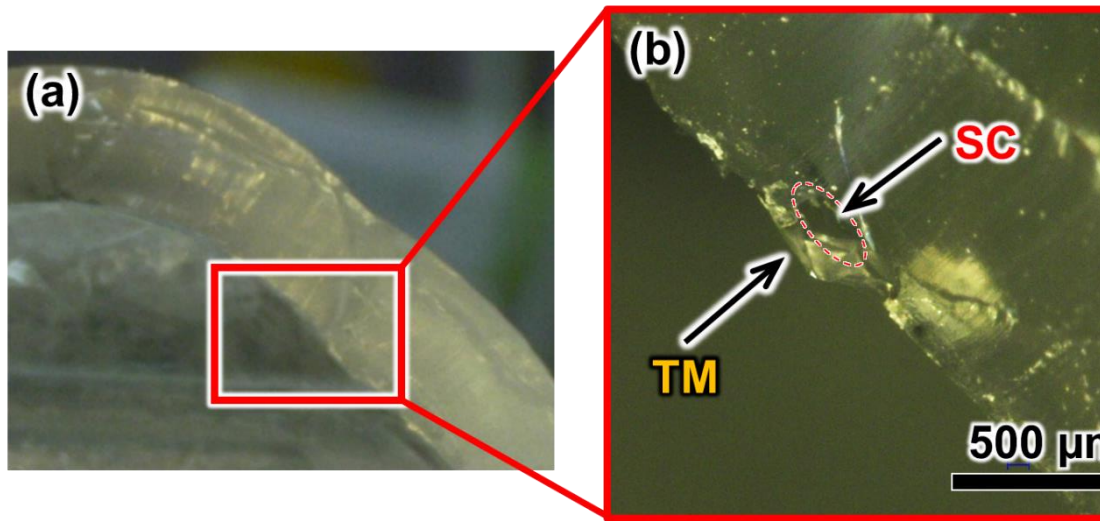


Figure 4.5. Sectional images of the fabricated eye model. (a) Cross-sectional image of the whole eye model. (b) High-magnification image of the angle for the tube structure of the SC covered with artificial TM.

### 4.3.3 Evaluation of the TM thickness

[Figure 4.6](#) shows the measured TM thickness as a function of the PVC concentration. We could control the thickness of the fabricated TM between approximately 20 and 80  $\mu\text{m}$  by adjusting the concentration of PVC to solvent. The thickness of human TM has a wide range of values (40–132  $\mu\text{m}$ ) [212]. Therefore, PVC with a concentration of 30% to 60% should fall within the range of thickness of human TM.

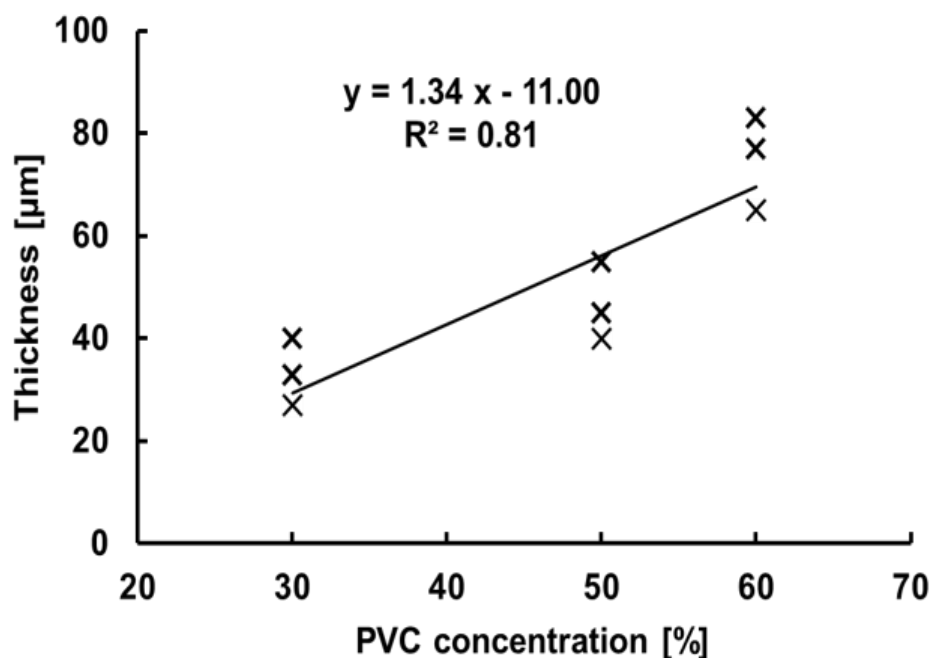


Figure 4.6. Relationship between the concentration of PVC solution and thickness of fabricated artificial trabecular meshwork.

#### 4.3.4 Evaluation of mechanical properties of the TM

The elastic modulus of human TM, in both normal and glaucomatous eyes, was measured in previous studies, and the values were 0.228–1.085 and 3–50 MPa, respectively [220,221]. [Figure 4.7](#) shows the stress–strain behavior of the fabricated TM for various PVC/DEHP ratios. [Table 4.2](#) summarizes the resulting elastic modulus, tensile strength, and strain at breaking for each mixture. We found that the elastic modulus of the PVC/DEHP (100/0) used in the fabrication of the TM is approximately three times the highest elastic modulus value of human TM tissue. By adding DEHP to the PVC solution, the elastic modulus of the fabricated TM can be tuned to match the elastic modulus of the human glaucoma TM. We could easily control the mechanical behavior of the fabricated TM using various concentrations of PVC/DEHP, as shown in [figure 4.8](#). The PVC/DEHP (99.5/0.5 to 98/2) ratio has an elastic modulus that fall within the wide range of elastic moduli of human TM tissue in an eye with glaucoma.

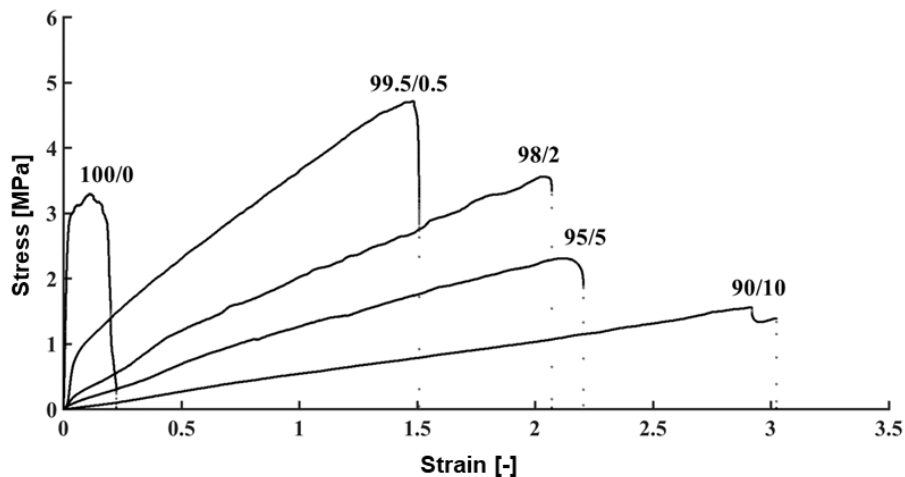


Figure 4.7. Stress–strain behavior of trabecular meshwork model. Numbers indicate the weight ratio of the PVC/DEHP mixture.

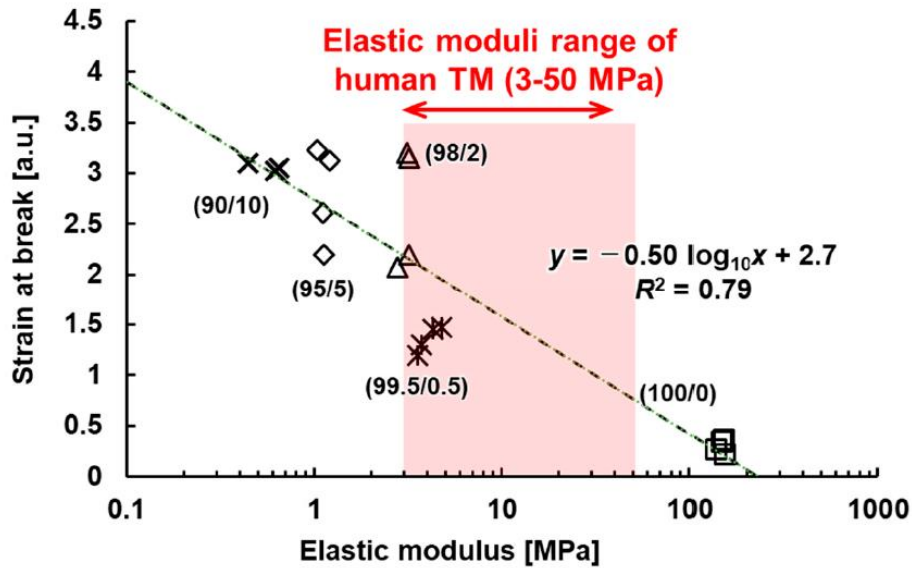


Figure 4.8. Elastic modulus and fracture strain of various concentrations of PVC/DEHP

Table 4.2 : Mechanical properties of PDMS and PVC/DEHP used in this study to replicate sclera and trabecular meshwork tissues, respectively.

| Tissues & Materials          | Elastic Modulus [MPa] | Tensile Strength [MPa] | Strain at Breaking [mm/mm] |
|------------------------------|-----------------------|------------------------|----------------------------|
| <b>Human Tissues</b>         |                       |                        |                            |
| Sclera                       | 2.0 [219]             | —                      | 0.2 [219]                  |
| TM tissue (normal eye)       | 0.2–1.1 [221]         | 2.0 [221]              | 0.06 [221]                 |
| TM tissue (glaucomatous eye) | 3.0–52.6 [220]        | —                      | —                          |
| <b>Artificial Materials</b>  |                       |                        |                            |
| PDMS                         | 1.3–2.9 [218]         | 3.5–7.6 [218]          | —                          |
| PVC/DEHP (100/0)             | 147 ± 6               | 3.0 ± 0.3              | 0.30 ± 0.06                |
| PVC/DEHP (99.5/0.5)          | 4.1 ± 0.5             | 4.0 ± 0.5              | 1.4 ± 0.2                  |
| PVC/DEHP (98/2)              | 3.1 ± 0.2             | 3.6 ± 0.9              | 2.7 ± 0.6                  |
| PVC/DEHP (95/5)              | 1.12 ± 0.06           | 2.3 ± 0.6              | 2.8 ± 0.5                  |
| PVC/DEHP (90/10)             | 0.6 ± 0.1             | 1.6 ± 0.2              | 3.1 ± 0.4                  |

#### 4.3.5 Simulation of surgery with the eye model

[Figure 4.9](#) shows the artificial eye model mounted on the Bionic-EyE™ to make the constraints of the surgery simulation similar to those in a real operation. [Figure 4.10](#) shows photographs and movie of the training with our proposed model. First, the surgeon attempted, using a goniotomy lens over the cornea, to identify the location of the SC. Then, an incision was made at the cornea limbus position to insert the microhook. Finally, the surgeon could embark to ablate part of the TM.

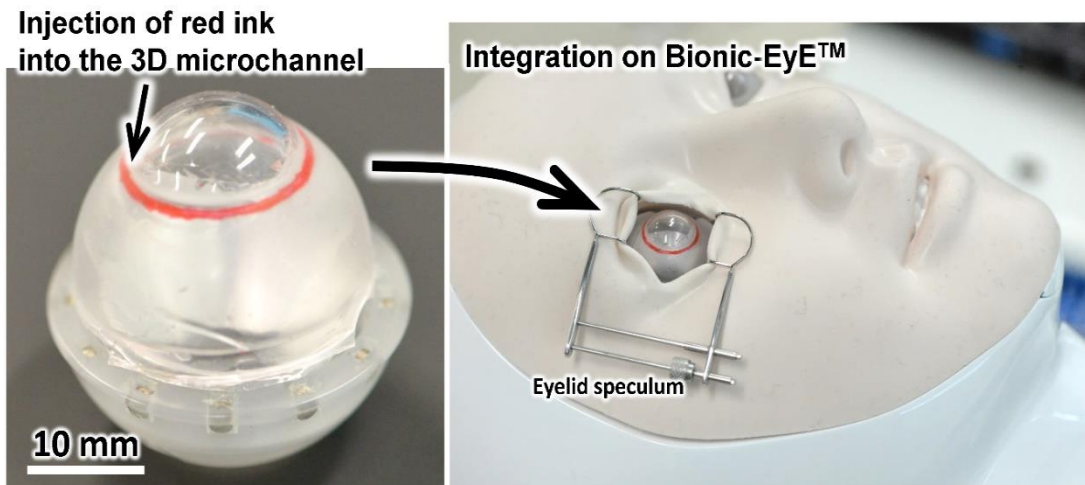


Figure 4.9. Photographs of the eye model installed on the Bionic-EyE™ for simulation of micro invasive glaucoma surgery.

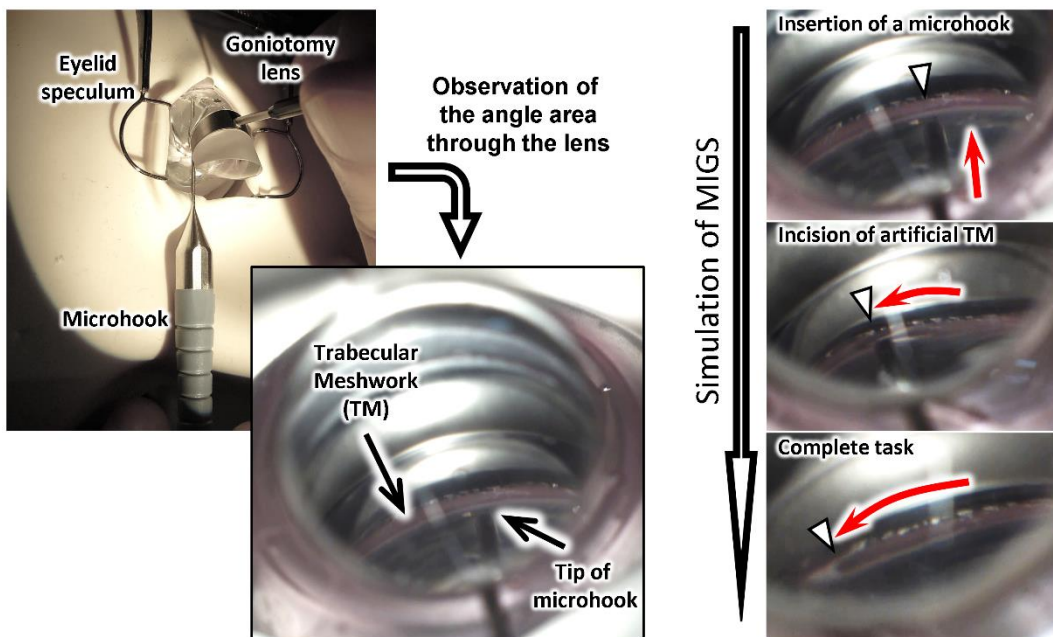


Figure 4.10. Photographs from the training of the micro-invasive glaucoma surgery with a microhook.

#### 4.4 Discussion

We developed a simple technique to fabricate a 3D microchannel over a spherical shape, such as an eyeball. Additionally, we used a blow molding method to fabricate a thin membrane covering the 3D microchannel to represent the TM. We applied these techniques to fabricate an eye surgery simulator that comprised a sclera with a clear cornea and 3D microchannel to represent the SC and TM to simulate an ab interno approach, a kind of MIGS. The proposed eye surgery simulator accurately represents the eye's shape and important anatomical structures, such as the SC and TM. The proposed fabrication methods, the 3D model made from a precision-machined, three-dimensional mold combined with polymer-molding and the blow-molding process used for the eyeball and TM exhibited several advantages: (1) a complex 3D microchannel, representing the SC, can be accurately produced with our proposed method; and (2) it allows the use of a wide variety of materials, e.g., transparent materials and soft ones that mimic human tissues. In fact, using the proposed fabrication methods, we succeeded in fabricating an eyeball and TM with mechanical properties that approach those of human tissues. Moreover, the blow-molding method enabled us to fabricate a TM over the spherical shape of the eye with a thickness that could be controlled to that of real tissue.

The proposed eye model reported herein exhibited several advantages compared with animal models, such as reproducibility and longer durability. The simulator has been designed to duplicate, as closely as possible, the MIGS procedures encountered in clinical situations. These features are introduced through the proposed fabrication methods used in making the simulator. The proposed eye surgery simulator would facilitate the education of novice

surgeons, allowing them to learn and practice basic skills for MIGS procedures while being evaluated objectively by an instructor.

One drawback of current fabrication methods is the syringe used in the blow-molding of the TM is fed manually. Therefore, even when we used the same concentration of PVC, the resulting thickness of the fabricated TM could have fairly large deviation, depending on the diameter of the balloon produced each time. However, from our TM measurements using the designed concentration ratio, the resulting thickness still fell within the range of human tissue, as shown in figure 4.6.

The proposed model and the materials used in their fabrication may not perfectly represent all of the mechanical properties of human tissues (e.g., they exhibit higher tensile strengths and breaking strain values), as summarized in Table 4.2. However, they serve as examples to validate that the fabrication methods reported in this paper and various polymer materials and their mixtures can be used. Furthermore, the proposed eye model and the current materials used in their fabrication would allow novice surgeons to learn the basic skills of the surgery. A preliminary assessment of the proposed model was performed with experienced surgeons, as shown in figures 4.9 and 4.10. A preliminary assessment revealed that the model could help novice eye doctors learn the basic skills of the surgery. Therefore, we succeeded in developing a novel training model for glaucoma surgery.

In the future, to obtain more similar characteristics, we will conduct a face validity study and ameliorate the material properties.



## 4.5 Summary

Simple techniques to fabricate a 3D microchannel and fabricate a thin membrane over a spherical shape were developed. Using these methods, 3D models were made using a precision-machined, three-dimensional mold. Additionally, using polymer molding and blow-molding methods, an eye model comprising a sclera with a clear cornea and 3D microchannel, which represent the SC, and TM was built. These methods are versatile because they replicate anatomical details with submillimeter resolution and permit a wide range of materials to be used. Additionally, we succeeded in installing the MIGS model into the Bionic-EyE™ and operated similar to an actual surgery. The proposed model can be used as a simulator for training novice surgeons on MIGS. A preliminary assessment by eye doctors showed that the model can help novice eye doctors to develop the basic skills of the surgery. We foresee a number of applications for the proposed eye model, besides simulation and training for the surgery, including medical device testing and surgical planning.

## **CHAPTER 5**

### **Conclusions and Future Outlook**

This chapter begins with the synopsis of the objectives that have been accomplished in this research. Then, potential future work is suggested for continuing the research.

#### **5.1 Conclusions**

This thesis presents the development of rapid fabrication techniques for the fabrication of 3D microchannel that emulates the natural shape of human blood vessel. Then, an eye surgery training simulator was developed, which has a 3D microchannel that represents SC, sclera with clear cornea and trabecular meshwork that cover the microchannel, as surgical simulator for glaucoma surgery. The detailed information is as follow;

Firstly, Chapter 1 provides a literature review of surgical simulation systems, with their advantages and disadvantages, are currently being used for surgery training and evaluation of medical devices. Then, we discussed the recent

advancement and progression of synthetic 3D models that are using as simulators for different medical applications.

In chapter 3, with the goal of creating micrometer-scale blood vessel models, we proposed 3D microchannel fabricated using photolithography and FME<sub>x</sub>. Photolithography with water transfer printing onto a 3D-printed model enabled us to quickly fabricate a 3D microscopic vessel with different depths and a large model size. The femtosecond laser exposure made it possible to fabricate part of the millimeter-scale structure with a submicrometer resolution in 3D. Also, we succeeded in obtaining a smooth surface independent of the minimum scanning line width of femtosecond laser exposure by using a chemically amplified resist that triggers acid diffusion. The acid diffusion phenomenon was essential for achieving a model with a smooth surface and circular cross-section. With the proposed FME<sub>x</sub> method, we can create 3D capillary vessel models that realistically mimic blood vessels. Our proposed methods can make an important contribution to the medical field and create an alternative to the use of animals for surgical training.

Then, in chapter 4, simple techniques to fabricate a 3D microchannel and a thin membrane over a spherical shape were developed. Using these methods, 3D models were made using a precision-machined, three-dimensional mold. Additionally, using polymer molding and blow-molding methods, an eye model comprising a sclera with a clear cornea and 3D microchannel, which represent the SC, and TM was built. These methods are versatile because they replicate anatomical details with submillimetre resolution and permit a wide range of materials to be used. Additionally, we succeeded in installing the MIGS model into the Bionic-EyE™ and operated similar to an actual surgery.

The proposed model can be used as a simulator for training novice surgeons on MIGS. A preliminary assessment by eye doctors showed that the model can help novice eye doctors to develop the basic skills of the surgery.

## **5.2 Future Outlook**

This thesis has developed an eye model with 3D microchannel, that simulate SC, and the important needed tissues, such as sclera and trabecular meshwork, having mechanical properties similar to human tissues, as an imitation model for glaucoma surgery. However, further optimisation of the fabrication methods and the materials used for the fabrication of model is required to give a higher performance for surgical training, implantable, tissue engineering applications. Certain suggestions for future research and progression are presented in the following sections.

### **5.2.1 For surgical training and planning applications**

One of the features that is lacked in the current synthetic model for surgical planning and training applications, is that it does not imitate the dynamic environments of the organ, such as pulsation in the blood vessels. In other words, it can be considered as a static synthetic model. Therefore, for more realistic simulation of the organ for the surgical training and rehearsal applications, implementation of such these dynamic features in the synthetic model are needed.

Another feature that is lacked in the model, is the sensors that could be embedded within the model for achieving a quantitative data about the performance of the surgeons. For better evaluation of surgeons' performance and for evaluation of assistant robotic systems used in the surgery, integration of the electronic devices, such as sensors, into the artificial models, to get a

quantitative feedback about surgeon's fulfilment, is in high demand. For example, for amelioration of the performance of novice surgeons, on performing a specific procedures of a surgery, we need to know the data of actions that performed by expert surgeons on the artificial tissues, such as forces exerted on the tissues, to compare it with actions of novices. Therefore, novice surgeons can improve and modify their performance based on the data achieved.

### **5.2.2 For tissue engineering and implantation applications**

Cardiovascular malady remains the leading cause of death in the world. In deep, coronary artery vessel is accounting more than 50% of the cardiovascular diseases. The golden remedy coronary artery vessel blockage is blood vessel bybass graft. The ideal biomimetic blood vessel model, which can be used for this treatment, should has good mechanical properties, mimic the real blood vessel, for long-term functionality. Moreover, the model should not hinder cell infiltration while promoting cell adhesion and proliferation. Therefore, more researches for using a combination of natural and synthetic polymers together, to produce a biomimetic small diameter vascular blood vessel, are required. For instance, adding collagen boost the biocompatibility of the biomimetic blood vessel and can naturally mimic the extracellular matrix, so himybrid materials of natural and synthetic polymers should be investigated for the production of biomimetic blood vessels.

## Bibliography

1. Rose, J.; Chang, D.C.; Weiser, T.G.; Kassebaum, N.J.; Bickler, S.W. The role of surgery in global health: analysis of United States inpatient procedure frequency by condition using the Global Burden of Disease 2010 framework. *PLoS One* **2014**, *9*, e89693.
2. Entezami, P.; Franzblau, L.E.; Chung, K.C. Mentorship in surgical training: a systematic review. *Hand* **2012**, *7*, 30–36.
3. Cloyd, J.; Holtzman, D.; O'Sullivan, P.; Sammann, A.; Tendick, F.; Ascher, N. Operating room assist: surgical mentorship and operating room experience for preclerkship medical students. *J. Surg. Educ.* **2008**, *65*, 275–282.
4. Cohen, M.S.; Jacobs, J.P.; Quintessenza, J.A.; Chai, P.J.; Lindberg, H.L.; Dickey, J.; Ungerleider, R.M. Mentorship, learning curves, and balance. *Cardiol. Young* **2007**, *17*, 164–174.
5. Randleman, J.B.; Wolfe, J.D.; Woodward, M.; Lynn, M.J.; Cherwek, D.H.; Srivastava, S.K. The resident surgeon phacoemulsification learning curve. *Arch. Ophthalmol.* **2007**, *125*, 1215–1219.
6. Lee, J.-S.; Hou, C.-H.; Yang, M.-L.; Kuo, J.Z.C.; Lin, K.-K. A different approach to assess resident phacoemulsification learning curve: analysis of both completion and complication rates. *Eye* **2009**, *23*, 683.
7. Taravella, M.J.; Davidson, R.; Erlanger, M.; Guiton, G.; Gregory, D. Characterizing the learning curve in phacoemulsification. *J. Cataract*

- Refract. Surg.* **2011**, *37*, 1069–1075.
8. Tarbet, K.J.; Mamalis, N.; Theurer, J.; Jones, B.D.; Olson, R.J. Complications and results of phacoemulsification performed by residents. *J. Cataract Refract. Surg.* **1995**, *21*, 661–665.
  9. Bell, C.M.; Hatch, W. V; Cernat, G.; Urbach, D.R. Surgeon volumes and selected patient outcomes in cataract surgery: a population-based analysis. *Ophthalmology* **2007**, *114*, 405–410.
  10. Bhagat, N.; Nissirios, N.; Potdevin, L.; Chung, J.; Lama, P.; Zarbin, M.A.; Fechtner, R.; Guo, S.; Chu, D.; Langer, P. Complications in resident-performed phacoemulsification cataract surgery at New Jersey Medical School. *Br. J. Ophthalmol.* **2007**, *91*, 1315–1317.
  11. Corey, R.P.; Olson, R.J. Surgical outcomes of cataract extractions performed by residents using phacoemulsification. *J. Cataract Refract. Surg.* **1998**, *24*, 66–72.
  12. Randleman, J.B.; Srivastava, S.K.; Aaron, M.M. Phacoemulsification with topical anesthesia performed by resident surgeons. *J. Cataract Refract. Surg.* **2004**, *30*, 149–154.
  13. Narendran, N.; Jaycock, P.; Johnston, R.L.; Taylor, H.; Adams, M.; Tole, D.M.; Asaria, R.H.; Galloway, P.; Sparrow, J.M. The Cataract National Dataset electronic multicentre audit of 55 567 operations: risk stratification for posterior capsule rupture and vitreous loss. *Eye* **2009**, *23*, 31.
  14. Carricondo, P.C.; Fortes, A.C.F.M.; Mourão, P. de C.; Hajnal, M.; Jose, N.K. Senior resident phacoemulsification learning curve. *Arq. Bras. Oftalmol.* **2010**, *73*, 66–69.
  15. Hashemi, H.; Mohammadpour, M.; Jabbarvand, M.; Nezamdoost, Z.; Ghadimi, H. Incidence of and risk factors for vitreous loss in resident-

- performed phacoemulsification surgery. *J. Cataract Refract. Surg.* **2013**, 39, 1377–1382.
16. Rutar, T.; Porco, T.C.; Naseri, A. Risk factors for intraoperative complications in resident-performed phacoemulsification surgery. *Ophthalmology* **2009**, 116, 431–436.
  17. Teus, M.A.; de Benito-Llopis, L.; Sánchez-Pina, J.M. Learning curve of laser-assisted subepithelial keratectomy: influence on visual and refractive results. *J. Cataract Refract. Surg.* **2007**, 33, 1381–1385.
  18. Kwong, A.; Law, S.K.; Kule, R.R.; Nouri-Mahdavi, K.; Coleman, A.L.; Caprioli, J.; Giacconi, J.A. Long-term outcomes of resident-versus attending-performed primary trabeculectomy with mitomycin C in a United States residency program. *Am. J. Ophthalmol.* **2014**, 157, 1190–1201.
  19. Reznick, R.K.; MacRae, H. Teaching surgical skills changes in the wind. *N. Engl. J. Med.* **2006**, 355, 2664–2669.
  20. Matsuoka, Y.; Howe, R.D. Robotics for surgery. *Annu. Rev. Biomed. Eng* **1999**, 1, 211–240.
  21. Davies, B. A review of robotics in surgery. *Proc. Inst. Mech. Eng. Part H J. Eng. Med.* **2000**, 214, 129–140.
  22. Dario, P.; Menciassi, A. Robotics for surgery. In Proceedings of the Proceedings of the Second Joint 24th Annual Conference and the Annual Fall Meeting of the Biomedical Engineering Society][Engineering in Medicine and Biology; 2002; Vol. 3, pp. 1813–1814.
  23. Jacob, B.P.; Gagner, M. Robotics and general surgery. *Surg. Clin. North Am.* **2003**, 83, 1405–1419.
  24. Varkarakis, I.M.; Rais-Bahrami, S.; Kavoussi, L.R.; Stoianovici, D. Robotic surgery and telesurgery in urology. *Urology* **2005**, 65, 840–846.



25. Lanfranco, A.R.; Castellanos, A.E.; Desai, J.P.; Meyers, W.C. Robotic surgery: a current perspective. *Ann. Surg.* **2004**, *239*, 14.
26. Dharia, S.P.; Falcone, T. Robotics in reproductive medicine. *Fertil. Steril.* **2005**, *84*, 1–11.
27. Guyton, S.W. Robotic surgery: the computer-enhanced control of surgical instruments. *Otolaryngol. Clin. North Am.* **2002**, *35*, 1303–1316.
28. Kwoh, Y.S.; Hou, J.; Jonckheere, E.A.; Hayati, S. A robot with improved absolute positioning accuracy for CT guided stereotactic brain surgery. *IEEE Trans. Biomed. Eng.* **1988**, *35*, 153–160.
29. Kim, V.B.; Chapman Iii, W.H.H.; Albrecht, R.J.; Bailey, B.M.; Young, J.A.; Nifong, L.W.; Chitwood Jr, W.R. Early experience with telemanipulative robot-assisted laparoscopic cholecystectomy using da Vinci. *Surg. Laparosc. Endosc. Percutaneous Tech.* **2002**, *12*, 33–40.
30. Bargar, W.L.; Bauer, A.; Börner, M. Primary and Revision Total Hip Replacement Using the Robodoc (R) System. *Clin. Orthop. Relat. Res.* **1998**, *354*, 82–91.
31. Unger, S.W.; Unger, H.M.; Bass, R.T. AESOP robotic arm. *Surg. Endosc.* **1994**, *8*, 1131.
32. Rininsland, H.H. Basics of robotics and manipulators in endoscopic surgery. *Endosc. Surg. Allied Technol.* **1993**, *1*, 154–159.
33. Taylor, R.H.; Funda, J.; Eldridge, B.; Gomory, S.; Gruben, K.; LaRose, D.; Talamini, M.; Kavoussi, L.; Anderson, J. A telerobotic assistant for laparoscopic surgery. *IEEE Eng. Med. Biol. Mag.* **1995**, *14*, 279–288.
34. Ballantyne, G.H. Robotic surgery, telerobotic surgery, telepresence, and telementoring. *Surg. Endosc. Other Interv. Tech.* **2002**, *16*, 1389–1402.
35. Satava, R.M. Surgical robotics: the early chronicles: a personal historical perspective. *Surg. Laparosc. Endosc. Percutaneous Tech.* **2002**, *12*, 6–16.

36. Kwon, D.-S.; Woo, K.Y.; Song, S.K.; Kim, W.S.; Cho, H.S. Microsurgical telerobot system. In Proceedings of the Proceedings. 1998 IEEE/RSJ International Conference on Intelligent Robots and Systems. Innovations in Theory, Practice and Applications (Cat. No. 98CH36190); 1998; Vol. 2, pp. 945–950.
37. Taylor, R.; Jensen, P.; Whitcomb, L.; Barnes, A.; Kumar, R.; Stoianovici, D.; Gupta, P.; Wang, Z.; Dejuan, E.; Kavoussi, L. A steady-hand robotic system for microsurgical augmentation. *Int. J. Rob. Res.* **1999**, *18*, 1201–1210.
38. Kumar, R.; Berkelman, P.; Gupta, P.; Barnes, A.; Jensen, P.S.; Whitcomb, L.L.; Taylor, R.H. Preliminary experiments in cooperative human/robot force control for robot assisted microsurgical manipulation. In Proceedings of the Proceedings 2000 ICRA. Millennium Conference. IEEE International Conference on Robotics and Automation. Symposia Proceedings (Cat. No. 00CH37065); 2000; Vol. 1, pp. 610–617.
39. Mitchell, B.; Koo, J.; Iordachita, I.; Kazanzides, P.; Kapoor, A.; Handa, J.; Hager, G.; Taylor, R. Development and application of a new steady-hand manipulator for retinal surgery. In Proceedings of the Proceedings 2007 IEEE International Conference on Robotics and Automation; 2007; pp. 623–629.
40. Hannaford, B.; Marbot, P.-H.; Moreyra, M.; Venema, S. A 5-axis mini direct drive robot for time delayed teleoperation. In Proceedings of the Proceedings of IEEE/RSJ International Conference on Intelligent Robots and Systems (IROS'94); 1994; Vol. 1, pp. 555–562.
41. Hunter, I.W.; Doukoglou, T.D.; Lafontaine, S.R.; Charette, P.G.; Jones, L.A.; Sagar, M.A.; Mallinson, G.D.; Hunter, P.J. A teleoperated microsurgical robot and associated virtual environment for eye surgery.

- Presence Teleoperators Virtual Environ.* **1993**, 2, 265–280.
42. Salcudean, S.E.; Yan, J. Towards a Force-Reflecting Motion-Scaling System for Microsurgery. In Proceedings of the IEEE International Conference On Robotics and Automation; 1993; Vol. 1, p. 2296.
  43. Tanikawa, T.; Arai, T.; Masuda, T. Development of micro manipulation system with two-finger micro hand. In Proceedings of the Proceedings of IEEE/RSJ International Conference on Intelligent Robots and Systems. IROS'96; 1996; Vol. 2, pp. 850–855.
  44. Fleming, I.; Balicki, M.; Koo, J.; Iordachita, I.; Mitchell, B.; Handa, J.; Hager, G.; Taylor, R. Cooperative robot assistant for retinal microsurgery. In Proceedings of the International conference on medical image computing and computer-assisted intervention; 2008; pp. 543–550.
  45. Ida, Y.; Sugita, N.; Ueta, T.; Tamaki, Y.; Tanimoto, K.; Mitsuishi, M. Microsurgical robotic system for vitreoretinal surgery. *Int. J. Comput. Assist. Radiol. Surg.* **2012**, 7, 27–34.
  46. Cianchetti, M.; Laschi, C.; Menciassi, A.; Dario, P. Biomedical applications of soft robotics. *Nat. Rev. Mater.* **2018**, 3, 143.
  47. Yang, G.-Z.; Bellingham, J.; Dupont, P.E.; Fischer, P.; Floridi, L.; Full, R.; Jacobstein, N.; Kumar, V.; McNutt, M.; Merrifield, R.; et al. The grand challenges of Science Robotics. *Sci. Robot.* **2018**, 3, eaar7650.
  48. Runciman, M.; Darzi, A.; Mylonas, G.P. Soft Robotics in Minimally Invasive Surgery. *Soft Robot.* **2019**.
  49. Nelson, B.J.; Kaliakatsos, I.K.; Abbott, J.J. Microrobots for minimally invasive medicine. *Annu. Rev. Biomed. Eng.* **2010**, 12, 55–85.
  50. Huang, T.-Y.; Sakar, M.S.; Mao, A.; Petruska, A.J.; Qiu, F.; Chen, X.-B.; Kennedy, S.; Mooney, D.; Nelson, B.J. 3D printed microtransporters: Compound micromachines for spatiotemporally controlled delivery of

- therapeutic agents. *Adv. Mater.* **2015**, *27*, 6644–6650.
51. Kim, Y.; Parada, G.A.; Liu, S.; Zhao, X. Ferromagnetic soft continuum robots. *Sci. Robot.* **2019**, *4*, eaax7329.
  52. Sutherland, L.M.; Middleton, P.F.; Anthony, A.; Hamdorf, J.; Cregan, P.; Scott, D.; Maddern, G.J. Surgical simulation: a systematic review. *Ann. Surg.* **2006**, *243*, 291.
  53. Valentine, R.; Padhye, V.; Wormald, P.-J. Simulation training for vascular emergencies in endoscopic sinus and skull base surgery. *Otolaryngol. Clin. North Am.* **2016**, *49*, 877–887.
  54. Dawson, D.L.; Meyer, J.; Lee, E.S.; Pevec, W.C. Training with simulation improves residents endovascular procedure skills. *J. Vasc. Surg.* **2007**, *45*, 149–154.
  55. Grantcharov, T.P.; Kristiansen, V.B.; Bendix, J.; Bardram, L.; Rosenberg, J.; Funch-Jensen, P. Randomized clinical trial of virtual reality simulation for laparoscopic skills training. *Br. J. Surg.* **2004**, *91*, 146–150.
  56. Issenberg, S.B.; McGaghie, W.C.; Hart, I.R.; Mayer, J.W.; Felner, J.M.; Petrusa, E.R.; Waugh, R.A.; Brown, D.D.; Safford, R.R.; Gessner, I.H.; et al. Simulation technology for health care professional skills training and assessment. *Jama* **1999**, *282*, 861–866.
  57. Satava, R.M. Accomplishments and challenges of surgical simulation. *Surg. Endosc.* **2001**, *15*, 232–241.
  58. Stadie, A.T.; Kockro, R.A.; Reisch, R.; Tropine, A.; Boor, S.; Stoeter, P.; Perneczky, A. Virtual reality system for planning minimally invasive neurosurgery. *J. Neurosurg.* **2008**, *108*, 382–394.
  59. Torkington, J.; Smith, S.G.; Rees, B.I.; Darzi, A. The role of simulation in surgical training. *Ann. R. Coll. Surg. Engl.* **2000**, *82*, 88.
  60. Sarker, S.K.; Patel, B. Simulation and surgical training. *Int. J. Clin. Pract.*

- 2007, 61, 2120–2125.
61. Satava, R.M. Surgical education and surgical simulation. *World J. Surg.* **2001**, 25, 1484–1489.
  62. Evgeniou, E.; Loizou, P. Simulation-based surgical education. *ANZ J. Surg.* **2013**, 83, 619–623.
  63. Dent, J.A. Current trends and future implications in the developing role of clinical skills centres. *Med. Teach.* **2001**, 23, 483–489.
  64. Maran, N.J.; Glavin, R.J. Low-to high-fidelity simulation--a continuum of medical education? *Med. Educ.* **2003**, 37, 22–28.
  65. Ramphal, P.S.; Coore, D.N.; Craven, M.P.; Forbes, N.F.; Newman, S.M.; Coye, A.A.; Little, S.G.; Silvera, B.C. A high fidelity tissue-based cardiac surgical simulator. *Eur. J. cardio-thoracic Surg.* **2005**, 27, 910–916.
  66. Hamstra, S.J.; Brydges, R.; Hatala, R.; Zendejas, B.; Cook, D.A. Reconsidering fidelity in simulation-based training. *Acad. Med.* **2014**, 89, 387–392.
  67. Munshi, F.; Lababidi, H.; Alyousef, S. Low-versus high-fidelity simulations in teaching and assessing clinical skills. *J. Taibah Univ. Med. Sci.* **2015**, 10, 12–15.
  68. Anastakis, D.J.; Regehr, G.; Reznick, R.K.; Cusimano, M.; Murnaghan, J.; Brown, M.; Hutchison, C. Assessment of technical skills transfer from the bench training model to the human model. *Am. J. Surg.* **1999**, 177, 167–170.
  69. Supe, A.; Dalvi, A.; Prabhu, R.; Kantharia, C.; Bhuiyan, P. Cadaver as a model for laparoscopic training. *INDIAN J. Gastroenterol.* **2005**, 24, 111.
  70. Dunnington, G.L. A model for teaching sentinel lymph node mapping and excision and axillary lymph node dissection. *J. Am. Coll. Surg.* **2003**, 197, 119–121.

71. Oram, O.; Gross, R.L.; Severin, T.D.; Feldman, R.M.; Orengo-Nania, S. A human cadaver eye model for anterior and posterior segment laser applications. *Ophthalmic Surgery, Lasers Imaging Retin.* **1994**, *25*, 449–451.
72. Carey, J.N.; Rommer, E.; Sheckter, C.; Minneti, M.; Talving, P.; Wong, A.K.; Garner, W.; Urata, M.M. Simulation of plastic surgery and microvascular procedures using perfused fresh human cadavers. *J. Plast. Reconstr. Aesthetic Surg.* **2014**, *67*, e42--e48.
73. Aboud, E.T.; Krisht, A.F.; O'Keeffe, T.; Nader, R.; Hassan, M.; Stevens, C.M.; Ali, F.; Luchette, F.A. Novel simulation for training trauma surgeons. *J. Trauma Acute Care Surg.* **2011**, *71*, 1484–1490.
74. Garrett Jr, H.E. A human cadaveric circulation model. *J. Vasc. Surg.* **2001**, *33*, 1128–1130.
75. Aboud, E.; Al-Mefty, O.; Ya \csargil, M.G. New laboratory model for neurosurgical training that simulates live surgery. *J. Neurosurg.* **2002**, *97*, 1367–1372.
76. Borirak-chanyavat, S.; Lindquist, T.D.; Kaplan, H.J. A cadaveric eye model for practicing anterior and posterior segment surgeries. *Ophthalmology* **1995**, *102*, 1932–1935.
77. Patel, S.P.; Sit, A.J. A practice model for trabecular meshwork surgery. *Arch. Ophthalmol.* **2009**, *127*, 311.
78. Carey, J.N.; Caldwell, A.M.; Coughlin, R.R.; Hansen, S. Building orthopaedic trauma capacity: IGOT international SMART course. *J. Orthop. Trauma* **2015**, *29*, S17--S19.
79. Imakuma, E.S.; Ussami, E.Y.; Meyer, A. Laparoscopic training model using fresh human cadavers without the establishment of penumoperitoneum. *J. Minim. Access Surg.* **2016**, *12*, 190.
80. Wagh, M.S.; Waxman, I. Animal models for endoscopic simulation.

*Gastrointest. Endosc. Clin. N. Am.* **2006**, *16*, 451–456.

81. Hedlund, C.S.; Hosgood, G.; Naugler, S. Surgical education: attitudes toward animal use in teaching surgery at Louisiana State University. *J. Vet. Med. Educ.* **2002**, *29*, 50–55.
82. Gaarder, C.; Naess, P.A.; Buanes, T.; Pillgram-Larsen, J. Advanced surgical trauma care training with a live porcine model. *Injury* **2005**, *36*, 718–724.
83. DeMasi, S.C.; Katsuta, E.; Takabe, K. Live animals for preclinical medical student surgical training. *Edorium J. Surg.* **2016**, *3*, 24.
84. Ueta, T.; Yamaguchi, Y.; Shirakawa, Y.; Nakano, T.; Ideta, R.; Noda, Y.; Morita, A.; Mochizuki, R.; Sugita, N.; Mitsuishi, M.; et al. Robot-assisted vitreoretinal surgery: Development of a prototype and feasibility studies in an animal model. *Ophthalmology* **2009**, *116*, 1538–1543.
85. Gwon, A. The rabbit in cataract/IOL surgery. In *Animal models in eye research*; Elsevier, 2008; pp. 184–204.
86. Mohammadi, S.F.; Mazouri, A.; Jabbarvand, M.; Rahman-A, N.; Mohammadi, A. Sheep practice eye for ophthalmic surgery training in skills laboratory. *J. Cataract Refract. Surg.* **2011**, *37*, 987–991.
87. Gressel, M.G.; Parrish II, R.K.; Folberg, R. 5-fluorouracil and glaucoma filtering surgery: I. An animal model. *Ophthalmology* **1984**, *91*, 378–383.
88. Tan, S.S.Y.; Sarker, S.K. Simulation in surgery: a review. *Scott. Med. J.* **2011**, *56*, 104–109.
89. Parra-Blanco, A.; González, N.; González, R.; Ortiz-Fernández-Sordo, J.; Ordieres, C. Animal models for endoscopic training: do we really need them? *Endoscopy* **2013**, *45*, 478–484.
90. Shurey, S.; Akelina, Y.; Legagneux, J.; Malzone, G.; Jiga, L.; Ghanem, A.M. The rat model in microsurgery education: classical exercises and

- new horizons. *Arch. Plast. Surg.* **2014**, *41*, 201.
91. Vázquez-Sequeiros, E.; de Miguel, D.B.; Foruny Olcina, J.R.; Gonzalez Martin, J.A.; Garcia, M.; Juzgado Lucas, D.; Garrido, E.; González, C.; Parra Blanco, A.; Arnau, M.R.; et al. Training model for teaching endoscopic submucosal dissection of gastric tumors. *Rev. Esp. Enfermedades Dig.* **2009**, *101*, 546.
  92. Fritscher-Ravens, A.; Cuming, T.; Dhar, S.; Parupudi, S.V.J.; Patel, K.; Ghanbari, A.; Holland, C.; Hadel, K.G.; Arlt, A.; Ellrichmann, M. Endoscopic ultrasound-guided fine needle aspiration training: evaluation of a new porcine lymphadenopathy model for in vivo hands-on teaching and training, and review of the literature. *Endoscopy* **2013**, *45*, 114–120.
  93. Cisler, J.J.; Martin, J.A. Logistical considerations for endoscopy simulators. *Gastrointest. Endosc. Clin.* **2006**, *16*, 565–575.
  94. Hochberger, J.; Maiss, J. Currently available simulators: ex vivo models. *Gastrointest. Endosc. Clin.* **2006**, *16*, 435–449.
  95. Ianacone, D.C.; Gnadt, B.J.; Isaacson, G. Ex vivo ovine model for head and neck surgical simulation. *Am. J. Otolaryngol.* **2016**, *37*, 272–278.
  96. Bauer, F.; Rommel, N.; Kreutzer, K.; Weitz, J.; Wagenpfeil, S.; Gulati, A.; Wolff, K.-D.; Kesting, M.R. A novel approach to teaching surgical skills to medical students using an ex vivo animal training model. *J. Surg. Educ.* **2014**, *71*, 459–465.
  97. Spiteri, A. V; Aggarwal, R.; Kersey, T.L.; Sira, M.; Benjamin, L.; Darzi, A.W.; Bloom, P.A. Development of a virtual reality training curriculum for phacoemulsification surgery. *Eye* **2014**, *28*, 78.
  98. Coleman, J.; Nduka, C.C.; Darzi, A. Virtual reality and laparoscopic surgery. *Br. J. Surg.* **1994**, *81*, 1709–1711.



99. Towers, A.; Field, J.; Stokes, C.; Maddock, S.; Martin, N. A scoping review of the use and application of virtual reality in pre-clinical dental education. *Br. Dent. J.* **2019**, *226*, 358–366.
100. Verma, D.; Wills, D.; Verma, M. Virtual reality simulator for vitreoretinal surgery. *Eye* **2003**, *17*, 71.
101. Kozak, I.; Banerjee, P.; Luo, J.; Luciano, C. Virtual reality simulator for vitreoretinal surgery using integrated OCT data. *Clin. Ophthalmol. (Auckland, NZ)* **2014**, *8*, 669.
102. Aggarwal, R.; Black, S.A.; Hance, J.R.; Darzi, A.; Cheshire, N.J.W. Virtual reality simulation training can improve inexperienced surgeons' endovascular skills. *Eur. J. Vasc. Endovasc. Surg.* **2006**, *31*, 588–593.
103. Tsang, J.S.; Naughton, P.A.; Leong, S.; Hill, A.D.K.; Kelly, C.J.; Leahy, A.L. Virtual reality simulation in endovascular surgical training. *Surg.* **2008**, *6*, 214–220.
104. Seibold, L.K.; Soohoo, J.R.; Ammar, D.A.; Kahook, M.Y. Preclinical investigation of ab interno trabeculectomy using a novel dual-blade device. *Am. J. Ophthalmol.* **2013**, *155*, 524–529.
105. De Visser, H.; Watson, M.O.; Salvado, O.; Passenger, J.D. Progress in virtual reality simulators for surgical training and certification. *Med. J. Aust.* **2011**, *194*, S38–S40.
106. Haque, S.; Srinivasan, S. A meta-analysis of the training effectiveness of virtual reality surgical simulators. *IEEE Trans. Inf. Technol. Biomed.* **2006**, *10*, 51–58.
107. Satava, R.M. Historical review of surgical simulation a personal perspective. *World J. Surg.* **2008**, *32*, 141–148.
108. Sagar, M.A.; Bullivant, D.; Mallinson, G.D.; Hunter, P.J. A virtual environment and model of the eye for surgical simulation. In

- Proceedings of the Proceedings of the 21st annual conference on Computer graphics and interactive techniques; 1994; pp. 205–212.
109. Sinclair, M.J.; Peifer, J.W.; Halebian, R.; Luxenberg, M.N.; Green, K.; Hull, D.S. Computer-simulated eye surgery: a novel teaching method for residents and practitioners. *Ophthalmology* **1995**, *102*, 517–521.
  110. Choi, K.-S.; Soo, S.; Chung, F.-L. A virtual training simulator for learning cataract surgery with phacoemulsification. *Comput. Biol. Med.* **2009**, *39*, 1020–1031.
  111. Khalifa, Y.M.; Bogorad, D.; Gibson, V.; Peifer, J.; Nussbaum, J. Virtual reality in ophthalmology training. *Surv. Ophthalmol.* **2006**, *51*, 259–273.
  112. Maiß, J.; Dumser, C.; Zopf, Y.; Nägel, A.; Krauss, N.; Hochberger, J.; Matthes, K.; Hahn, E.G.; Schwab, D. Hemodynamic efficacy of two endoscopic clip devices used in the treatment of bleeding vessels, tested in an experimental setting using the compact Erlangen Active Simulator for Interventional Endoscopy (compactEASIE) training model. *Endoscopy* **2006**, *38*, 575–580.
  113. Datta, V.; Mandalia, M.; Mackay, S.; Darzi, A. The PreOp flexible sigmoidoscopy trainer. *Surg. Endosc. Other Interv. Tech.* **2002**, *16*, 1459–1463.
  114. Tuggy, M.L. Virtual reality flexible sigmoidoscopy simulator training: impact on resident performance. *J Am Board Fam Pr.* **1998**, *11*, 426–433.
  115. Sedlack, R.E.; Kolars, J.C. Validation of a computer-based colonoscopy simulator. *Gastrointest. Endosc.* **2003**, *57*, 214–218.
  116. Cohen, J.; Cohen, S.A.; Vora, K.C.; Xue, X.; Burdick, J.S.; Bank, S.; Bini, E.J.; Bodenheimer, H.; Cerulli, M.; Gerdes, H.; et al. Multicenter, randomized, controlled trial of virtual-reality simulator training in acquisition of competency in colonoscopy. *Gastrointest. Endosc.* **2006**, *64*,

- 361–368.
117. Carter, F.J.; Schijven, M.P.; Aggarwal, R.; Grantcharov, T.; Francis, N.K.; Hanna, G.B.; Jakimowicz, J.J. Consensus guidelines for validation of virtual reality surgical simulators. *Surg. Endosc. Other Interv. Tech.* **2005**, *19*, 1523–1532.
  118. Seymour, N.E. Virtual reality in general surgical training. *Eur. Surg.* **2005**, *37*, 298–303.
  119. McCloy, R.; Stone, R. Virtual reality in surgery. *Bmj* **2001**, *323*, 912–915.
  120. Aggarwal, R.; Grantcharov, T.P.; Eriksen, J.R.; Blirup, D.; Kristiansen, V.B.; Funch-Jensen, P.; Darzi, A. An evidence-based virtual reality training program for novice laparoscopic surgeons. *Ann. Surg.* **2006**, *244*, 310.
  121. Peugnet, F.; Dubois, P.; Rouland, J.F. Virtual reality versus conventional training in retinal photocoagulation: a first clinical assessment. *Comput. Aided Surg. Off. J. Int. Soc. Comput. Aided Surg.* **1998**, *3*, 20–26.
  122. Cai, Y.; Chui, C.; Ye, X.; Wang, Y.; Anderson, J.H. VR simulated training for less invasive vascular intervention. *Comput. Graph.* **2003**, *27*, 215–221.
  123. Guo, S.; Qu, M.; Gao, B.; Guo, J. Deformation of the catheter and 3D blood vessel model for a VR-based catheter system. In Proceedings of the 2013 IEEE International Conference on Mechatronics and Automation; 2013; pp. 861–866.
  124. Guo, J.; Guo, S.; Xiao, N.; Dauteuille, T. A VR-based training system for vascular interventional surgery. In Proceedings of the 2013 ICME International Conference on Complex Medical Engineering; 2013; pp. 575–579.
  125. Gao, B.; Guo, S.; Xiao, N.; Guo, J. Development of a 3D blood vessel model for the Simulation of the Minimally Invasive Surgery. In

- Proceedings of the 2012 IEEE International Conference on Mechatronics and Automation; 2012; pp. 1393–1398.
126. Palter, V.N.; Grantcharov, T.P. Simulation in surgical education. *Cmaj* **2010**, *182*, 1191–1196.
  127. Thomson, J.E.; Poudrier, G.; Stranix, J.T.; Motosko, C.C.; Hazen, A. Current status of simulation training in plastic surgery residency programs: A review. *Arch. Plast. Surg.* **2018**, *45*, 395.
  128. Kaschwich, M., Matysiak, F., Bouchagiar, J., Dell, A., Bayer, A., Horn, M., & Kleemann, M. An Endovascular Simulator based on Exchangeable 3D-printed Real Vascular Pathologies as Alternative to the use of Animals. *Trans. Addit. Manuf. Meets Med.* **2019**, *1*.
  129. Chong, C.K.; How, T. V; Black, R.A.; Shortland, A.P.; Harris, P.L. Development of a simulator for endovascular repair of abdominal aortic aneurysms. *Ann. Biomed. Eng.* **1998**, *26*, 798–802.
  130. Wang, X.; Ph, D.; Yan, Y.; Zhang, R.; Ph, D.; Al, W.E.T. Recent Trends and Challenges in Complex Organ Manufacturing. **2010**, *16*.
  131. He, Y.; Xue, G.; Fu, J. prostheses with the desktop 3D printer. **2014**, 1–7.
  132. Kelley, D.J.; Farhoud, M.; Meyerand, M.E.; Nelson, D.L.; Ramirez, L.F.; Dempsey, R.J.; Wolf, A.J.; Alexander, A.L.; Davidson, R.J. Creating physical 3D stereolithograph models of brain and skull. *PLoS One* **2007**, *2*, e1119.
  133. Centre, U.G.H.N.; Science, B.E.; Engineering, B. Biomodels of Bone : A Review. **2005**, *33*, 1295–1311.
  134. Iyer, M.N.; Han, D.P. An eye model for practicing vitreoretinal membrane peeling. *Arch. Ophthalmol.* **2006**, *124*, 108–110.
  135. Rengier, F.; Mehndiratta, A.; Von Tengg-Kobligk, H.; Zechmann, C.M.; Unterhinninghofen, R.; Kauczor, H.U.; Giesel, F.L. 3D printing based on

- imaging data: Review of medical applications. *Int. J. Comput. Assist. Radiol. Surg.* **2010**, *5*, 335–341.
136. Giannopoulos, A.A.; Mitsouras, D.; Yoo, S.-J.; Liu, P.P.; Chatzizisis, Y.S.; Rybicki, F.J. Applications of 3D printing in cardiovascular diseases. *Nat. Rev. Cardiol.* **2016**, *13*, 701–718.
137. Hussain, T.; Gomez-Cia, T.; Valverde, I.; others Potential of 3D-printed models in planning structural interventional procedures. *Interv. Cardiol.* **2015**, *7*, 343–350.
138. Marro, A.; Bandukwala, T.; Mak, W. Three-dimensional printing and medical imaging: a review of the methods and applications. *Curr. Probl. Diagn. Radiol.* **2016**, *45*, 2–9.
139. Vukicevic, M.; Mosadegh, B.; Min, J.K.; Little, S.H. Cardiac 3D printing and its future directions. *JACC Cardiovasc. Imaging* **2017**, *10*, 171–184.
140. Sun, Z.; Lee, S.-Y. A systematic review of 3-D printing in cardiovascular and cerebrovascular diseases. *Anatol. J. Cardiol.* **2017**, *17*, 423.
141. Müller, A.; Krishnan, K.G.; Uhl, E.; Mast, G. The application of rapid prototyping techniques in cranial reconstruction and preoperative planning in neurosurgery. *J. Craniofac. Surg.* **2003**, *14*, 899–914.
142. D'Urso, P.S.; Hall, B.I.; Atkinson, R.L.; Weidmann, M.J.; Redmond, M.J. Biomodel-guided stereotaxy. *Neurosurgery* **1999**, *44*, 1084–1093.
143. D Urso, P.S.; Williamson, O.D.; Thompson, R.G. Biomodeling as an aid to spinal instrumentation. *Spine (Phila. Pa. 1976)*. **2005**, *30*, 2841–2845.
144. Yoo, S.-J.; Spray, T.; Austin III, E.H.; Yun, T.-J.; van Arsdell, G.S. Hands-on surgical training of congenital heart surgery using 3-dimensional print models. *J. Thorac. Cardiovasc. Surg.* **2017**, *153*, 1530–1540.
145. Kiraly, L.; Tofeig, M.; Jha, N.K.; Talo, H. Three-dimensional printed prototypes refine the anatomy of post-modified Norwood-1 complex

- aortic arch obstruction and allow presurgical simulation of the repair. *Interact. Cardiovasc. Thorac. Surg.* **2015**, *22*, 238–240.
146. Yoo, S.J.; Spray, T.; Austin, E.H.; Yun, T.J.; van Arsdell, G.S. Hands-on surgical training of congenital heart surgery using 3-dimensional print models. *J. Thorac. Cardiovasc. Surg.* **2017**, *153*, 1530–1540.
  147. Bernhard, J.C.; Isotani, S.; Matsugasumi, T.; Duddalwar, V.; Hung, A.J.; Suer, E.; Baco, E.; Satkunasivam, R.; Djaladat, H.; Metcalfe, C.; et al. Personalized 3D printed model of kidney and tumor anatomy: a useful tool for patient education. *World J. Urol.* **2016**, *34*, 337–345.
  148. Wake, N.; Chandarana, H.; Huang, W.C.; Taneja, S.S.; Rosenkrantz, A.B. Application of anatomically accurate, patient-specific 3D printed models from MRI data in urological oncology. *Clin. Radiol.* **2016**, *71*, 610–614.
  149. Kusaka, M.; Sugimoto, M.; Fukami, N.; Sasaki, H.; Takenaka, M.; Anraku, T.; Ito, T.; Kenmochi, T.; Shiroki, R.; Hoshinaga, K. Initial experience with a tailor-made simulation and navigation program using a 3-D printer model of kidney transplantation surgery. In Proceedings of the Transplantation proceedings; 2015; Vol. 47, pp. 596–599.
  150. Borenstein, J.T.; Terai, H.; King, K.R.; Weinberg, E.J.; Kaazempur-Mofrad, M.R.; Vacanti, J.P. Microfabrication technology for vascularized tissue engineering. *Biomed. Microdevices* **2002**, *4*, 167–175.
  151. Lanza, R.; Langer, R.; Vacanti, J.P. *Principles of tissue engineering*; Academic press, 2011;
  152. Borenstein, J.T.; Weinberg, E.J.; Orrick, B.K.; Sundback, C.; Kaazempur-Mofrad, M.R.; Vacanti, J.P. Microfabrication of three-dimensional engineered scaffolds. *Tissue Eng.* **2007**, *13*, 1837–1844.
  153. Golden, A.P.; Tien, J. Fabrication of microfluidic hydrogels using

- molded gelatin as a sacrificial element. *Lab Chip* **2007**, *7*, 720–725.
154. Norotte, C.; Marga, F.S.; Niklason, L.E.; Forgacs, G. Scaffold-free vascular tissue engineering using bioprinting. *Biomaterials* **2009**, *30*, 5910–5917.
  155. Fedorovich, N.E.; Alblas, J.; de Wijn, J.R.; Hennink, W.E.; Verbout, A.J.; Dhert, W.J.A. Hydrogels as extracellular matrices for skeletal tissue engineering: state-of-the-art and novel application in organ printing. *Tissue Eng.* **2007**, *13*, 1905–1925.
  156. Wheeler, T.D.; Stroock, A.D. The transpiration of water at negative pressures in a synthetic tree. *Nature* **2008**, *455*, 208.
  157. Therriault, D.; White, S.R.; Lewis, J.A. Chaotic mixing in three-dimensional microvascular networks fabricated by direct-write assembly. *Nat. Mater.* **2003**, *2*, 265.
  158. Fujii, T. PDMS-based microfluidic devices for biomedical applications. *Microelectron. Eng.* **2002**, *61*, 907–914.
  159. Ikeda, S.; Arai, F.; Fukuda, T.; Negoro, M.; Irie, K. An in vitro patient-specific biological model of the cerebral artery reproduced with a membranous configuration for simulating endovascular intervention. *J. Robot. Mechatronics* **2005**, *17*, 327–334.
  160. Matsushima, M.; Tercero, C.; Ikeda, S.; Fukuda, T.; Arai, F.; Negoro, M.; Takahashi, I. Photoelastic stress analysis in blood vessel phantoms: three-dimensional visualization and saccular aneurysm with bleb. *Int. J. Med. Robot. Comput. Assist. Surg.* **2011**, *7*, 33–41.
  161. Nakano, T.; Itoyama, T.; Yoshida, K.; Sawada, Y.; Ikeda, S.; Fukuda, T.; Matsuda, T.; Negoro, M.; Arai, F. Multiscale fabrication of a transparent circulation type blood vessel simulator. *Biomicrofluidics* **2010**, *4*, 46505.
  162. Tanaka, S.; Harada, K.; Ida, Y.; Tomita, K.; Kato, I.; Arai, F.; Ueta, T.;

- Noda, Y.; Sugita, N.; Mitsuishi, M. Quantitative assessment of manual and robotic microcannulation for eye surgery using new eye model. *Int. J. Med. Robot. Comput. Assist. Surg.* **2015**, *11*, 210–217.
163. Arai, F.; Fukuda, T.; Ikeda, S.; Negoro, M.; Takahashi, I. Rapid production of an in vitro anatomical model of human cerebral arteries based on CT images. In Proceedings of the Proceedings of 2002 International Symposium on Micromechatronics and Human Science; 2002; pp. 41–46.
164. Queijo, L.; Lima, R. PDMS anatomical realistic models for hemodynamic studies using rapid prototyping technology. In Proceedings of the 6th World Congress of Biomechanics (WCB 2010). August 1-6, 2010 Singapore; 2010; pp. 434–437.
165. Torres, I.O.; De Luccia, N. A simulator for training in endovascular aneurysm repair: the use of three dimensional printers. *Eur. J. Vasc. Endovasc. Surg.* **2017**, *54*, 247–253.
166. Kaneko, N.; Mashiko, T.; Ohnishi, T.; Ohta, M.; Namba, K.; Watanabe, E.; Kawai, K. Manufacture of patient-specific vascular replicas for endovascular simulation using fast, low-cost method. *Sci. Rep.* **2016**, *6*, 39168.
167. Neequaye, S.K.; Aggarwal, R.; Van Herzeele, I.; Darzi, A.; Cheshire, N.J. Endovascular skills training and assessment. *J. Vasc. Surg.* **2007**, *46*, 1055–1064.
168. Itagaki, M.W. Using 3D printed models for planning and guidance during endovascular intervention: a technical advance. *Diagnostic Interv. Radiol.* **2015**, *21*, 338.
169. Hayakawa, T.; Kato, I.; Arai, F.; Mitsuishi, M.; Sugita, N.; Harada, K.; Tanaka, S.; Noda, Y.; Ueta, T. Retinal vessel model fabricated on a



- curved surface structure for a simulation of microcannulation. *ROBOMECH J.* **2016**, *3*, 19.
170. Omata, S.; Someya, Y.; Masuda, T.; Hayakawa, T.; Harada, K.; Mitsuishi, M.; Totsuka, K.; Araki, F.; Takao, M.; Aihara, M.; et al. A surgical simulator for peeling the inner limiting membrane during wet conditions. *PLoS One* **2018**, *13*, e0196131.
171. Ikeda, S.; Arai, F.; Fukuda, T.; Negoro, M.; Irie, K.; Takahashi, I. An in vitro patient-tailored model of human cerebral artery for simulating endovascular intervention. In Proceedings of the International Conference on Medical Image Computing and Computer-Assisted Intervention; 2005; pp. 925–932.
172. Beauchamp, M.J.; Nordin, G.P.; Woolley, A.T. Moving from millifluidic to truly microfluidic sub-100- $\mu\text{m}$  cross-section 3D printed devices. *Anal. Bioanal. Chem.* **2017**, *409*, 4311–4319.
173. Ho, C.M.B.; Ng, S.H.; Li, K.H.H.; Yoon, Y.-J. 3D printed microfluidics for biological applications. *Lab Chip* **2015**, *15*, 3627–3637.
174. Itoga, K.; Yamato, M.; Kobayashi, J.; Kikuchi, A.; Okano, T. Cell micropatterning using photopolymerization with a liquid crystal device commercial projector. *Biomaterials* **2004**, *25*, 2047–2053.
175. Noda, D.; Matsumoto, Y.; Setomoto, M.; Hattori, T. Fabrication of coil lines with high aspect ratio for electromagnetic actuators. In Proceedings of the 2007 International Symposium on Micro-NanoMechatronics and Human Science; 2007; pp. 436–441.
176. Ito, H.; England, W.P.; Ueda, M. Chemical amplification based on acid-catalyzed depolymerization. *J. Photopolym. Sci. Technol.* **1990**, *3*, 219–233.
177. Schlegel, L.; Ueno, T.; Hayashi, N.; Iwayanagi, T. Determination of acid diffusion in chemical amplification positive deep ultraviolet resists. *J.*

- Vac. Sci. Technol. B Microelectron. Nanom. Struct. Process. Meas. Phenom.* **1991**, *9*, 278–289.
178. ASAKAWA, K. Diffusion of acid and activation energy of positive chemical amplification resist. *J. Photopolym. Sci. Technol.* **1993**, *6*, 505–514.
179. Asakawa, K.; Ushirogouchi, T.; Nakase, M. Effect of remaining solvent on sensitivity, diffusion of acid, and resolution in chemical amplification resists. *J. Vac. Sci. Technol. B Microelectron. Nanom. Struct. Process. Meas. Phenom.* **1995**, *13*, 833–839.
180. Chen, Q.; Li, G.; Zhao, J. CURVED SU-8 structure fabrication based on the acid-diffusion effect. In Proceedings of the 2011 IEEE 24th International Conference on Micro Electro Mechanical Systems; 2011; pp. 225–228.
181. Yamagishi, Y.; Masuda, T.; Takei, N.; Owaki, H.; Matsusaki, M.; Akashi, M.; Arai, F. Three-Dimensional Assembly of Multilayered Tissues. *Procedia CIRP* **2013**, *5*, 201–204.
182. Futai, N.; Gu, W.; Takayama, S. Rapid Prototyping of Microstructures with Bell-Shaped Cross-Sections and Its Application to Deformation-Based Microfluidic Valves. *Adv. Mater.* **2004**, *16*, 1320–1323.
183. Hayakawa, T.; Fukada, S.; Arai, F. Fabrication of an on-chip nanorobot integrating functional nanomaterials for single-cell punctures. *IEEE Trans. Robot.* **2013**, *30*, 59–67.
184. Tomita, K.; Nakano, T.; Onda, K.; Fukuda, T.; Matsuda, T.; Negoro, M.; Arai, F. Fabrication of 3D capillary vessel simulator using femtosecond laser and mask hybrid exposure. In Proceedings of the 2011 International Symposium on Micro-NanoMechatronics and Human Science; 2011; pp. 300–302.
185. Juodkazis, S.; Mizeikis, V.; Seet, K.K.; Miwa, M.; Misawa, H. Two-

- photon lithography of nanorods in SU-8 photoresist. *Nanotechnology* **2005**, *16*, 846.
186. Sun, H.-B.; Tanaka, T.; Kawata, S. Three-dimensional focal spots related to two-photon excitation. *Appl. Phys. Lett.* **2002**, *80*, 3673–3675.
187. Kneebone, R. Simulation in surgical training: educational issues and practical implications. In Proceedings of the Medical education; Wiley Online Library, 2003; Vol. 37, pp. 267–277.
188. Yamaguchi, H.; Saito, T.; Shiraishi, Y.; Arai, F.; Morimoto, Y.; Yuasa, A. Quantitative study on appearance of microvessels in spectral endoscopic imaging. *J. Biomed. Opt.* **2015**, *20*, 36005.
189. Sakuma, S.; Kuroda, K.; Tsai, C.-H.D.; Fukui, W.; Arai, F.; Kaneko, M. Red blood cell fatigue evaluation based on the close-encountering point between extensibility and recoverability. *Lab Chip* **2014**, *14*, 1135–1141.
190. Tham, Y.-C.; Li, X.; Wong, T.Y.; Quigley, H.A.; Aung, T.; Cheng, C.-Y. Global prevalence of glaucoma and projections of glaucoma burden through 2040: a systematic review and meta-analysis. *Ophthalmology* **2014**, *121*, 2081–2090.
191. Quigley, H.A.; Broman, A.T. The number of people with glaucoma worldwide in 2010 and 2020. *Br. J. Ophthalmol.* **2006**, *90*, 262–267.
192. Goel, M.; Picciani, R.G.; Lee, R.K.; Bhattacharya, S.K. Aqueous humor dynamics: a review. *Open Ophthalmol. J.* **2010**, *4*, 52.
193. Lee, W.R. The pathology of the outflow system in primary and secondary glaucoma. *Eye* **1995**, *9*, 1.
194. Spileers, W.; Goethals, M. Structural changes of the lamina cribrosa and of the trabeculum in primary open angle glaucoma (POAG). *Bull. Soc. Belge Ophtalmol.* **1992**, *244*, 27.
195. Tamm, E.R. The trabecular meshwork outflow pathways: structural and

- functional aspects. *Exp. Eye Res.* **2009**, *88*, 648–655.
196. GRANT, W.M. Clinical measurements of aqueous outflow. *AMA Arch. Ophthalmol.* **1951**, *46*, 113–131.
197. GRANT, W.M. Experimental aqueous perfusion in enucleated human eyes. *Arch. Ophthalmol.* **1963**, *69*, 783–801.
198. Brubaker, R.F. Targeting outflow facility in glaucoma management. *Surv. Ophthalmol.* **2003**, *48*, S17--S20.
199. Pillunat, L.E.; Erb, C.; Jünemann, A.G.M.; Kimmich, F. Micro-invasive glaucoma surgery (MIGS): a review of surgical procedures using stents. *Clin. Ophthalmol. (Auckland, NZ)* **2017**, *11*, 1583.
200. Fingeret, M.; Dickerson Jr, J.E. The role of minimally invasive glaucoma surgery devices in the management of glaucoma. *Optom. Vis. Sci.* **2018**, *95*, 155.
201. Agrawal, P.; Bradshaw, S.E. Systematic literature review of clinical and economic outcomes of micro-invasive glaucoma surgery (MIGS) in primary open-angle glaucoma. *Ophthalmol. Ther.* **2018**, *7*, 49–73.
202. Richter, G.M.; Coleman, A.L. Minimally invasive glaucoma surgery: current status and future prospects. *Clin. Ophthalmol. (Auckland, NZ)* **2016**, *10*, 189.
203. Saheb, H.; Ahmed, I.I.K. Micro-invasive glaucoma surgery: current perspectives and future directions. *Curr. Opin. Ophthalmol.* **2012**, *23*, 96–104.
204. Kaplowitz, K.; Schuman, J.S.; Loewen, N.A. Techniques and outcomes of minimally invasive trabecular ablation and bypass surgery. *Br. J. Ophthalmol.* **2014**, *98*, 579–585.
205. Akura, J.; Pokharel, K. Artificial lens for cataract surgery practice 2014.
206. Van Dalen, J.T.W.; Carda, D.D. Model human eye and face manikin for

- use therewith 2014.
207. Bernal, A. Ophthalmic surgical simulation system 2016.
  208. Kamei, K. ichiro; Mashimo, Y.; Koyama, Y.; Fockenberg, C.; Nakashima, M.; Nakajima, M.; Li, J.; Chen, Y. 3D printing of soft lithography mold for rapid production of polydimethylsiloxane-based microfluidic devices for cell stimulation with concentration gradients. *Biomed. Microdevices* **2015**, *17*.
  209. Borenstein, J.T.; Tupper, M.M.; MacK, P.J.; Weinberg, E.J.; Khalil, A.S.; Hsiao, J.; García-Cardena, G. Functional endothelialized microvascular networks with circular cross-sections in a tissue culture substrate. *Biomed. Microdevices* **2010**, *12*, 71–79.
  210. Beebe, D.J.; Mensing, G.A.; Walker, G.M. Physics and applications of microfluidics in biology. *Annu. Rev. Biomed. Eng.* **2002**, *4*, 261–286.
  211. Tanito, M.; Sano, I.; Ikeda, Y.; Fujihara, E. Microhook ab interno trabeculotomy, a novel minimally invasive glaucoma surgery, in eyes with open-angle glaucoma with scleral thinning. *Acta Ophthalmol.* **2016**, *94*, e371--e372.
  212. Dietlein, T.S.; Jacobi, P.C.; Lüke, C.; Krieglstein, G.K. Morphological variability of the trabecular meshwork in glaucoma patients: implications for non-perforating glaucoma surgery. *Br. J. Ophthalmol.* **2000**, *84*, 1354–1359.
  213. Vieira, M.G.A.; Da Silva, M.A.; Dos Santos, L.O.; Beppu, M.M. Natural-based plasticizers and biopolymer films: A review. *Eur. Polym. J.* **2011**, *47*, 254–263.
  214. Strobl, G. *The physics of polymers: Concepts for understanding their structures and behavior*; 2007; ISBN 9783540252788.
  215. Stevens, K.R.; Ungrin, M.D.; Schwartz, R.E.; Ng, S.; Carvalho, B.;

- Christine, K.S.; Chaturvedi, R.R.; Li, C.Y.; Zandstra, P.W.; Chen, C.S.; et al. InVERT molding for scalable control of tissue microarchitecture. *Nat. Commun.* **2013**, *4*.
216. Khetani, S.R.; Bhatia, S.N. Microscale culture of human liver cells for drug development. *Nat. Biotechnol.* **2008**, *26*, 120–126.
217. Gallab, M.; Tomita, K.; Omata, S.; Arai, F. Fabrication of 3D Capillary Vessel Models with Circulatory Connection Ports. *Micromachines* **2018**, *9*, 101.
218. Johnston, I.D.; McCluskey, D.K.; Tan, C.K.L.; Tracey, M.C. Mechanical characterization of bulk Sylgard 184 for microfluidics and microengineering. *J. Micromechanics Microengineering* **2014**, *24*.
219. Friberg, T.R.; Lace, J.W. A comparison of the elastic properties of human choroid and sclera. *Exp. Eye Res.* **1988**, *47*, 429–436.
220. Camras, L.J.; Stamer, W.D.; Epstein, D.; Gonzalez, P.; Yuan, F. Circumferential tensile stiffness of glaucomatous trabecular meshwork. *Investig. Ophthalmol. Vis. Sci.* **2014**, *55*, 814–823.
221. Camras, L.J.; Stamer, W.D.; Epstein, D.; Gonzalez, P.; Yuan, F. Differential effects of trabecular meshwork stiffness on outflow facility in normal human and porcine eyes. *Investig. Ophthalmol. Vis. Sci.* **2012**, *53*, 5242–5250.

## Accomplishments

1. Mahmoud Gallab, Seiji Omata, Kanako Harada, Mamoru Mitsuishi, Kiyohito Totsuka, Fumiyuki Araki, Muneyuki Takao, Makoto Aihara and Fumihito Arai. Development of a Spherical Model with a 3D Microchannel: an Application of Glaucoma Surgery. *Micromachines*, 10 (5), 297, April, 2019. (Cover Article)
2. Mahmoud Gallab, Kyohei Tomita, Seiji Omata, and Fumihito Arai. Fabrication of 3D Capillary Vessel Models with Circulatory Connection Ports. *Micromachines*, 9 (3), 101, February, 2018.
3. Mahmoud Gallab, Seiji Omata, Kanako Harada, Mamoru Mitsuishi, Kiyohito Totsuka, Fumiyuki Araki, Muneyuki Takao, Makoto Aihara and Fumihito Arai. Eye Surgery Simulator for the Training of Minimally Invasive Glaucoma Surgery Skills. IEEE international conference on cyborg and bionic systems, Shenzhen, China, 2018.
4. Mahmoud Gallab, Seiji Omata, Kanako Harada, Mamoru Mitsuishi, Kiyohito Totsuka, Fumiyuki Araki, Muneyuki Takao, Makoto Aihara and Fumihito Arai. Surgical Simulator for Training of Minimally Invasive Glaucoma Surgery. International Symposium on Micro-Nano Mechatronics and Human Science, Japan, 2018.

5. Mahmoud Gallab, Seiji Omata, and Fumihito Arai. A novel eye-surgery simulator of glaucoma surgery with a bionic eye model. International Symposium on Micro-Nano Mechatronics and Human Science, Japan, 2017.
  
6. Seiji Omata, Mahmoud Gallab, Kanako Harada, Mamoru Mitsuishi, Kiyohito Totsuka, Fumiyuki Araki, Muneyuki Takao, Makoto Aihara and Fumihito Arai. Bionic-EyE: Eye Model for Simulating Glaucoma Operation. ROBOMECH Conference, Kitakyushu, Japan 2018.